UPPSALA
UNIVERSITET

Digital Comprehensive Summaries of Uppsala Dissertations from the Faculty of Science and Technology 2069

Combining Electrochemistry and Photoelectron Spectroscopy for the Study of Li-ion Batteries

IDA KÄLLQUIST

ACTA
UNIVERSITATIS
UPSALIENSIS
UPPSALA
2021

ISSN 1651-6214
ISBN 978-91-513-1285-9
URN urn:nbn:se:uu:diva-452281

Dissertation presented at Uppsala University to be publicly examined in Siegbahnsalen, Ångströmlaboratoriet, Lägerhyddsvägen 1, Uppsala, Friday, 22 October 2021 at 09:15 for the degree of Doctor of Philosophy. The examination will be conducted in English. Faculty examiner: Doctor Hendrik Bluhm (Fritz Haber Institute of the Max Planck Society).

Abstract
Källquist, I. 2021. Combining Electrochemistry and Photoelectron Spectroscopy for the Study of Li-ion Batteries. *Digital Comprehensive Summaries of Uppsala Dissertations from the Faculty of Science and Technology* 2069. 123 pp. Uppsala: Acta Universitatis Upsaliensis. ISBN 978-91-513-1285-9.

In this thesis photoelectron spectroscopy (PES) is combined with electrochemistry to investigate the electrochemical processes that occur at the electrode/electrolyte interfaces in lithium-ion batteries (LIBs). LIB systems are studied by the use of both ex situ PES, where electrodes are electrochemically pre-cycled and subsequently measured by PES, and operando PES, where electrodes are cycled during PES measurements.

Ex situ PES is used to determine the main degradation mechanisms of a novel high capacity material, Li_2VO_2F. The capacity fade seen for Li_2VO_2F. is found to be related to an irreversible oxidation of the active material at high voltages, and a continuous surface layer formation at low voltages. To decrease the capacity fading three strategies for optimizing the interface are investigated. The results show that a surface coating of AlF3 most efficiently can mitigate electrolyte reduction, while boron containing electrolyte additives and transition metal substitution more successfully limit the oxidation of the active material.

A large part of the work performed in this thesis has been devoted towards developing a methodology suitable for conducting operando ambient pressure photoelectron spectroscopy (APPES) measurements on LIB systems. A general connection between the theory of PES and electrochemistry is made, where in particular a model suitable for interpreting operando APPES results on solid/liquid interfaces is suggested. The model is further developed for the specific case of LIB interfaces. The results from the operando studies show that the kinetic energy shifts of the liquid electrolyte measured by APPES can be correlated to the electrochemical reactions occurring at the interface. If no charge transfer occurs, the kinetic energy shift is proportional to the applied voltage. During charge transfer the behavior is more complex, and the kinetic energy shifts are related to the change in chemical potential of the working electrode.

In summary, this thesis exemplifies how both ex situ and operando PES are highly useful techniques for the study of LIB battery interfaces. The possibilities of both techniques are highlighted, and important considerations for an accurate interpretation of the PES results are also discussed.

Keywords: Li-ion battery, battery interfaces, electrochemistry, electrochemical potential, photoelectron spectroscopy, operando, ambient pressure photoelectron spectroscopy

Ida Källquist, Department of Physics and Astronomy, Condensed Matter Physics of Energy Materials, Box 516, Uppsala University, SE-751 20 Uppsala, Sweden.

ISSN 1651-6214
ISBN 978-91-513-1285-9
URN urn:nbn:se:uu:diva-452281 (http://urn.kb.se/resolve?urn=urn:nbn:se:uu:diva-452281)

Till min farmor – när jag blir ”stor” hoppas jag på att vara lika cool som du.

List of Papers

This thesis is based on the following papers, which are referred to in the text by their Roman numerals.

I Lindgren, F., Rehnlund, D., **Källquist, I**., Nyholm, L., Edström, K., Hahlin, M. & Maibach, J. (2017). Breaking Down a Complex System: Interpreting PES Peak Positions for Cycled Li-ion Battery Electrodes. *The Journal of Physical Chemistry C*, 121:27303-27312.

II Maibach, J., **Källquist, I**., Maibach, J., Källquist, I., Andersson, M., Urpelainen, S., Edström, K., Rensmo, H., Siegbahn, H., Hahlin, M. (2019). Probing a battery electrolyte drop with ambient pressure photoelectron spectroscopy. *Nature Communications,* 10(1):3080.

III **Källquist, I**., Lindgren, F., Lee, M.-T., Shavorskiy, A., Edström, K., Rensmo, H., Nyholm, L., Maibach, J., Hahlin, M. (2021). Probing Electrochemical Potential Differences over the Solid/Liquid Interface in Li-Ion Battery Model Systems. *ACS Applied Materials & Interfaces*, 13(28):32989-32996

IV **Källquist, I**., Ericson, T., Lindgren, F., Chen, H., Shavorskiy, A., Maibach, J., Hahlin, M. (2021). Potentials in Li-ion batteries probed by operando ambient pressure photoelectron spectroscopy. *Submitted manuscript.*

V **Källquist, I**., Ericson, T., Erbing, A., Odelius, M., Lindgren, F., Lee, M.-T., Shavorskiy, A., Rensmo, H., Maibach, J., Hahlin, M. (2021). Operando ambient pressure photoelectron spectroscopy of solid/liquid interfaces in Li-ion batteries. *In manuscript.*

VI **Källquist, I**., Naylor, A.J., Baur, C., Chable, J., Kullgren, J., Fichtner, M., Edström, K., Brandell, D., Hahlin, M. (2019). Degradation Mechanisms in Li2VO2F Li-Rich Disordered Rock-Salt Cathodes. *Chemistry of Materials*, 31(16), 6084-6096.

VII Baur, C., **Källquist, I**., Chable, J., Chang, J. H., Johnsen, R. E., Ruiz-Zepeda, F., Ateba Mba, J.-M., Naylor, A.J., García-Lastra, J.M., Vegge, T., Klein, F., Schür, A.R., Norby, P., Edström K., Hahlin, M., Fichtner, M. (2019). Improved cycling stability in high-capacity Li-rich vanadium containing disordered rock salt oxyfluoride cathodes. *Journal of Materials Chemistry A*, 7(37):21244-21253.

VIII **Källquist, I**., Martin, J.-F., Naylor, A. J., Baur, C., Fichtner, M., Colin, J.-F., Brandell, D., Edström, K., Hahlin, M. (2020). Influence of Electrolyte Additives on the Degradation of Li2VO2F Li-Rich Cathodes. *The Journal of Physical Chemistry C*, 124(24):12956-12967.

IX Naylor, A. J., **Källquist, I**., Peralta, D., Martin, J.-F., Boulineau, A., Colin, J.-F., Baur, C., Chable, J., Fichtner, M., Edström, K., Hahlin, M., Brandell, D. (2020). Stabilization of Li-Rich Disordered Rocksalt Oxyfluoride Cathodes by Particle Surface Modification. *ACS Applied Energy Materials*, 3(6):5937-5948.

Reprints were made with permission from the publishers.

Comments on participation

The papers included in this thesis are the result of joint efforts. In Paper I, my main contribution was to the data analysis and discussions. In Paper II and IX, I contributed with experimental work, data analysis, discussions and part of the writing. In Paper III-VI and Paper VIII, where I am first author, I have been the main responsible for the data analysis, interpretation, discussions and writing. I have also to a large extent been involved in planning, preparing and performing all the photoelectron spectroscopy measurements. In Paper VII, I was the main responsible for the photoelectron spectroscopy experiments, data analysis and writing.

Extended bibliography

The following are publications to which the author has contributed that are not included in the present thesis:

Zhu, S., Scardamaglia, M., Kundsen, J., Sankari, R., Tarawneh, H., Temperton, R., Pickworth, L., Cavalca, F., Wang, C., Tissot, H., Weissenrieder, J., Hagman, B., Gustafson, J., Kaya, S., Lindgren, F., **Källquist, I**., Maibach, J., Hahlin, M., Boix, V., Gallo, T., Rehman, F., D'Acunto, G., Schnadt, J., Shavorskiy, A. (2021). HIPPIE: a new platform for ambient-pressure X-ray photoelectron spectroscopy at the MAX IV Laboratory. *Journal of synchrotron radiation,* 28 Pt 2, 624-636

Naylor, A., Maibach, J., **Källquist, I**., Makkos, E., Roberts, M. R., Younesi, R., Hahlin, M., Brandell, D., Islam, M.S. Bruce, P.G., Edström, K. (2018). Energy-Tuned Photoelectron Spectroscopy of Lithium-Ion Battery Cathodes: Revealing Oxygen Redox Activity and Investigating New Materials. In *ECS Meeting Abstracts* (No. 4, p. 215). IOP Publishing.

Edström, K., Maibach, J., **Källquist, I**., Lindgren, F., & Hahlin, M. (2019). Ambient Pressure XPS Studies of Liquid Solid Interfaces in Batteries. In *ECS Meeting Abstracts* (No. 3, p. 167). IOP Publishing.

Contents

Abbreviations

AM	Active Material
APPES	Ambient Pressure Photoelectron Spectroscopy
BE	Binding Energy
CB	Carbon Black
CC	Current Collector
CE	Counter Electrode
DMC	Dimethyl Carbonate
DRS	Disordered Rock-Salt
EC	Ethylene Carbonate
ESCA	Electron Spectroscopy for Chemical Analysis
HOMO	Highest Occupied Molecular Orbital
IMFP	Inelastic Mean Free Path
KE	Kinetic Energy
LCO	Lithium Cobalt Oxide, $LiCoO_2$
LIB	Lithium Ion Battery
LiTFSI	Lithium bis(trifluoromethanesulfonyl)imide
LTO	Lithium Titanate Oxide, $Li_4Ti_5O_{12}$
LUMO	Lowest Unoccupied Molecular Orbital
MO	Metal Oxide
NMC	Lithium Nickel Manganese Cobalt Oxide, $LiNi_xMn_yCo_zO_2$
PC	Propylene Carbonate
PE	Photoelectron
PES	Photoelectron Spectroscopy
RE	Reference Electrode
SEI	Solid Electrolyte Interphase
TM	Transition Metal
UHV	Ultra-High Vacuum
WE	Working Electrode

Elektrokemi och fotoelektronspektroskopi för studier av Li-jonbatterier

Litiumjonbatterier är i dagsläget förstahandsvalet för batterier som används i portabel elektronik, som till exempel mobiltelefoner, datorer och kameror. Anledningen till detta är att Li-jonbatterier har en hög energidensitet, d.v.s. en stor mängd energi kan lagras i förhållande till batteriets vikt (eller volym). Detta är kanske den viktigaste parametern för batterier som vi dagligen bär med oss, men inte den enda viktiga faktorn som ett batteri behöver uppfylla.

Utöver en hög energilagringskapacitet, så bör ett batteri också hålla länge, och kunna cyklas många gånger (en battericykel = en upp- och urladdning) med bibehållen kapacitet. Batteriet ska gärna gå att ladda snabbt, vilket kan vara extra viktigt till exempel för elbilar som ska köras långt och behöver laddas under vägen. Dessutom måste batteriet förstås vara säkert att använda, och materialen som används ska helst finnas i en stor mängd, och vara billiga och miljövänliga.

Ofta är det tyvärr så att de batterimaterial som kan ge högst energidensitet, inte är de som kan cyklas flest gånger. Detta hänger ihop med att energirika material typiskt är kemiskt reaktiva, vilket innebär att det finns en risk för att diverse oönskade ”sidoreaktioner” sker. Dessa kan leda till nedbrytning av batteriets komponenter och i värsta fall även vara en säkerhetsrisk genom värmeutveckling och i extremfall explosioner. Ett av de långsiktiga målen med forskningen i den här avhandlingen handlar därför om att hitta strategier för att designa batterier med både hög energidensitet och lång hållbarhet.

Upp- och urladdningen av ett Li-jonbatteri sker genom transport av Li-joner och elektroner mellan den positiva och negativa elektroden. Laddningarna avges och tas upp vid elektroderna i s.k. redoxreaktioner. Elektronerna transporteras genom en yttre elektrisk krets, medan Li-jonerna transporteras inne i batteriet genom en elektrolyt. Elektrolyten är i de flesta fall en vätska som består av ett organiskt lösningsmedel och ett litiumjonsalt. I gränsskiktet mellan elektrod och elektrolyt sker de redoxreaktioner som ansvarar för energiomvandlingen i batteriet. En redoxreaktion sker vid en speciell spänning, vilken bestäms av materialets kemiska egenskaper och kallas för elektrodens redoxpotential. Skillnaden mellan redoxpotentialen för den positiva elektroden och den negativa elektroden ger batteriets totala spänning. Ju högre spänning batteriet har, desto mer energi kan lagras.

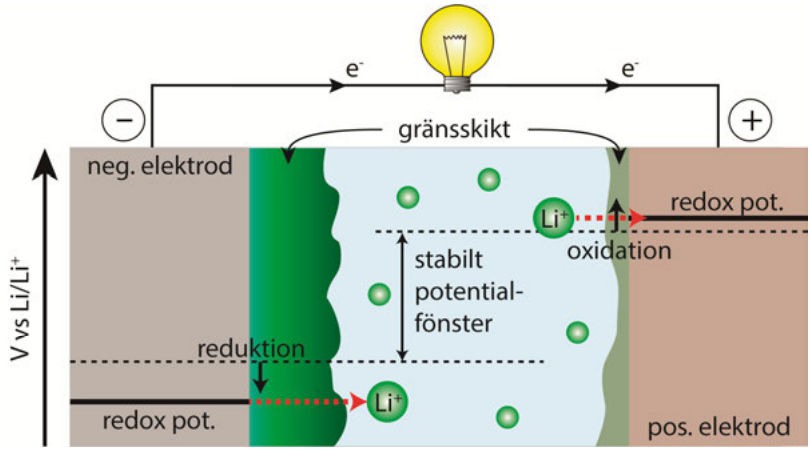

Figur 1: Illustration av gränsskikten i ett litiumjonbatteri, som bildas när elektrodernas redoxpotential ligger utanför elektrolytens stabila potentialfönster.

En nackdel med höga spänningar är att de vanligaste batterielektrolyterna i detta fall inte är stabila, utan kan oxideras vid höga potentialer, och reduceras vid låga potentialer. Dessa reaktioner leder till att gränsskikt bildas på elektroderna, vilket är illustrerat i Figur 1.

Uppbyggnaden av gränsskikt är ett exempel på sidoreaktioner som kan ske i ett batteri. I dessa sidoreaktioner konsumeras elektroner och Li-joner som sedan inte kan frigöras igen (s.k. irreversibla reaktioner). Detta leder till att en del av energin som går åt till att ladda batteriet inte fås tillbaka när batteriet laddas ur. I vissa sidoreaktioner kan även delar av elektrodmaterialet brytas ner, vilket gör att batteriet tappar en del av sin kapacitet. Om dessa sidoreaktioner fortgår kommer lite kapacitet att tappas i varje cykel, tills batteriet så småningom inte fungerar alls. För många kommersiella batterier sker detta efter omkring 500-1000 cykler, d.v.s. efter 2-3 år för ett batteri som laddas dagligen.

För att öka livslängden både på dagens batterier och möjliga framtida batterimaterial, så handlar mycket om att optimera gränsskikten i batteriet. Syftet med detta är att i möjligaste mån begränsa sidoreaktionerna, utan att förhindra de önskade redoxreaktionerna. För att kunna göra det, är det första steget att förstå vilka reaktioner som sker vid ytan, och vad som är anledningen till att batteriet bryts ned. När detta är kartlagt går det att använda olika strategier för att modifiera ytkemin och förbättra gränsskiktens egenskaper. Detta är något som undersöks i avhandlingen med hjälp av elektrokemiska och spektroskopiska metoder.

De elektrokemiska metoderna kan bl.a. användas för att studera mängden laddning (Li-joner och elektroner) som kan lagras i batteriet, elektrodernas redoxpotentialer och hur snabbt reaktionerna sker. Genomatt utföra många cykler går det också att undersöka hur batteriets kapacitet avtar över tid, och hur lång cykling påverkar t.ex. resistans och spänning för batteriet.

Spektroskopiska metoder används för att studera den kemiska sammansättningen av elektrodytan. I det här arbetet har främst tekniken fotoelektronspektroskopi använts. Grundprincipen för denna teknik är att ett material som bestrålas med ljus (fotoner) av tillräckligt hög energi, kommer avge elektroner med olika kinetisk energi. Den kinetiska energin för de frigjorda elektronerna kan mätas, och med hjälp av den kända energin för fotonerna går det då att räkna ut elektronernas bindningsenergi. Bindningsenergin är specifik för olika grundämnen, kemiska tillstånd, och den elektrostatiskastuderas potential som elektronen frigjordes ifrån. På det här sättet är det möjligt att identifiera olika grundämnen, deras kemiska omgivning och eventuella potentialskillnader i ett prov.

Den här avhandlingen är en sammanläggning, i vilken nio artiklar ingår. Gemensamt för alla nio artiklarna är att fotoelektronspektroskopi har använts för att studera gränsskikt i Li-jonbatterier. I de studier som genomfördes först (Artikel I och VI-IX) har batterielektroderna först cyklats elektrokemiskt, för att sedan tas isär och undersökas med hjälp av fotoelektronspektroskopi i vakuum (*ex situ* mätningar). I denna metod är omgivningen under mätningarna *inte* representativ för det riktiga batteriet. Trots det, kan gränsskiktens karaktär såsom tjocklek och sammansättning studeras efter olika många cykler. I artikel VI studeras ett nytt positivt elektrodmaterial, Li_2VO_2F, som potentiellt skulle kunna leverera dubbelt så hög energidensitet som de kommersiella material som används idag. För att detta material ska vara användbart måste dock dess cyklingsprestanda förbättras väsentligt. Den här studien visar att nedbrytningen av materialet hänger ihop med en instabil struktur, där vanadinoxiden kan reagera med saltet i elektrolyten. Detta resulterar i att materialet gradvis bryts ner och inte längre kan cyklas, vilket förklarar den snabbt avtagande kapaciteten.

I Artikel VII-IX studeras olika sätt att förbättra cyklingsprestandan för samma material. Tre olika strategier utvärderas och resultaten visar att elektrodmaterialets prestanda kan förbättras genom: (i) dopning av materialet, där en del av vanadinet byts ut mot järn eller titan. Detta stabiliserar materialets struktur (Artikel VII). (ii) Tillsatser till elektrolyten, där framförallt bor-salter visar sig kunna skydda elektrodmaterialet från oxidation genom att forma ett skyddande ytlager (Artikel VIII). (iii) En ytbeläggning av elektrodmaterialet, som fysiskt blockerar lösningsmedlet från att reagera med elektroden och på så sätt minskar uppbyggnaden av ett tjockt ytlager som leder till förlorad kapacitet (Artikel IX).

För att få mer information kring formering, laddningsöverföring och andra kinetiska egenskaper hos gränsskikten i batterier, krävs metoder där ytorna kan studeras samtidigt som batteriet cyklas (*operando* mätningar). Tidigare har det inte funnits många ytkänsliga metoder för vilka detta är möjligt. I denna avhandling har en stor del av arbetet därför handlat om att utveckla en metodik för att studera gränsskikt i Li-jonbatterier med fotoelektron-spektroskopi under cykling. För att kunna utföra dessa experiment måste

många praktiska utmaningar beaktas. Exempelvis krävs ett högre tryck under mätningarna för att kunna introducera en vätska (elektrolyt), och ett tunt vätskelager måste skapas för att kunna mäta på elektrolyten och elektroden samtidigt. Dessutom måste uppställningen vara lämplig för elektrokemisk cykling.

För att förstå och tolka resultaten från mätningarna krävs även en förståelse för vilka spektroskopiska och elektrokemiska principer som kan appliceras på systemet. Detta illustreras i Artikel I, där de (elektrokemiska) potentialskillnader som kan uppstå mellan olika faser när batteriets spänning ändras leder till skift i den uppmätta bindningsenergin. För att förstå uppkomsten av dessa potentialskillnader mellan t.ex. elektroden och elektrolyten kan *operando* mätningar göras. I artikel II-V görs fotoelektronspektroskopimätningar under tryck ”nära” normalt lufttryck (~1 mbar jämfört med ~10^{-7} mbar som används för fotoelektronspektroskopi i vakuum). I artikel II karakteriseras och undersöks stabiliteten hos en flytande elektrolyt. Denna studie är en viktig förstudie för att sedan kunna undersöka gränsskiktet mellan elektrolyt och elektrod. I artikel III och IV studeras en batterielektrolyt *operando* under cykling. I artikel III undersöks två modellsystem bestående av metallelektroder, och i artikel IV cyklas ett välkänt negativt elektrodmaterial, $Li_4Ti_5O_{12}$. I artikel V studeras till sist gränsskiktet mellan elektrod och elektrolyt *operando* för två olika positiva elektrodmaterial, NMC och LCO.

Resultaten från *operando* mätningarna visar att denna metodik kan användas för att direkt mäta kemiska och elektrokemiska potentialskillnader mellan elektroden och elektrolyten i ett batteri. Mätningarna inkluderade i artikel V är första gången någonsin som ett litiumjonbatteri med flytande elektrolyt mäts på detta sätt. Resultaten i artikel III-V visar att *operando* fotoelektronspektroskopi har stor potential att ge en ökad förståelse för de elektrokemiska processer som sker i ett batteri, men illustrerar också flera medföljande mätsvårigheter. Många av dessa kan säkert övervinnas med fortsatt instrument- och metodutveckling, men det är också viktigt att komma ihåg att även när tekniken har mognat, så innebär närvaron av en vätska en stor skillnad mot *ex situ* mätningar i vakuum. Detta gör att teknikerna (*ex situ* och *operando*) har olika för- och nackdelar och kan användas för olika vetenskapliga frågeställningar. Enligt mig bör *operando* fotoelektron-spektroskopi därför ses som ett komplement till *ex situ*, snarare än en utveckling eller ersättning av den mer traditionella mätmetoden. Jag tror att båda dessa varianter av fotoelektronspektroskopi kommer vara till stor nytta i utvecklingen av morgondagens batterier, och hoppas att den som läser denna avhandling får en uppfattning om hur de båda kan användas.

1 Introduction

30 years ago, lithium ion batteries (LIBs) were introduced to the energy storage market by Sony Corporation [1-3]. Since then, the technology has revolutionized the marked for portable electronics, and has become a crucial part in the development of a more sustainable society [4, 5]. The importance of the LIB technology was highlighted in 2019, when the Nobel Prize in Chemistry was awarded to J. B. Goodenough, M. S. Whittingham and A. Yoshino for the development of "the world's most powerful battery" [6]. Today, a LIB probably power most of your wireless electric devices, such as mobile phones, laptops, cameras and electrical tools.

To further implement LIBs in e.g., electrical vehicles and for renewable energy storage, there is a need to improve both the energy density and the cycle life of today's battery materials [1, 7]. Thus, there is an ongoing search for new materials in which a large amount of lithium can be inserted and extracted reversibly. In order to make this search more efficient, there is a need to better understand the electrochemical reactions occurring in a LIB. In particular, it is of high interest to study the battery interfaces, as the majority of all reactions in a LIB occur at the interface between the electrode materials and the Li-ion containing electrolyte. This includes both the redox reactions responsible for the energy storage in the battery, and different side reactions that cause battery degradation.

Despite the large number of studies performed on LIBs, there are still fundamental questions remaining regarding the kinetics and mechanisms responsible for the formation of surface layers at the battery interfaces. To answer these questions, there is a need for experimental techniques that can probe the battery interfaces on an atomic level during cycling (*operando*). Due to the limited availability of surface sensitive *operando* techniques, and the complexity of the battery interfaces, the knowledge regarding these interfacial processes up until today remains scarce [8-10]. This thesis aims to target these challenges.

1.1 Scope of the thesis

The main purpose of the work performed in this thesis is to increase the understanding of the processes occurring at the interfaces in LIBs. In order to do this, LIB systems are investigated primarily by electrochemical methods and photoelectron spectroscopy (PES) studies. Electrochemical methods are used to understand the characteristics of the battery such as energy density, energy efficiency and cycle life, while PES is used to characterize the atomic and electronic structure of battery materials and interfaces. A major part of the work has been directed towards combining these two methods, by the development of a methodology to perform *operando* APPES measurements on solid/liquid interfaces in LIB systems. This development has involved both practical and theoretical aspects.

The implementation of these measurements on solid/liquid LIB interfaces put high demands on the experimental setup. Thus, practical aspects that has been considered include for example the design of a suitable electrochemical setup, developing the measurement procedure, and evaluating effects of synchrotron radiation on the liquid electrolyte. The theoretical work has been focused on how the *operando* APPES results can be interpreted and understood. In order to do this, it is not only necessary to understand the working principle of a LIB, but also to have an understanding of electrochemical and photoelectron spectroscopic processes in general. While the theory of both electrochemistry and PES already is rather well-known, the combination of the two is intricate and more rarely described. Thus, significant work has also been devoted to the understanding of how these two research fields can be combined, and how such combined theory can be used to further understand the interfacial processes occurring at the battery interfaces.

In the thesis experimental results on LIB interfaces are presented from both *ex situ* and *operando* spectroscopic studies. This research is presented in detail in the nine articles that constitutes the basis for this thesis. These articles can be divided into two main topics. Paper I-V focus on understanding the charge transfer reactions and the potential differences over the solid/liquid interface. In order to do this, the development of a methodology for *operando* APPES measurements on LIB system has been essential. In Paper VI-IX the focus is placed on understanding the chemical degradation reactions occurring at the LIB interfaces and how these can be prevented by different means to stabilize the interface. From the results a further understanding of the characteristics of the LIB interfaces can be gained, which is a necessity for the continuous development of today's LIB.

1.1.1 A note on the structure of this thesis

The work performed in this thesis concerns energy material physics. This is to a large extent an interdisciplinary subject, bridging towards chemistry and materials science. To understand the results, a solid background of two large research areas; photoelectron spectroscopy and electrochemistry, is necessary.

Thus, in an attempt to allow readers of different backgrounds to better follow the results, I have included a rather extensive background in Chapter 2-4. First, the principles governing the properties of a LIB is presented (Chapter 2), followed by what I tried to make a comprehensive summary of the necessary theoretical background for both electrochemistry (Chapter 3) and PES (Chapter 4). This background may be considered "textbook knowledge", which a reader in the respective field probably already is familiar with.

In Chapter 5 a connection between core concepts used in electrochemistry and PES is made, and some common sources of misunderstandings in between the fields are addressed. In this way Chapter 5 bridges to the results of this thesis, which are presented in Chapter 6 and 7. These two chapters are the core of the thesis work, but they may be difficult to comprehend without the knowledge presented in the previous chapters.

Thus, as someone who spent years working on the interpretation of the results in Chapter 6, I would urge you to read this chapter with curiosity (the first time), and possibly not expect to follow all my reasoning at once. However, my hope is that with this thesis in hand, the process of interpreting *operando* APPES spectra of LIB systems will be less confusing than it first was for me.

2 Li-ion batteries

In this chapter the components and general working principle of a LIB are presented. Further, it is explained how the chemistry of the battery materials is crucial for the properties of the LIB, such as the energy density and cycle life. There are a number of different requirements on LIBs, and a vast selection of possible materials with different advantages and disadvantages. A large number of books and reviews can be found on this topic [1, 3, 11, 12]. Here, the focus has been narrowed down to the materials used in this thesis.

2.1 LIB components

The functionality of a rechargeable battery, such as a LIB, builds upon the conversion between chemical and electrical energy by reversible redox reactions. In a LIB the redox reactions involve the movement of Li-ions and electrons. During charge, Li-ions and electrons are moved from the positive electrode[1] (higher reduction potential) to the negative electrode[2] (lower reduction potential). The charging process requires electrical energy, which is stored in the battery as chemical compounds with higher chemical potential compared to the pristine (or discharged) materials. During discharge the process is reversed, and the Li-ions and electrons spontaneously return to the positive electrode. The stored chemical energy can then be used to perform electrical work.

For a LIB to operate, several components are required. These are schematically illustrated in Figure 2.1. First and foremost, two electrodes are needed, the positive and the negative electrode. These contain the active materials (AMs) that are responsible for the energy storage in the battery. In order to transfer charged species (electrons and Li-ions) between the electrodes, other components are also necessary. For ion transport, the

[1] In the battery community often called cathode. However, according to the electrochemical definition the cathode is the electrode that is reduced, i.e., the positive electrode will only be the cathode during discharge. To avoid confusion, the term positive electrode will instead be used throughout this thesis.

[2] In the battery community often also called anode. However, according to the electrochemical definition the anode is the electrode that is oxidized, i.e., the negative electrode will only be the anode during discharge. To avoid confusion, the term negative electrode will instead be used throughout this thesis.

electrodes are connected by an electrolyte that is an ion conductor and an electronic insulator. Often the electrolyte is added to the battery cell by soaking a separator in the liquid electrolyte. The separator is placed in between the electrodes to prevent a short circuit. The separator is usually a thin porous membrane that is electrically insulating but ion permeable. In this way the separator prevents electron transport, but allows for transport of Li-ions.

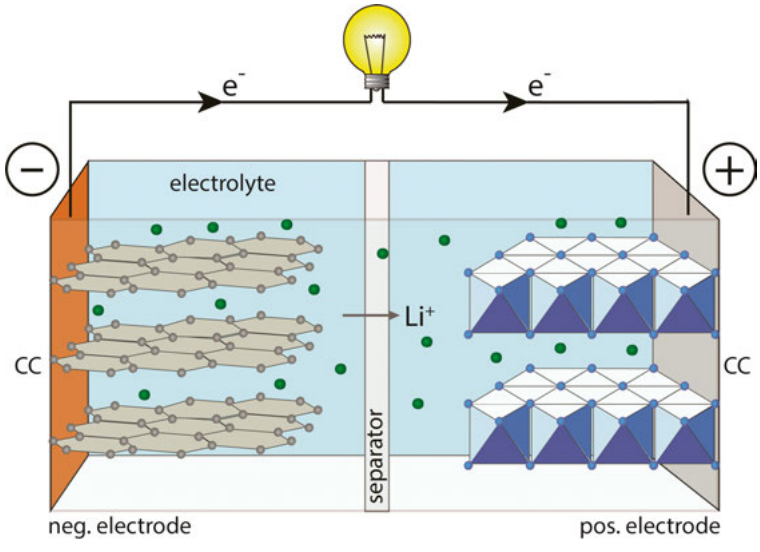

Figure 2.1: Illustration of the battery parts as well as the discharge process in a Li-ion battery.

The transfer of electrons between the electrodes occurs in an outer circuit, where the movement of electrons can be used to perform electrical work. This is achieved by contacting each electrode to a current collector (CC). The purpose of the CC is to conduct electrons, without interfering with the redox reactions occurring at the electrodes. Thus, metals that are inert at the voltages used for each electrode are typically chosen as CCs.

Finally, the battery components are also enclosed by a casing, to protect the components and to avoid contact with air (not shown in Figure 2.1). The battery design of a full cell or battery pack is outside the scope of this thesis, but it can be noted that this optimization is crucial for the energy density of the final commercial product [13, 14].

2.2 LIB properties

The great success of LIBs for portable electrical devices stems from their high energy density, compared to other battery chemistries such as nickel-metal hydride, nickel cadmium or lead-acid [15]. The high energy density of LIBs

can to a large extent be attributed to the properties of Li. Li is the most electropositive element (i.e., has the lowest reduction potential of all elements), and is thus an ideal choice for high-voltage batteries. Due to the small size and light weight of the Li-ion, it can also relatively easily be inserted into many different materials.

However, the energy density is not the only important factor for a battery. Ideally, a battery should also be quick to charge, have a long shelf and cycle life, be safe, environmentally friendly and preferably cheap. All together, these are heavy demands to put on a single battery, and fulfilling them all at once is not trivial. Depending on the application, certain properties may be particularly important, although a baseline needs to be surpassed in all areas. Several LIB chemistries are already commercially available and the functionality of the LIB has been proven. Thus, today's research efforts in particular focus on further improving energy density and cycle life [1, 3, 16].

The amount of energy that can be converted in a LIB depends on the (average) voltage of the battery, as well as the amount of charge that can be transferred. The voltage is determined by the difference in reduction potential between the positive and negative electrode. The reduction potential of an electrode is in turn determined by the electrochemical reaction(s) occurring at the electrode/electrolyte interface (see further Section 3.1). The amount of charge that can be stored in the battery depends on the number of Li-ions and electrons that can be reversibly transferred between the electrodes. This property is denoted the capacity and is often reported in mA h. For comparison between different materials or batteries, the specific capacity is also used. In this case the capacity is reported as gravimetric capacity (mA h g^{-1}) or volumetric capacity (mA h cm^{-3}).

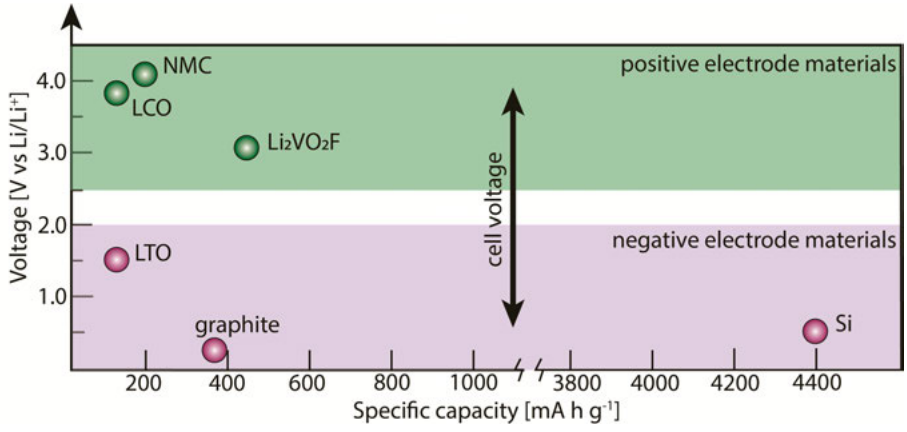

Figure 2.2: Redox potentials and gravimetric capacities for some common battery materials mentioned in this thesis

In Figure 2.2 redox potentials and specific capacities for LIB materials mentioned in this thesis (see Section 2.4) are shown. The variety of materials into which lithium can be inserted, gives several choices for negative electrode materials. However, finding chemically stable materials from which a lot of lithium can be taken out is more difficult. As a result, negative electrode materials with very high capacities can be found, but the capacities of positive electrode materials are more limited. Thus, the positive electrode material is usually the bottleneck for the overall capacity of the battery [17-19].

Unfortunately, maximizing the energy density is often linked to stability and safety issues, as highly reactive materials are packed together in a small volume to achieve this. High voltages can increase the risk for unwanted side reactions with subsequent capacity losses. Violent side reactions in a damaged or overcharged battery can also lead to short circuits, heat generation and in the worst case scenario even explosions [20-22]. Materials that have a large capacity are generally also more prone to material degradation, as a result of lattice strains caused by volume changes and/or exposure of new surfaces to the electrolyte as Li is inserted and removed [12, 23, 24].

The issues with safety and stability suggest that the question of finding "ideal" battery materials is more complex than only finding materials with high capacities. Thus, a more interesting parameter than the maximum (theoretical) energy density of a battery, is often the capacity retention or cycle life. In battery testing, the cycle life is commonly evaluated by testing how many cycles the battery can perform while maintaining >80 % of its initial capacity [25-27]. In order to find battery materials with both good cycling performance and high energy density, the key is often to understand and control the interfacial chemistry [8-10, 24, 28].

2.3 Interphases in LIBs

As most reactions in a LIB are heterogeneous (i.e., occurring at the electrode/electrolyte interfaces) gaining an understanding of the interfacial properties and processes is highly important to improve the overall battery performance.

In an ideal LIB, the chemical redox reactions are (thermodynamically) reversible and no side reactions occur. In this scenario, both the cell voltage and the capacity would be constant and equal during charge and discharge. A battery like this would be possible to use for an infinite amount of cycles with an unchanged capacity. In reality, such an ideal battery does not exist. Instead, the large voltage range and reactive materials of high energy density materials are inevitably linked to a number of possible side reactions, including electrolyte degradation of both solvent and salt, oxygen loss from the lattice structure, TM dissolution etc. [29-32]. In particular, most liquid electrolytes are not stable at the reduction and oxidation potentials used in LIBs (especially

for high-voltage LIBs). This is illustrated in Figure 2.3, where electrolyte degradation leads to formation of two interphase layers. In this case, preventing any side reactions at all from happening would require the use of another electrolyte. However, often it is sufficient to make sure that the side reactions are self-limiting, and only occurs during the first (few) battery cycle(s). This can be achieved by the formation of passivating interphase layers.

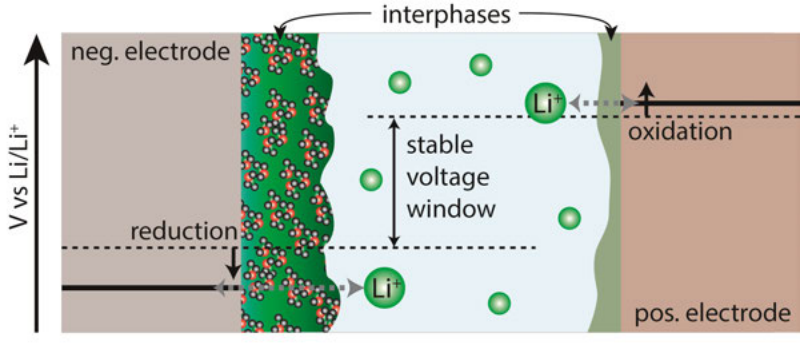

Figure 2.3: Schematic illustration of lithium insertion/extraction potentials as well as the electrolyte stability window. The black lines (representing the redox potential) of the positive and negative electrode are outside the stability window of the electrolyte, resulting in a reduction/oxidation at the electrode interfaces.

2.3.1 Interphase formation

The degradation products formed from the side reactions in a LIB can either be dissolved in the electrolyte, or stay at the electrode surface where they build up an electrode/electrolyte interphase. The interphase layers often contain a mix of organic and inorganic compounds, and vary in thickness, flexibility and ionic conductivity depending on the chemistry of the battery materials. The properties of the interphase layer are of utmost importance for the long-term battery performance [9, 10, 33-35].

Especially on negative electrodes interphase layers are often observed, as most AMs have a reduction potential well below the reduction potential of most common electrolytes. This gives a relatively thicker interphase (compared to the positive electrode side), made up from solvent reduction products as well as inorganic material stemming from salt degradation. On the negative electrode the interphase layer is often referred to as the solid electrolyte interphase (SEI).

On positive electrodes the interphase layers are usually less prominent, since the operating voltages for these often are close to or within the stability window of the electrolyte. Additionally, the lithium transition metal oxides typically used as positive electrodes have a rather stable structure, with strong covalent bonds and a native surface film, making them less susceptible to

degradation reactions with the electrolyte [28, 36]. For these reasons, a smaller number of studies have been performed on the positive electrode interphase. However, during recent years the importance of also these interphases has been recognized, especially for high-voltage materials [37-40]. The nomenclature of this interphase is less consistent, and terms such as the "solid permeable interface" (SPI) [37, 41, 42] or the "cathode electrolyte interphase" (CEI) [43, 44] have been used. In this thesis the term interphase layer is used to refer to the interphase both at the positive and negative electrode.

The ability to form a beneficial surface layer is one of the most important factors when choosing the electrolyte for a LIB. An ideal interphase layer should be (Li-)ion permeable, electronically insulating, mechanically stable, and chemically stable. It should also be limited in thickness, as the available battery capacity is consumed during its formation. A stable interphase should have a good adhesion to the electrode, not dissolve in the electrolyte, and be flexible enough to accommodate for any volume changes of the electrode. In addition, the formed degradation products should be chemically inert towards both the electrode and the electrolyte [9, 28, 35]. If the interphase layer on the other hand is unstable or only cover part of the electrode the side reactions can continue, until the battery eventually no longer is operational.

2.3.2 Characterization of LIB interphases

The importance of battery interphases can be recognized by the numerous studies performed within the area. Especially for the SEI layer there are several reviews on the topic [8-10, 28, 34, 35]. Also, the interfaces of positive electrode materials have been investigated in for example references [8, 36, 37, 45, 46]. Different methods used for characterization of the electrode/electrolyte interfaces range from imaging techniques such as SEM and TEM, to various spectroscopy methods, diffraction and electrochemical measurements [47]. The diverse methods give complementary information about the interphase properties such as structure, composition, functional groups and resistivity.

The current knowledge about interphase layers in LIBs to a large extent stem from ex situ experiments and/or from measurements only including the solid electrode. In these cases, only a static picture of the interphase can be gained, and the measurement environment will not accurately represent the real battery environment. To further understand the interphase layers, there is a need for methods where the interphase formation can be studied during cycling, i.e., for *operando* measurement under realistic conditions. Several techniques that previously have been used for *ex situ* material characterization are currently being developed to allow for this type of measurements [47]. This thesis contributes to this work by the development of a methodology for performing *operando* APPES on solid/liquid interfaces in LIBs (Chapter 6).

2.4 Materials used in LIBs

Today's state-of-the-art LIBs typically comprises a graphite based negative electrode, a layered lithium transition metal oxide positive electrode, and a carbonate based electrolyte containing a lithium salt [1, 3, 7, 12, 48, 49]. These materials have been thoroughly studied and the composition of the electrodes and electrolyte have been optimized to achieve a good cycling performance (~1 000 cycles).

The energy density of these cells are limited by the capacity of the positive electrode, which is ~150-200 mA h g^{-1} [50-52]. This is only around half of the theoretical capacity of a graphite negative electrode (372 mA h g^{-1}) [53], and thus there is a need to find positive electrode materials with higher capacities to most effectively increase the overall capacity of the battery. To increase the capacity, so-called Li-rich materials are of high interest, where more than one Li can be removed per transition metal (TM).

In this thesis a novel high capacity material, Li_2VO_2F, is investigated. For the *operando* APPES measurements, a number of model systems and common LIB materials are also investigated. The general properties of the materials studied in this thesis are discussed below.

2.4.1 Negative electrode materials

Depending on their lithiation mechanism, negative electrode materials can be divided into three categories; insertion/intercalation materials, conversion materials and alloying materials [11, 15, 54]. In this thesis one material of each category is investigated by *operando* APPES. A gold and a copper electrode/electrolyte interface are investigated as model systems of an alloying anode and a conversion anode, respectively (Paper III). As an intercalation material $Li_4Ti_5O_{12}$ (LTO) is chosen, due to its very flat lithiation potential characteristic of a first order phase transition reaction (Paper IV).

2.4.1.1 Intercalation materials

In an intercalation material the Li-ions are stored in vacant sites in the lattice structure of the material. This often leads to a relatively low volume expansion and a highly reversible cycling. The amount of Li that can be stored depends on the size and number of vacant sites in the lattice structure, but as Li is incorporated within the host structure, intercalation materials often have rather limited theoretical capacities.

In this thesis the intercalation material LTO is studied [55]. During lithiation LTO undergo a first order phase transition from spinel $Li_4Ti_5O_{12}$ to rock salt $Li_7Ti_5O_{12}$ at 1.55 V vs. Li/Li^+ according to [56, 57]:

$$Li_4Ti_5O_{12} + 3Li^+ + 3e^- \leftrightarrow Li_7Ti_5O_{12}. \quad (2.1)$$

The insertion of 3 Li into the original spinel phase results in a partial reduction of Ti from Ti^{4+} to Ti^{3+} and gives a theoretical capacity of 175 mA h g^{-1}. During the electrochemical lithiation Li is inserted into empty octahedral sites, giving a minimal volume expansion of only ~0.2 %. The relatively high reduction potential can also effectively limit side reactions at the negative electrode. Together these properties make LTO a relatively safe negative electrode material (compared to e.g., graphite) with a very long cycle life (~10 000 cycles) [58]. By synthesizing the material with nano-sized particles, LTO also shows great power performance and is suitable for fast charging [59]. However, the lower theoretical capacity and higher voltage as compared to graphite, gives a significantly lower energy density.

The energy density of LTO can be increased by further lithiation of the rock salt phase $Li_7Ti_5O_{12}$ towards $Li_9Ti_5O_{12}$. Previous studies have shown that this reaction can occur at potentials below 1 V vs. Li/Li^+, where the maximum of the second reduction peak has been seen around 0.7 V vs. Li/Li^+ [60, 61]. By charging to ~0 V vs. Li/Li^+ reversible capacities of up to ~230 mA h g^{-1} have been observed [60]. In this case, reduction of the electrolyte cannot generally be avoided due to the low voltages used [28, 62-64].

2.4.1.2 Alloying and conversion materials

Alloying and conversion materials can give significantly higher energy densities compared to intercalation materials. For alloying materials, the theoretical capacity depends on the solubility of Li in the original phase. One of the most investigated alloying materials is silicon, with a very appealing theoretical capacity of 4 200 mA h g^{-1}, resulting from the formation of the alloy $Li_{4.4}Si$ [65-67].

For conversion materials the theoretical capacity is determined by the general conversion-displacement reaction:

$$MO + 2Li^+ + 2e^- \leftrightarrow M + Li_2O, \qquad (2.2)$$

where M is a transition metal, such as Co, Ni, Cu or Fe among others [68-70]. The conversion reaction begins with an amorphization of the lattice, and thereafter metal nanoparticles are formed. Conversion electrodes can deliver gravimetric capacities of over 500 mA h g^{-1} [69]. However, both alloying and conversion materials typically show large volume changes during cycling, leading to stability issues and poor cycling performance [65, 67, 71].

In this thesis the lithiation of Au and Cu is studied by *operando* APPES. The use of pure metal/metal oxides serves as an easier model system of a "real" LIB electrode, which are often composites. Au undergoes an alloying reaction with lithium around and below 0.2 V vs Li/Li^+ according to [72]:

$$Au + x\ Li^+ + x\ e^- \leftrightarrow Li_xAu, \qquad (2.3)$$

where the maximum amount x of Li that can be alloyed with Au corresponds to approximately 3 Li per Au. During the lithiation of Au two main plateaus can be seen in the voltage curve. The first one, located around 0.16 V vs Li/Li^+, correspond to Li_xAu, where $x \leq 1$. A second plateau corresponding to a Li content of $x \leq 2.5$ is seen around 0.06 V vs Li/Li^+. During delithiation a total of three plateaus can be distinguished, corresponding to three different delithiated Li_xAu phases.

For the Cu electrode the conversion reaction with Li of the native copper oxides is studied. Conversion from Cu oxides to Li_2O occur according to [73]:

$$Cu_2O + 2\,Li^+ + 2\,e^- \leftrightarrow 2\,Cu + Li_2O, \tag{2.4}$$

and

$$CuO + 2\,Li^+ + 2\,e^- \leftrightarrow Cu + Li_2O. \tag{2.5}$$

The reduction of Cu^{2+} to Cu and Cu^+ to Cu occurs around 2.1 V and 1.4 V vs. Li/Li^+, respectively. However, the voltage is highly dependent on the particle size, and a large polarization is often seen [74]. The theoretical capacity is 674 mA h g^{-1} for CuO and 375 mA h g^{-1} for the heavier Cu_2O. Upon re-oxidization of Cu, it seems mainly Cu_2O is formed [73]. In this regard similar capacities are seen for both CuO and Cu_2O after the first (formation) cycle. High experimental capacities have been measured for both oxides, often even higher than the theoretical capacities due to side reactions and/or a contribution from electrical double layer charging [74-76].

2.4.2 Positive electrode materials

The choice of material for the positive electrode in commercial LIBs is almost exclusively a lithium transition metal oxide [17, 52]. The TM used is typically cobalt, nickel, manganese, or a combination thereof. The general half-cell reaction for these materials can be written:

$$LiMO_2 \leftrightarrow Li^+ + e^- + MO_2, \tag{2.6}$$

where M indicates the TM. The structure of these materials is typically either layered or spinel, with Li incorporated in between layers or channels of MO_6-octahedra. These structures as well as the rock-salt structure mentioned below are illustrated in Figure 2.4.

If all the Li is taken out from these structures, this often give an unstable structure that can cause material breakdown and capacity loss [77-80]. If the material structure is severely changed, it might not be possible to re-insert the extracted Li. The practical capacity of these positive electrode material must therefore be based on how much Li that can be reversibly cycled. Often the

practical capacity is significantly lower than the theoretical capacity (based on removing all lithium from the material).

In this thesis two layered transition metal oxides; lithium cobalt oxide ($LiCoO_2$, LCO) and lithium nickel manganese cobalt oxide ($LiNi_xMn_yCo_{1-x-y}O_2$, NMC), are investigated. In addition, a newly developed Li-rich disordered rock-salt (DRS) material, Li_2VO_2F, is investigated as a possible high capacity positive electrode material.

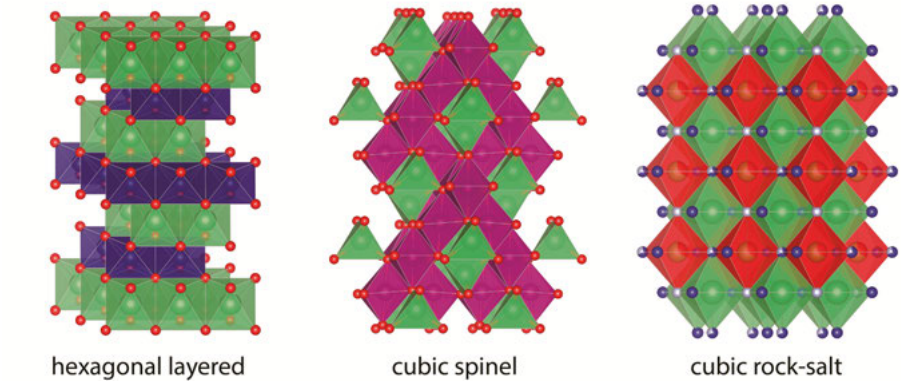

Figure 2.4: Material structure of three different types of positive electrode materials.

2.4.2.1 Layered lithium transition metal oxides

LCO and NMC have the same layered hexagonal structure, where Li is located in layers between MO_6-octahedra (see Figure 2.4). The presence of positively charged Li, stabilizes the structure by screening the negatively charged O.

Upon removal of Li, LCO undergoes a number of phase transitions [50, 77, 81]. Initially, an insulator-metal transition occurs in the range of ~75-95 % Li [82]. Around 50 % remaining Li, at a voltage of 4.2 V vs. Li/Li^+, LCO undergoes a transition to an ordered structure [81, 83]. Both these are second order phase transitions. Upon further delithiation (charging up to 4.5 V) the stacking of the Co-O layers changes, which severely stresses the material structure and lowers the Li diffusivity. Because of the instability of the fully delithiated structure, the cycling of LCO is often limited to the removal of 0.5 Li per TM, corresponding to a practical capacity of ~140 mA h g^{-1}. Significant efforts have been put into stabilizing the material towards further delithiation by the use of e.g., doping and surface modifications [84].

The properties of the layered lithium transition metal oxides can be improved by using a mixture of different TMs. One of the most successful materials is NMC, where Ni, Mn and Co are mixed to gain the beneficial properties of each element [85]. In NMC, delithiation is first coupled to an oxidation of Ni from Ni^{2+} to Ni^{4+}, followed by an oxidation of Co^{3+} to Co^{4+} at higher voltages [86, 87]. Mn is believed to be redox inactive in the Mn^{4+} state [88], but improves the stability of the crystal structure. Depending on

application, the ratio between the different TMs can be altered. NMC electrodes can deliver practical capacities up to around 200 mA h g^{-1}, and are also more stable, safe and conductive compared to the pure TM oxides. However, despite these improvements the capacity is still significantly lower compared to the capacity of graphite.

To improve the energy density of the current positive electrode materials further, one searches for Li-rich materials that can incorporate more than one Li per TM. This can be achieved by substituting some of the Ni/Mn/Co in the layered structure for Li. In this way the capacity can be increased to ~300 mA h g^{-1}, at a high average voltage of 3.7 V vs. Li/Li^+. However, to commercialize these materials the cycling stability needs to be improved [89-92].

2.4.2.2 Li-rich disordered rock-salt materials

Due to the limited Li diffusion in ordered rock-salt structures, materials exhibiting this structure were for a long time not considered for use in LIBs. However, when starting to explore Li-rich materials, it was found that a percolating network for Li diffusion was created in DRS structures where Li and TMs are randomly distributed on the cation site [93, 94]. This discovery opened up for a large variety of new possible positive electrode materials that theoretically can cycle more than one Li per TM.

Li-rich DRS materials are now of high interest for LIB applications due to their high theoretical capacities, without phase transitions or large volume expansion [93-96]. In order to access the full theoretical capacity, either a multi-electron redox couple or a reversible anionic redox activity is necessary [80, 97, 98]. In this respect, Li_2VO_2F is an attractive material since the V^{3+}/V^{5+} redox couple that can be used to fully compensate for the extraction of two Li. This can be compared to the corresponding oxide Li_2VO_3, in which V is in the 4+ oxidation state in the pristine material. In this case only one Li can be compensated by the oxidation of V, and further Li removal must be compensated by oxidation of O. Li_2VO_2F has an attractive theoretical capacity of 462 mA h g^{-1} according to the (de)lithiation reaction [99, 100]:

$$Li_2VO_2F \leftrightarrow 2Li^+ + 2e^- + VO_2F. \qquad (2.7)$$

Experimentally, a maximum capacity of ~400 mA h g^{-1} has been measured during cycling at low C-rates. However, the long-term cycling performance of Li_2VO_2F is unsatisfactory with rapid capacity fading and increased polarization upon cycling. This behavior has also been seen for other Li-rich materials, and is suggested to be linked to a loss of oxygen as a result of anionic redox activity [80, 101-103]. In this thesis the mechanisms behind the material degradation of Li_2VO_2F is investigated (Chapter 7).

2.4.3 Electrolytes

The electrolyte's function in the battery is to transport ions between the electrodes. In order to do so, the electrolyte should have a high ionic conductivity, determined by the viscosity and dielectric constant of the solvent [28, 63]. Additionally, for the long-term battery performance the electrolyte should have a low volatility and good cycling stability. In order to function well in high-voltage batteries, the electrolyte either needs to have a sufficient voltage stability window, or be able to operate outside its stability window by forming a well-functioning interphase layer [8, 28, 35, 36, 40, 63].

The most commonly used electrolytes for lithium batteries are liquid electrolytes consisting of an organic solvent and a soluble lithium salt [28, 63, 64, 104, 105]. These electrolytes have a very good ionic conductivity, but are not stable at the low voltages required to lithiate graphite electrodes. Thus, their use is dependent on the formation of a passivating interphase layer [8, 106]. Liquid electrolytes are often also volatile and flammable, which can cause safety issues [15, 63, 104, 105]. To improve safety, fire-retardant additives can be used. It is also common to add small amounts of electrolyte additives to further tune the composition of the interphase layers [39, 107, 108]. Electrolyte additives are further discussed in Chapter 7.

A safer and more stable option for high-voltage LIBs (>5 V) is offered by the use of solid electrolytes [109, 110] or ionic liquids [111, 112]. These electrolytes provide new possibilities in terms of stability, safety and battery design. However, the ionic conductivity at room temperature is poor, and needs to be improved to be a viable replacement for liquid electrolytes.

In this thesis only liquid electrolytes are studied. The solvents used include ethylene carbonate (EC), dimethyl carbonate (DMC), propylene carbonate (PC) or a mixture of these. The main electrolyte salts used are lithium hexafluorophosphate ($LiPF_6$), lithium bis(trifluoromethanesulfonyl)imide (LiTFSI) and lithium perchlorate ($LiClO_4$). $LiPF_6$ is the most commonly used salt for LIBs. However, degradation of the PF_6-anion can cause HF formation upon reaction with trace amounts of water [113, 114]. Due to the reactivity of the PF_6-anion it can sometimes be preferable to use other salts, in particular if there is a risk for gas release as HF is highly toxic.

2.5 Sample preparation

Several different LIB materials have been investigated by electrochemistry and photoelectron spectroscopy in this thesis. Some of the battery electrodes have been prepared in the home lab at Ångström Advanced Battery center (ÅABC), while other electrodes have been prepared in collaboration with other universities (Karlsruhe Institute of Technology, Helmholtz Institute Ulm, French Alternative Energies and Atomic Energy Commission). Details

on sample preparation for each study can be found in the experimental section of the papers included in this thesis. For all studies it has been important to ensure that the studied sample surfaces are not significantly altered by the sample preparation or measurement method.

For the studies of solid/liquid interfaces with *operando* APPES the main challenge in terms of sample preparation is to design an electrochemical cell setup that functions as a regular battery, while the liquid phase should be thin enough to see through with APPES (further discussed in Section 6.2). To limit the liquid absorption of the electrode, thin film samples containing only the active material prepared were used for some of the *operando* APPES measurements. These films were prepared by sputter deposition in collaboration with Karlsruhe Institute of Technology.

For *ex situ* samples measured in ultra-high vacuum (UHV), only the solid parts of the interphase can be studied. For these studies the samples are electrochemically cycled prior to the PES measurements. In this case several batteries are cycled and stopped at different state-of-charge and/or after a different number of cycles for comparison. When dismounting the battery cells to prepare samples for PES measurements, it is important that the interphase remains (largely) unaffected. Therefore, the electrode to be studied is extracted and gently rinsed with DMC to remove salt residues and excess solvent from the electrode. Previous studies have shown that the washing can alter the SEI composition slightly by removing solvable components [115-117], but overall the changes are not significant for short washing times [118]. To avoid further chemical reactions, the samples are handled in an argon filled glovebox during preparation, and stored in an argon/vacuum environment during transport.

3 Electrochemical systems

In this chapter some basic concepts and principles of electrochemical systems are outlined. Current models and descriptions of the solid/liquid interface is presented, as well as the electrochemical characterization techniques used in this thesis. A more rigorous description of the different terms, concepts and methods described here can be found in electrochemistry textbooks [119-121].

3.1 Principles of electrochemistry

The field of electrochemistry concerns the relation between chemical and electrical effects, i.e., the study of chemical reactions where electrons are transferred from one species to another. Electrochemistry incorporates many different processes, including corrosion, electroplating, electrosynthesis, and – as in the subject of this thesis – electrical energy storage. Although the general principles of electrochemistry can be applied to any electrochemical system, the focus here is on the necessary fundamental concepts and definitions needed to understand the properties of the electrode/electrolyte interfaces in a battery.

3.1.1 The electrochemical cell

A simple electrochemical cell consists of two electrodes. The electrode where oxidation occurs is called the anode, and the electrode where reduction occurs is called the cathode. If the chemical reaction is spontaneous (e.g., discharge of a battery) the cell is called a Galvanic cell, and if the chemical reaction is driven by electrical energy (e.g., charging of a battery) the cell is called an electrolytic cell.

The definition of the term electrode in electrochemistry refers to the electric conductor in contact with an ionic conductor, i.e., the whole interface [121, 122]. However, in this thesis the term electrode will be used according to the more technical definition, where the electrode only refers to the electronic conductor. The term half-cell or electrode/electrolyte interface will instead be used to refer to the whole interface.

The electronic conductor (electrode) is often a solid metal or semiconductor (or a composite). The electrolyte is typically a liquid solution with ions, although also ionic liquids and solid electrolytes are used. Since the electrolyte

is an electronic insulator, transport of electrons between the electrodes in the cell can only occur through an outer circuit. Ions can on the other hand move from electrode to electrode through the electrolyte.

When electrochemical methods are employed to study chemical reactions occurring at a single electrode, a three-electrode setup is often used. A simple setup is illustrated in Figure 3.1. The electrode under study is called the working (or indicator) electrode (WE). The voltage of the WE is measured against a reference electrode (RE). The third electrode is called the counter (or auxiliary) electrode (CE). This electrode is used to draw a current through the cell. The voltage and current can be controlled and/or measured by a potentiostat.

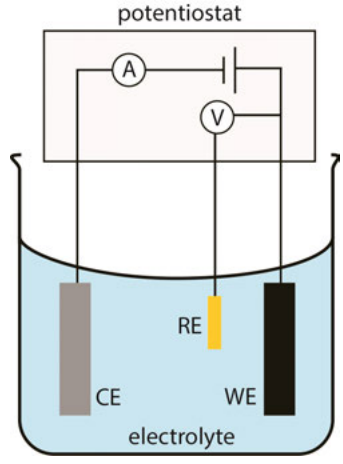

Figure 3.1: Simple illustration of a three-electrode cell. A current flow between the WE and CE, while the WE voltage is measured versus a RE.

3.1.2 Potentials in electrochemistry

A "potential" is a measure of the capacity of a system to perform work, or in other words, its ability to convert energy from potential energy to e.g., kinetic energy or electrical energy. In electrochemistry, the ability of a system to perform work is measured by the *electrochemical potential* $\bar{\mu}$, and the work is performed by converting chemical (potential) energy to electrical energy.

The electrochemical potential of a species i in a phase α ($\bar{\mu}_i^{\alpha}$) is defined as the energy needed to bring the species i from a reference state (usually vacuum at infinity) and add it to the phase α [119, 123]. The species can be an electron or an ion, and the phase can be an electrode or an electrolyte. If possible, a species will spontaneously move from a phase with higher $\bar{\mu}_i$ to a phase with lower $\bar{\mu}_i$. At thermodynamic equilibrium, $\bar{\mu}$ of all species is equal in all phases, and no net movement of species occurs [119, 123].

Conceptually, $\bar{\mu}_i^{\alpha}$ can be divided into one contribution from the chemical potential, and one contribution from the electrostatic potential according to:

$$\bar{\mu}_i^\alpha = \mu_i^\alpha + z_i F \phi^\alpha, \tag{3.1}$$

where μ_i^α is the chemical potential of species i in phase α, z_i is the signed charge number of i (e.g., +1, -1), F is the Faraday constant and ϕ the electrostatic potential of the phase. In this case the unit of $\bar{\mu}_i^\alpha$ and μ_i^α is given in J/mol. This unit is commonly used in chemistry and thermodynamics. However, when electrochemistry is combined with PES it is more convenient to use the unit electronvolts (eV), which simplifies the connection between electrochemical potentials and electron energies measured by PES, as will be discussed in detail in Chapter 5. In this case the corresponding form of Eq. (3.1) becomes

$$\bar{\mu}_i^\alpha = \mu_i^\alpha + z_i \phi^\alpha. \tag{3.2}$$

Throughout this thesis the electrochemical potential will be described by Eq. (3.2), and $\bar{\mu}_i^\alpha$ and μ_i^α will always be referred to in eV.

Even though both contributions to the electrochemical potential stem from Coulomb forces, the difference in length scale makes the separation introduced in Eq. (3.2) useful. In this way, the chemical potential μ represents the contribution to the electron energy stemming from the local chemical environment, while the electrostatic potential ϕ only includes long-range forces equivalent to applying an external electric field to a phase. Thus, μ is a property characteristic of the chemical composition, while ϕ is independent of the chemical properties and affect all species with the same charge in the same way.

The chemical potential is defined as the derivative of the Gibbs free energy with respect to the number of particles n_j at constant temperature T, constant pressure P, and constant concentration of all other species $n_{j\neq i}$:

$$\mu_i^\alpha = \left(\frac{\partial G_{int}}{\partial n_i}\right)_{T,P,n_{j\neq i}}, \tag{3.3}$$

where G_{int} is the Gibbs *chemical* free energy, excluding contributions from long-range electrostatic effects [119]. Since μ_i^α depends on the temperature, pressure and activity of the species i, a standard state is defined for T=25°C, P=1 atm and a_i=1. Standard state conditions are often indicated by the superscript 0. At non-standard conditions μ_i^α can be referenced to the standard state according to:

$$\mu_i^\alpha = \mu_i^{0,\alpha} + RT \ln a_i^\alpha, \tag{3.4}$$

where R is the gas constant, T the temperature and the activity a_i is defined as $a_i = \gamma_i c_i$, where γ_i is the activity coefficient and c_i the concentration.

3.1.3 Cell voltage and Gibbs free energy

The voltage of an electrode (vs. a RE) is defined as the energy required to move a unit *positive* charge to the electrode from a (arbitrary) reference. This measurement can be carried out with a common voltmeter, which measures the flow of electrons, driven by a difference in electron electrochemical potential [124]. Because of the sign convention, the measured electrode voltage (or electrode potential[3]) equals the negative of the electron electrochemical potential of the electrode:

$$E_{WE} = -\bar{\mu}_e^{WE}, \tag{3.5}$$

where E is the electrode voltage versus an arbitrary reference, $\bar{\mu}_e$ the electron electrochemical potential versus the same arbitrary reference, and WE refers to the working electrode.

Practically, a voltmeter cannot measure the absolute voltage of a single electrode, but only the voltage difference between two electrodes. The voltage difference between the positive and negative electrode in an electrochemical cell (e.g., a battery) is called the cell voltage (or cell potential[3]) and is equal to the negative of the electron electrochemical potential difference:

$$E_{cell} = -(\bar{\mu}_e^{\mathrm{pos}} - \bar{\mu}_e^{\mathrm{neg}}). \tag{3.6}$$

From these definitions it follows that the voltage is a measurement of the increase or decrease in the free energy of the electron as it moves from one electrode to the other. The total energy (work) that can be converted in the electrical cell is thus equal to the cell voltage multiplied with the total charge (q_{tot}) of the electrons that can be transferred [119]:

$$W = q_{tot} * E_{cell}. \tag{3.7}$$

In thermodynamics, the total energy that can be converted in a chemical reaction is denoted by the change in Gibbs free energy, ΔG. If no external electric fields are present, the Gibbs free energy (G) is determined only by the chemical potential and $G = G_{int}$, (see Eq. (3.3)). G_{int} should not be confused with $\bar{G}$, the Gibbs *electrochemical* free energy, where also contributions from electrostatic potentials are included [122]. In thermodynamics, common practice is to simply use G as the Gibbs free energy, and it is often not specified if this refers to the chemical or electrochemical Gibbs free energy.

To understand this, it is necessary to recall that thermodynamic relations (strictly) only can be applied to systems at thermodynamic equilibrium. If a

[3] In literature, "electrode potential" and "cell potential" is commonly used. However, using the term "potential" without specifying the species, phase and type of potential can cause misinterpretations. Throughout this thesis "electrode voltage" and "cell voltage" is used instead, to specify that this refers to an electron electrochemical potential difference.

reaction is at thermodynamic equilibrium, an infinitesimal change in the direction of a driving force (e.g., a current) will reverse the direction of the process (e.g., the chemical reaction) [119]. This can only be the case if the driving force for the process already is infinitesimal, i.e., the system is essentially always at equilibrium. Traversing such a reaction would take an infinite amount of time, and hence strict thermodynamic equilibrium is rarely achieved in practice.

For the purpose of studying electrochemical systems, one may instead consider a practical equilibrium [119]. A process that proceeds in such a way that thermodynamic equations can be applied to a desired accuracy, can be considered to be at practical equilibrium. In order for a chemical reaction to be practically reversible, the reaction (naturally) has to be chemically reversible. In addition, the applied perturbation needs to be sufficiently small, so that the time to re-establish equilibrium is minor compared to the timescale of the measurement. From this condition it follows that the practical reversibility of a reaction not only depends on the chemical reaction, but also on the measurement conditions. This is important for the assumptions that can be made for the electrochemical cell, which will be further discussed in the context of *operando* APPES measurements in Chapter 6.

For an electrochemical reaction to be thermodynamically reversible, the voltage during the reaction has to be constant. If the voltage is constant, the electrostatic potential of the electrodes does not change and no electrical work is performed. From this it follows that $\Delta G = \Delta G_{int} = \Delta \bar{G}$. Thus, for a thermodynamically reversible reaction, the energy available for conversion only depends on the chemical potential of the products and reactants. Under these conditions one can write the common relation [119, 122]:

$$|\Delta G| = nF|E_{cell}|, \tag{3.8}$$

where n is the number of moles of electrons and F is Faraday's constant.

The thermodynamic quantity ΔG (J/mol) is associated with a sign. A negative sign signifies that energy is released from the system, and a positive sign that energy is gained by the system. The measured cell voltage is on the other hand independent of the direction of the reaction. To accommodate for this discrepancy, the construct "electromotive force" (EMF) is used.

The EMF (E_{rxn}) of an electrochemical cell is assigned to the cell reaction and equals the negative of the difference in $\bar{\mu}_e$ between the cathode and anode:

$$E_{rxn} = -(\bar{\mu}_e^{cathode} - \bar{\mu}_e^{anode}). \tag{3.9}$$

When the direction of the reaction is reversed, the electrode that was cathode becomes the anode (and vice versa), and the sign of the EMF changes. By convention, the EMF has a positive sign when the reaction is spontaneous [119]. By using the concept of EMF one can write:

$$\Delta G = -nFE_{rxn}, \tag{3.10}$$

Similarly, for standard conditions Eq. (3.10) becomes:

$$\Delta G^0 = -nFE^0_{rxn}. \tag{3.11}$$

Now, by using the relation [119, 122]:

$$\Delta G = \Delta G^0 + RT \ln Q, \tag{3.12}$$

where Q is the reaction quotient (determined from the activities of the species in the reaction), one arrives at the Nernst equation:

$$E_{rxn} = E^0_{rxn} + \frac{RT}{nF} \ln Q. \tag{3.13}$$

The Nernst equation relates the EMF of the reaction to the activities of the electroactive species. This relation is highly useful to derive thermodynamic quantities from electrochemical measurements, and likewise to predict electrochemical behavior from thermodynamic data. However, whenever thermodynamics are considered together with electrochemistry, it is important to remember that **thermodynamic relations only apply during (practical) thermodynamic equilibrium**. Electrochemical measurements can on the other hand be (and often are) carried out on systems at non-equilibrium.

3.1.4 Half-cell reactions and electrode potentials

The absolute voltage (in this thesis defined as the voltage versus a point in vacuum at infinity) of an electrode cannot be measured by electrochemical methods. However, since the chemical reactions between two phases depend on the voltage *difference*, there is often no need to determine absolute voltages for electrochemical purposes. Rather, one is interested in relative voltages of different electrodes or redox reactions. To compare voltages of different electrodes, a standard RE is often applied in electrochemical measurements. Any electrode with a known electrode voltage that remains fixed during the measurements can be used as a RE. This can be achieved for any electrode where a reversible redox reaction occurs at a sufficiently low rate so that the activities of the participating species remain constant (see Eq. (3.13)).

The primary reference used in electrochemical literature is the standard hydrogen electrode (SHE) [119-121]. The SHE consists of a platinum electrode in a 1 atm H_2 gas atmosphere, immersed in a solution containing 1.0 M H^+. The platinum electrode does not participate in the reaction, but is used as an electrode conductor and a catalyst. The voltage of the SHE is governed by the half-cell reaction occurring at the Pt surface:

$$2H^+ + 2e^- \leftrightarrow H_2. \quad (3.14)$$

The voltage of the SHE at standard conditions has been arbitrarily chosen to 0 V (on the SHE scale) [119-121]. Similarly, the reduction potential of the half-cell reaction (also called half-reaction EMF) where hydrogen ions are reduced to hydrogen gas is also set to 0 V. In this way, the standard electrode voltage (E^0) of any other electrode can be determined versus the SHE.

E^0 is determined by the redox couple O^+/R present at the electrode. In accordance with the definition of the EMF for the cell reaction, E^0 is equal to the EMF of the half-reaction where an oxidized species O^+ is reduced to R. The EMF of the reversed half-reaction (R is oxidized to O^+) has the same magnitude, but opposite sign. Tabulated values for the reduction potential of various redox couples at standard conditions can be found in electrochemical literature [125, 126] and in chemical handbooks [127].

In a practical measurement, it might be more convenient to use another RE than the SHE. The reference of choice often depends on the chemistry of the system. A common choice for water-based systems is the Ag/AgCl reference, and for studies of LIBs a Li/Li^+ reference is most often used. Thus, when reporting electrode voltages, one always need to specify versus what RE the voltage is measured. For a Li/Li^+ reference, voltages would be reported as "V vs. Li/Li^+". This is the standard in this thesis, unless otherwise indicated. Since the standard reduction potential (vs. SHE) of both the Ag^+/Ag and Li^+/Li redox couples are known, voltages measured versus these electrodes can be converted to voltages vs. SHE as needed.

Since it is possible to measure the voltage of any electrode versus the SHE, it would be enough to determine the absolute voltage of the SHE to calculate the absolute voltage of any other electrode. An absolute voltage scale would be of interest to connect electrochemical measurements to spectroscopic measurements of Fermi levels or work functions [128-130]. Numerous calculations and experiments have been performed to estimate the absolute voltage of the SHE, but due to different assumptions and uncertainties there is no general agreement on an exact value [131, 132]. Depending on how the "absolute" voltage is defined, values between 4–4.5 V have been suggested for the SHE.

3.2 Solid/liquid interfaces

In electrochemistry, one is often interested in the charge transfer and reactions occurring at the solid/liquid interfaces. The kinetics of a reaction involving transfer of charged species over an interface (as opposed to only neutral particles), depends both on the difference in chemical potential of the products and reactants, and on the difference in electrostatic potential between the

phases (i.e., on the electrochemical potential difference) [119-121, 123]. The difference in $\bar{\mu}_e$ between two electrodes can be altered by applying an external voltage. In this way it is possible to initiate or change the rate of a redox reaction occurring in the cell by changing the electrode voltage(s).

In this section some different models used to describe solid/liquid interfaces are presented. This includes the two ideal cases of an ideal polarizable and an ideal non-polarizable electrode. Further, a few models of the electrical double layer (EDL) present at an ideal polarizable interface are described. It is also discussed how the voltage drop over a solid/liquid interface during charge transfer depends on the occurring redox reaction(s).

3.2.1 Ideal polarizable and ideal non-polarizable electrodes

If charge transfer cannot occur over a solid/liquid interface, regardless of the voltage applied, the electrode is called an ideal polarizable electrode (or interface) [119, 120, 133]. Charging of an ideal polarizable electrode results in a behavior similar to a capacitor, where one of the phases gains an excess positive charge, and the other phase an equal amount of excess negative charge. Since no redox reactions can occur, any change in voltage difference over such an interface solely stems from an electrostatic potential difference, built up by the charge separation at the interface. In this case a small current will cause a large change in electrode voltage. Any electrode/electrolyte interface will behave as an ideal polarizable interface at voltage regions where no charge transfer occurs. Electrodes that show ideal polarizable behavior in a large voltage region can for example be useful to determine the voltage stability region of electrolyte solutions [134, 135].

In the opposite case, when charge transfer can occur reversibly over the solid/liquid interface, the voltage will be constant even when a current is passed through the electrode. If the voltage is fixed regardless of the size of current, the electrode is termed an ideal non-polarizable electrode (or interface) [119]. In this case, an excess/deficiency of electrons at the electrode is immediately compensated by a reduction/oxidation of an available redox couple, and the electrode voltage remains constant. An electrode or interface will behave as an ideal non-polarizable electrode if the number of transferred electrons (i.e., the current) is much smaller than the concentration of available reduced and oxidized species. This type of electrode is suitable for use as a RE in electrochemical measurements [119].

In practice, no electrode can behave as an ideal polarizable interface for all voltages. Similarly, no real electrode can remain ideal non-polarizable upon passage of an infinite current. However, in certain voltage and current ranges, it is possible to find real electrode/electrolyte interfaces that behave in this way, and thus the concepts are still useful.

3.2.2 The electrical double layer

In case of an ideal polarizable interface, a charged interface will be built up at the electrode/electrolyte interface when the electrode voltage is changed. The whole region incorporating the excess charges is called the EDL. This term stems from the first model used to describe this interface, introduced by Helmholtz in the 1850s [136]. In Helmholtz's model, only purely electrostatic interactions are considered. In this case the ions line up close to the electrode surface, with the distance from the surface determined by the radius of the solvation shell. This is illustrated in Figure 3.2a. In this model the (electrostatic) potential drop is linear and located in between the two arrays of charges, exactly analogous to a parallel-plate capacitor. The charge stored is in this case directly related to the applied voltage according to [119-121]:

$$q = \frac{\varepsilon\varepsilon_0}{d} V = C * V, \qquad (3.15)$$

where ε is the dielectric constant of the medium, ε_0 the permittivity of vacuum, d the distance between the charges, V the voltage and C the capacity.

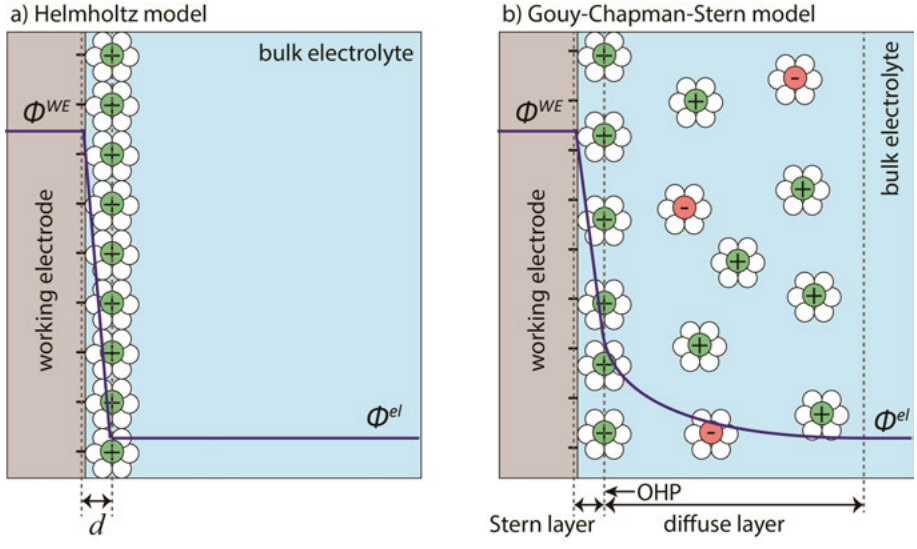

Figure 3.2: Illustration of the Helmholtz model (a), and the Gouy-Chapman-Stern model (b) of the electrical double layer.

The simple model suggested by Helmholtz describes the EDL between highly conductive phases rather well, where a large number of movable charges exists. In highly conductive phases no electrical fields can exist within the phase at equilibrium, and any excess charge is strictly confined to the surface. In this case the distance d is constant, and the capacity can be considered independent of voltage.

For electrolytes with low ion concentrations, the Helmholtz model does not give an accurate description of the charged interface. In this case the thickness of the charged interface layer will vary, depending on the interplay between different forces causing ion movement, including electrostatic, chemical and thermal effects [119]. The charge excess is still highest close to the surface, but in this case the region with excess charges stretches over a larger distance, called the diffuse layer. The thickness of the diffuse layer depends on the electrode voltage and the ion concentration of the electrolyte. A higher voltage or ion concentration increases the electrostatic interactions, and thus decreases the thickness of the diffuse layer.

For a more realistic view of the EDL, several additional models have been developed. A description of the EDL incorporating thermal movement was suggested independently by Gouy and Chapman [137, 138]. In this model a statistical mechanical approach is used to describe the voltage drop over the diffuse layer. In the limiting case for low concentrations and small potential differences, the potential drop becomes an exponential function. For interfaces close to the point of zero charge, the Gouy-Chapman model gives a good description of the charged interface [119]. However, as the concentration or the voltage increases, the capacities are highly overestimated since the ions are viewed as point charges that can be located arbitrary close to the electrode surface. Physically, d will be limited by the size of the (solvated) ions.

By combining the Helmholtz model and the Gouy-Chapman model a decent description of the charged interface at the electrode/electrolyte interface is given. This was first done by Stern [139]. In this model, the closest distance a solvated ion can get to the electrode surface defines the outer Helmholtz plane (OHP), which also defines the boundary of the Stern layer (or compact layer) of the EDL. In the Stern layer the voltage drop is linear, as defined by the Helmholtz capacitor. Ions located further away from the electrode than the OHP make up the diffuse layer. In this region the potential profile is described by the Gouy-Chapman model. The total capacitance of the charged interface is given by these two capacitances in series [119]. This model, illustrated in Figure 3.2b, is called the Gouy-Chapman-Stern model.

None of these original models consider additional effects stemming from the chemistry of the ions and solvent, including full polarization of the solvent, specific adsorption of ions at the surface and ion pairing effects in the EDL. These properties were later discussed by e.g., Frumkin [140], Grahame [141] and Parsons [142, 143]. Today, both new experimental techniques [144, 145] and more detailed theoretical models [146, 147] are used to describe the EDL.

For the electrolytes used in this thesis the ion concentration is high enough to ensure a large number of charge carriers. In this regard the double layer thickness will be very thin (~a few Å) and a linear voltage drop located immediately at the electrode/electrolyte interface serves as a good approximation of the EDL [119, 121].

3.2.3 Charge transfer over the solid/liquid interface

When charge transfer occurs over a solid/liquid interface, changes in both the chemical (μ) and electrostatic potential (ϕ) of both phases can occur. A change in chemical composition can lead to a change in μ, while the transfer of charge also alters ϕ. In general, ϕ can be changed much faster than μ, and reaching equilibrium for a charged species thus requires transfer of far fewer species compared to a neutral species. It can also be noted that the equilibrium of a species is separated from the equilibrium of the overall redox reaction. In this way equilibrium of a mobile species can be established even though the overall redox reaction is not in equilibrium [119, 120].

If two initially uncharged phases ($\phi = 0$) are put into contact, a difference in μ of a transferable species, say an electron, will cause electron transfer from the phase with higher μ_e to the phase with lower μ_e. The transfer of electrons results in an excess of electrons in one phase, and a deficiency of electrons in the other. This gives an electrostatic potential difference (or Galvani potential difference) $\Delta\phi$ at the phase boundary. When z*$\Delta\phi$ (-$\Delta\phi$ in the case of an electron) exactly compensates $\Delta\mu_e$, the electron electrochemical potentials ($\bar{\mu}_e$) are equal and electronic equilibrium is achieved. If the voltage of one phase thereafter is changed, the equilibrium will be disturbed, and electron transfer will once again occur until equilibrium is re-established. Depending on the kinetics of the reaction this process can be slow or fast, but given sufficient time equilibrium will be established. The voltage drop over an interface in electronic equilibrium is always zero.

If the transferable species over the solid/liquid instead is an ion (e.g., as in the case of an LIB) the electrochemical potential of the ion is equilibrated. If charge transfer of electrons cannot occur, there may in this case be a difference in $\bar{\mu}_e$ (i.e., a voltage drop) over the interface. If the electrode voltage is changed under these circumstances, this can also affect the ionic equilibrium. In this case the voltage drop over the solid/liquid interface may vary as a function of electrode voltage. This voltage drop can be directly studied by APPES (see Chapter 6).

3.2.3.1 Reaction rate and overpotential

The rate of a reaction involving charge transfer over an interface depends not only on the usual kinetic variables of a chemical reaction (temperature, pressure, concentration etc.) but also on mass transfer to the interface and on different surface effects [119, 121]. For a redox reaction, the reaction rate is proportional to the current, which can be measured as a function of applied voltage. In such measurements, the standard electrode voltage (E^0) determined from thermodynamics is an interesting point of reference.

A deviation from E^0 during a redox reaction is termed polarization. The polarization is equal to the difference between the measured voltage (E) and the standard electrode voltage E^0 and is called the overpotential η:

$$\eta = E - E^0. \quad (3.16)$$

A larger overpotential (in magnitude) correspond to a lower energy efficiency, i.e., more electrical energy is needed to charge the electrochemical cell, compared to the energy that can be used for electrical work during discharge. The difference in these energies correspond to energy dissipated as heat. For an ideal thermodynamically reversible reaction the overpotential is zero, and the energy efficiency is 100 %. For most practical systems the overpotential deviates from zero, and increases with an increased current.

The overpotential stems from the inherent sluggishness of the redox reaction. In this way the reaction can be thought of as a resistance in an electric circuit, where the total resistance consists of the resistance (or more correctly, impedance) from each reaction step; including mass transfer, charge transfer, and any preceding chemical reactions. A slow reaction (step) will give rise to a high resistance, and a fast reaction a low resistance. The overall rate of the reaction will be limited by the slowest reaction step, called the rate determining step. At steady-state conditions all reaction steps occur at the same rate, limited by the slowest process. The current flowing under these conditions is called the limiting current.

In addition to the overpotential associated with the redox reaction, there can also be a resistance stemming from the transport of a current in the bulk electrolyte, denoted iR_s. This contribution is usually separated from the overpotential, as it is a purely ohmic voltage drop that is characteristic of the bulk electrolyte solution, and not the electrode reaction. The measured voltage of an electrode when a current is drawn can then be described by [119]:

$$E = E^0 + \eta + iR_s. \quad (3.17)$$

During reduction of the WE both η and iR_s are negative, and during oxidation both terms are positive. The iR_s contribution can be minimized by using electrolytes with a low resistance and/or by cell design. In these cases the iR_s-drop can often be neglected (see also Section 6.2.3).

3.3 Electrochemical methods

Electrochemical methods can be used to evaluate e.g., the redox potential of a reaction, the capacity of an electrode, and/or the resistance of a cell. In this section the principles of the potentiostat (used to perform the electrochemical cycling) and some of the most common electrochemical methods used to test batteries are presented. For a more complete description of the many available electrochemical techniques, there are several textbooks on the topic, including e.g., references [119, 121].

3.3.1 The potentiostat

In most electrochemical measurements performed in this thesis a potentiostat (that also can operate as a galvanostat) is used to control and measure the voltage/current in a three-electrode setup. The potentiostat controls the voltage between the WE and RE by adjusting the current flow between CE and WE [119, 121]. In a two-electrode setup, the CE also acts as RE.

The potentiostat uses a feedback loop to compare the measured voltage of the WE (vs. the RE) to the input voltage set by the user. If the measured WE voltage is too high/low, the cell current is altered until the measured WE voltage equals the input voltage. The feedback loop functions by the use of operational amplifiers (op-amps). The op-amps measure the voltage difference between two inputs, and give an output voltage equal to this difference multiplied by a scale factor. To measure the voltage difference directly, the scale factor is 1 (unity gain). In a feedback loop the scale factor is usually a large number (~10^5) to quickly adjust a small difference in voltage.

In Figure 3.3 a simple schematic of a potentiostat is shown, illustrating the main components of the potentiostat; the electrometer, the current-to-voltage (I/E) converter, the signal circuit, and the control amplifier. These general components are common for most potentiostats, although the precise setup of different instruments may vary [148, 149]. The electrometer and the I/E converter are unity gain amplifiers that are used to measure the voltage and the current of the cell, respectively. The signal circuit is used to convert the user input (e.g., cut-off voltages, current values, potential steps etc.) from numbers to a voltage signal by a digital-to-analog converter. The input voltage set by the user and the measured voltage is compared in the control amplifier. To convert the potentiostat to a galvanostat (i.e., control the current rather than the voltage), the feedback to the control amplifier is changed from voltage to current.

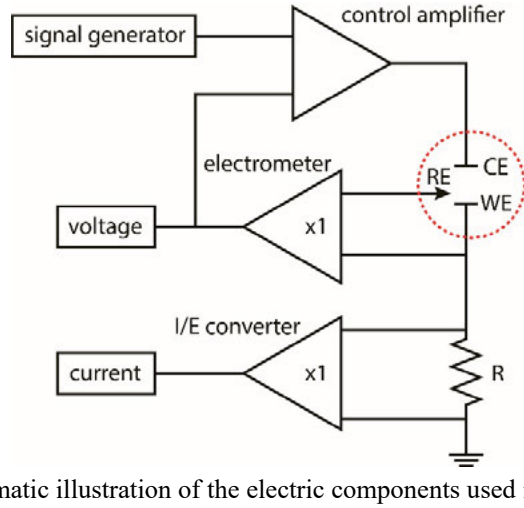

Figure 3.3: Schematic illustration of the electric components used in a potentiostat.

3.3.2 Controlled current cycling

In galvanostatic cycling, the current is controlled while the cell voltage is measured as a function of time [119, 121]. This technique is typically used to charge and discharge a cell during a fixed time, determined by the applied current in relation to the capacity of the battery/electrode. Either a two electrode cell or a three-electrode cell can be used. In a two electrode setup only the (total) cell voltage can be measured. In a three-electrode setup also the individual voltages of the WE and CE can be measured (vs. the RE).

When an electrochemical cell is charged a (constant) current is flowing from the negative electrode to the positive electrode, and to discharge the cell the current is reversed. The resulting cycling curve gives information of the total charge that can be cycled within the cell. In Figure 3.4 an example is shown for one cycle of LTO and NMC. The shape of the voltage curve also gives information regarding the reduction potential and type of reaction. A flat voltage plateau indicates a first order phase transition with a fixed equilibrium voltage. A more sloping voltage curve is characteristic of a single phase reaction, where lithium is intercalated gradually into the same phase [56, 150].

Often several full cycles are performed to evaluate coulombic efficiency and capacity retention. The coulombic efficiency is a measure of the ratio between extracted charge and inserted charge. The capacity retention measures the (often discharge) capacity as a function of cycle number. Together these two parameters give a good indication of the reversibility of the chemical reactions and the cycle life.

Another important parameter for galvanostatic cycling is the C-rate. The C-rate denotes how fast the charge/discharge is performed, in number of charges per hour. A C-rate of 1C corresponds to one full charge (or discharge) in 1 hour (i.e., a full cycle takes 2 hours) and a C-rate of 10C corresponds to one charge in 6 minutes. By varying the C-rate, information about the kinetics of the redox reaction can be gained. Low C-rates are used to test the materials under practical equilibrium, and high C-rates are used to evaluate the power capability, determining how fast the battery can be charged.

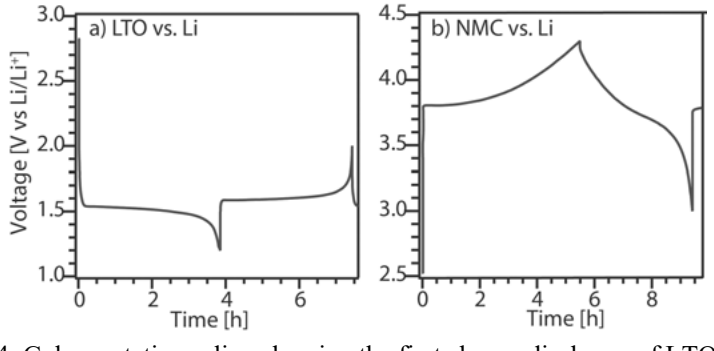

Figure 3.4: Galvanostatic cycling showing the first charge-discharge of LTO (a) and NMC (b) cycled versus Li metal.

3.3.3 Controlled potential cycling

Two common controlled potential techniques are potentiostatic cycling and cyclic voltammetry [119, 121]. In potentiostatic cycling a fixed voltage is applied in a potential step, and the current response is measured as a function of time. Often the voltage is stepped from a value where no faradaic reactions occur, to a value where a reduction/oxidation reaction takes place. The voltage steps can also be varied, in order to probe the current at a given time as a function of voltage (overpotential). In this case applying a larger overpotential usually gives a larger current. Potentiostatic cycling have been used in the *operando* APPES measurements presented in Paper III-V.

In the case of a mass transfer limited reaction, the reaction rate of the redox reaction is so fast that a reactant arriving at the surface immediately reacts, and the concentration of the reactant is essentially zero at the electrode surface. In this case the reaction rate is determined by how fast the reactant can be brought to the electrode surface. For a mass transfer limited reaction the current will decay proportional to $t^{-1/2}$ [119].

Cyclic voltammetry is useful to determine the reduction potential of a reaction. In cyclic voltammetry the voltage is scanned at a fixed scan rate between an upper and a lower cut-off voltage, and the current is measured as a function of voltage. An example for a Cu electrode is shown in Figure 3.5. Reduction and oxidation reactions will result in current peaks in the cyclic voltammogram. When the WE voltage is lowered reduction reactions can occur, and when the scan rate is reversed the corresponding oxidation reactions can be studied. For fast scan rates the current is typically limited by diffusion, and the measurement gives information about the mass transport properties. Using slow scan rates, information regarding the kinetics of the charge transfer reaction can instead be gained.

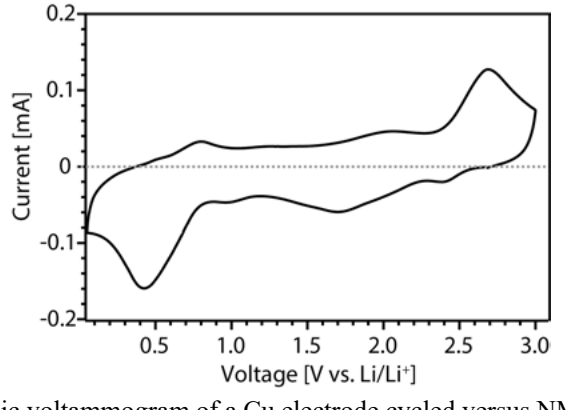

Figure 3.5: Cyclic voltammogram of a Cu electrode cycled versus NMC.

4 Photoelectron spectroscopy[4]

In photoelectron spectroscopy (PES), the interaction between light (photons) and matter is used to study the electronic states of materials. In this chapter a short background on the electronic structure of matter is first given. Thereafter the general principles of PES are presented. This is the primary technique used in all work performed in this thesis. In the last section a description of some of the experimental setups used for the work in this thesis is included.

4.1 The electronic structure of matter

In order to understand and develop the macroscopic properties of a material, it is often necessary to study the atomic composition, and the electronic structure of the atoms in the material. The electronic structure is a result of the electromagnetic forces between nuclei and electrons, and will determine the character of the chemical bonds that hold the atoms together in a material. Depending on the character of the bonding, many physical and chemical properties of a material can be explained. In this section a short introduction to the electronic structure of atoms, molecules and solids is presented.

4.1.1 The quantum mechanical description of the atom

The results in this thesis are to a large extent based on electron energies measured by PES, which can give information about the chemical composition of a sample. The interpretation of these results would not be possible without the historical work performed in the field of atomic physics and quantum mechanics in the early 20th century. In the following brief summary of some of this work, a few key concepts that serves as a foundation for the interpretation of the PES results are highlighted. For a rigorous description of these findings, the reader is referred to one of the many textbooks on the matter [151-154].

One of the most important findings in this regard, stems from experiments performed by e.g., Kirchoff and Bunsen in the 1850s [155]. They observed that atoms only emit or absorb light of specific wavelengths, which are

[4]Section 4.2 and 4.3 is partly based on the corresponding sections of my Licentiate thesis: Källquist, I. (2019). Interfaces in Li-ion batteries seen through photoelectron spectroscopy.

characteristic of the atom under study. This implied that the energy of an atom only could be changed by certain discrete values. This was later visualized in the simple picture of an atom presented by Bohr in 1913 [156]. In Bohr's model negatively charged electrons move in circular orbits around the positively charged nucleus. Each orbit is located at a specific distance from the nucleus, corresponding to a certain allowed electron energy. The electron energies associated with a specific atom are characteristic of that element, and depend for example on the charge of the nucleus and the electrons' interactions with each other. The energy required to remove an electron from the atom is also referred to as the electron's binding energy (BE). The BEs of the electrons in an atom can be used as a "fingerprint" to detect different elements in a sample. This basic principle is the foundation of the PES measurements.

To determine the allowed energies of an electron moving around a nucleus in an atom, the dual nature of the electron – behaving as both a particle and a wave – can be considered. This relationship between the wave and particle properties was described by de Broglie in 1923 [157, 158]. Heisenberg and Schrödinger also made significant contributions to the understanding of electron energies by developing the field of quantum mechanics in the 1920s. Heisenberg described the probabilistic nature of particles on the atomic scale, stating that values of energy, momentum and position of such a particle can only be determined within certain uncertainties [159]. To determine the expected value of these quantities, one need to consider the probability of finding the particle in certain positions. The probability of finding a particle at a certain position is derived from the wave function Ψ. Once the wave function is known, the average position, energy and momentum of a particle can be calculated. The wave function and corresponding allowed energies for a particle can be found by solving the Schrödinger equation [160]:

$$\mathcal{H}\Psi = E\Psi, \tag{4.1}$$

where $\mathcal{H}$ is the Hamiltonian operator, Ψ the wave function of the particle and E is the energy eigenvalues. $\mathcal{H}$ describes the different contributions to the total energy of the particle (e.g., kinetic energy, potential energy).

In quantum mechanics one way of describing an electron in an atom is by the use of four quantum numbers[5]. The principal quantum number *n*, describes the energy level and is given from the energy eigenvalues of the Hamiltonian. The available principle quantum numbers *n*=1, 2, 3, etc. correspond to the main electron shell (also called the K-, L-, M-shell etc.). These energy levels are also described by Bohr's model. However, the circular orbits used by Bohr cannot accurately describe the spatial distribution of the electrons around the nucleus. In quantum mechanics the electron orbitals are described by *n*, the

[5] For a thorough description, see e.g., references [151]-[154].

orbital angular momentum quantum number l, and the magnetic quantum number m_l. The symmetry of the orbital is described by l and give the subshells, labelled s, p, d, f, etc. The s- and p-orbitals are schematically illustrated in Figure 4.1. The available energy states within each subshell is given by m_l. The forth number is the spin quantum number, m_s, describing the spin of the electron. In this thesis n and l are used to describe the measured electron energy levels of different elements (e.g., C 1s, Co 2p).

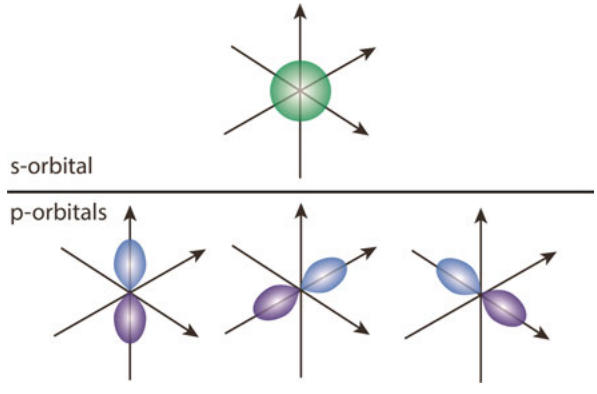

Figure 4.1: Illustration of the symmetry of the s- and p-orbitals.

4.1.2 From atoms to solids

The outermost electrons in an atom are called the valence electrons, while the inner electrons are called the core electrons. The valence electrons participate in the chemical bonds that can be formed between two or more atoms in a chemical compound.

In solids, three main types of bonding are often described [161, 162]. In a pure ionic bond, one atom gives away one or more valence electrons to another atom, resulting in the formation of a positive and a negative ion. In this case the electrons are localized around a single nucleus, and the interaction between the ions are largely described by Coulomb forces between these ions. In a pure covalent bond, valence electrons are equally shared between two atoms. In this case the shared electron(s) can be located around any of the two nuclei, and the atoms are held together largely as a consequence of the interactions among these electrons. In reality, most chemical bonds are combination of these two extremes, where the valence electrons are shared, but the electron density is higher around one (e.g., the more electronegative) atom. This type of bonding is also found in molecules. In a metallic bond, the valence electrons of many atoms are shared. This results in a bonding where positive ion cores are surrounded by (essentially) freely moving valence electrons.

When atoms are combined into molecules, solids, or liquids, the allowed electron energies can be altered. This is schematically illustrated in Figure 4.2. The electrons closest to the nuclei are typically tightly bound to the core of a

single atom and are not directly involved in the chemical bonds. The interaction of a core electron with other atoms is thus minor, and these orbitals will keep their atomic character. However, for valence electrons, the character of the orbitals and the allowed electron energies can be significantly altered in a solid or molecule compared to the free atom. This is a result of the additional interactions a valence electron in a solid will experience, compared to a valence electron in a free atom. According to the Pauli exclusion principle [161, 162], two interacting electrons cannot have the same quantum state. To accommodate for this, any identical atomic orbitals must be split into new orbitals when atoms are combined. For molecules, these are referred to as molecular orbitals. The highest occupied molecular orbital is called the HOMO, and the lowest unoccupied molecular orbital is called the LUMO.

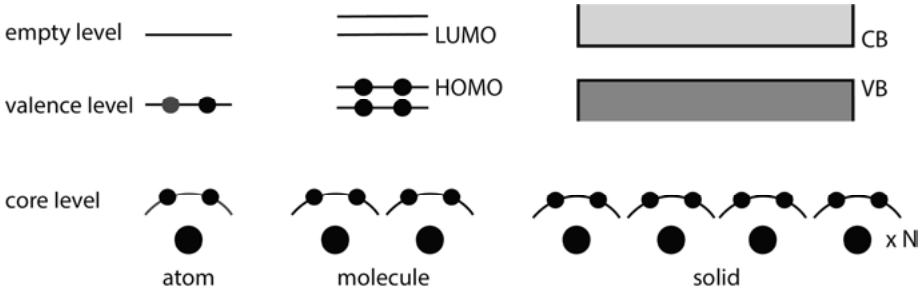

Figure 4.2: Illustration of the nature of different electron energy levels in an atom, a molecule, and a solid. In molecules and solids valence electrons are shared to form chemical bonds, which results in the formation of new orbitals/energy bands.

For solids, the atomic orbitals will be combined into many close lying energy levels, which for macroscopic solids are so closely spaced that they essentially form a continuous band of allowed electron energies. In this case, the available states can be divided into an upper band (the conduction band, CB) and a lower band (the valence band, VB). The VB contains mostly filled states, and the CB mostly empty states. The bands can either overlap (as in a metal) or be separated by a band gap (as in semiconductors or insulators).

To define the energy required to add an electron to a solid, the concept Fermi level (E_F) is used. E_F is defined as the energy level where the probability of electron occupation is exactly ½ [161, 162]. If a free electron in vacuum is used as the energy reference, energy is typically released to the surrounding when an electron is added to the material (i.e., the "required" energy is negative). At 0 K all available energy states up to E_F is filled, and all states above E_F are empty. At room temperature, the thermal motion will result in a symmetrical statistical distribution (Fermi-Dirac distribution) for the occupancy probability of energy levels around E_F. As a result, some available states above E_F can be filled, and some states below E_F can be empty. E_F represents the average energy change associated with adding/removing an electron from the material.

4.2 Principles of photoelectron spectroscopy

PES is a photon-in electron-out technique that builds on the photoelectric effect [163, 164]. A photoelectron (PE) spectrum is typically recorded by measuring the number of detected PEs as a function of their binding energy (BE) or kinetic energy (KE).

From a quick survey spectrum, shown in Figure 4.3 for a gold electrode, the overall composition of the sample can be evaluated from the positions and intensities of the PE peaks. For more detailed information, PEs stemming from specific orbitals can be measured with higher resolution. In the following sections it is described how PES can be used to analyze the chemical composition and (local) electrochemical potential of a sample. Most emphasis is put on how to interpret the spectra, with a special focus on considerations for electrochemical systems.

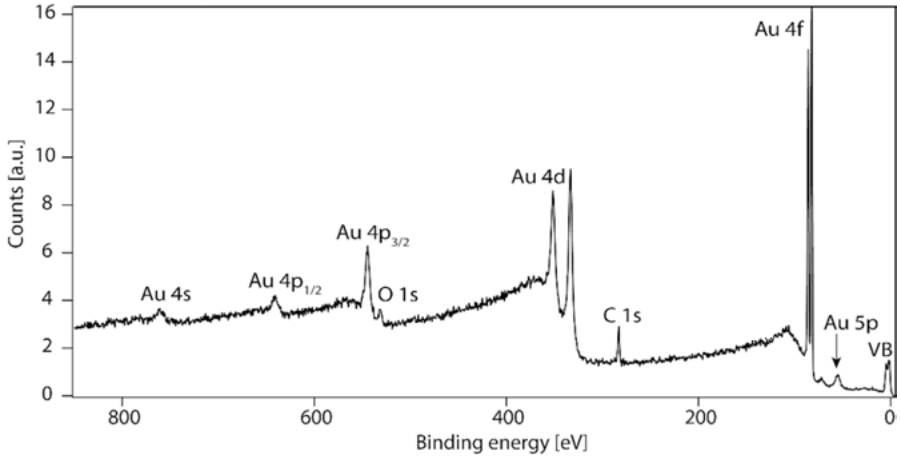

Figure 4.3: Survey spectrum of a gold electrode.

4.2.1 The photoelectric effect

As first discovered by Hertz in the 1880s [165], and later described by Einstein [166], the probability of creating sparks between electrically isolated metal objects is enhanced by the irradiation of photons. This phenomenon is called the photoelectric effect, and describes the process whereby photoionization occurs as a result of light-matter interaction. Photoionization can occur if the energy of the photons is higher than a certain threshold energy, corresponding to the minimum energy required to emit an electron from the sample. For a condensed sample, this energy is called the work function, Φ.

The energy is conserved in the photoionization process. This means that if the photon energy $h\nu$ is larger than the energy necessary to remove an electron from the sample, the remaining energy of the photon will be converted to KE. The photoelectric effect can be described by the equation:

$$KE_{max} = h\nu - \Phi, \quad (4.2)$$

where KE_{max} is the maximum kinetic energy of the emitted PE, $h\nu$ is the incoming photon energy and Φ the work function.

4.2.2 Binding energies

The BE is, in a simplistic way, a measurement of how strongly an electron is bound in a sample. In PES, the BE is often given as a positive number, corresponding to the energy required to remove an electron from its orbital. In condensed matter (solids and liquids), the BE is often defined with respect to the Fermi level (E_F) [163]. The additional energy required to move an electron from E_F to the vacuum level (V_{sample}) is equal to the work function Φ. In this case the KE of the emitted PE can be determined according to:

$$KE = h\nu - BE - \Phi_{sample}. \quad (4.3)$$

where Φ_{sample} depends both on the "chemistry" (the attraction of the electrons at the Fermi level to the material) and on the electronic structure of the surface. Due to the asymmetric environment at an interface, a surface dipole typically exists at the sample surface. To escape from the sample, the PE need to pass the resulting electrostatic field, denoted by the surface electrical potential χ. The interaction of the PE with the surface dipole results in a gain/loss of KE, depending on the direction of the electric field.

Both χ and Φ depend on the surface properties (crystal orientation, contaminations etc.) of the material, rather than the bulk properties. Thus, it can be different for different samples of the same bulk material. Because of this, it can be helpful to reference BEs towards E_F of the sample, to facilitate the comparison of BEs of the same element in different samples. This is similar to the conceptual separation of the electrochemical potential into the chemical and electrostatic potential, used in electrochemistry.

4.2.2.1 Measuring binding energies with PES

According to Eq. (4.3), the BE of an electron can be estimated by measuring the KE of the outgoing PE. If the BE is referenced versus E_F, the defined BE is independent of Φ_{sample}. However, to actually detect and measure the KE of the PE, it has to leave the sample and enter the electron analyzer. This means that the PE in practice is affected by the surface dipole, and any other external electrical fields, on its trajectory from sample to analyzer. To account for this, the sample is generally electrically connected to the electron analyzer during PES measurements. In this way E_F of a conductive sample is aligned with E_F of the spectrometer. This facilitates the interpretation of obtained BEs.

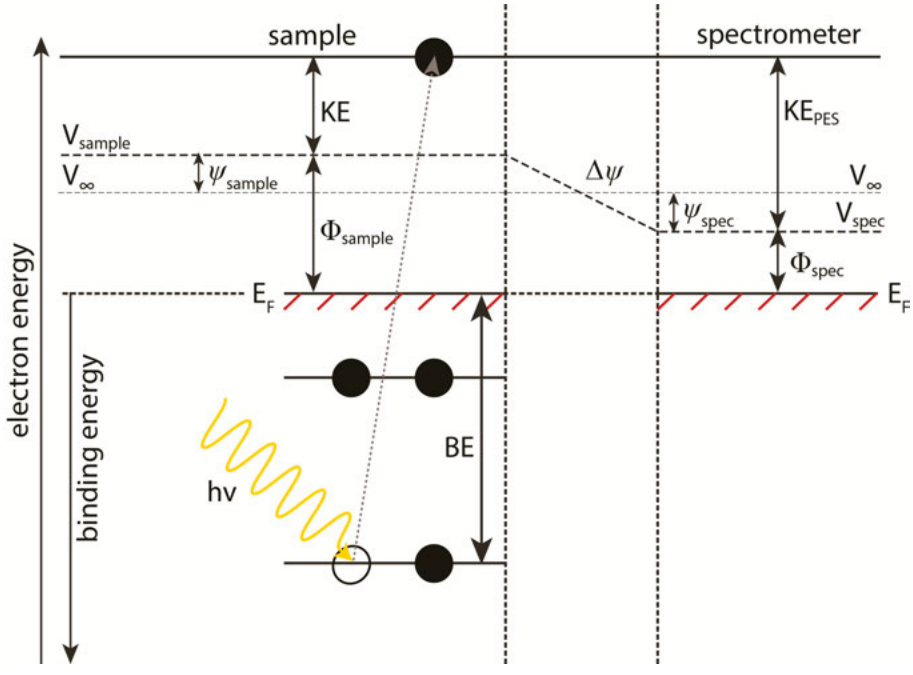

Figure 4.4: Illustration of the different energy levels in the sample and spectrometer. In the figure it is assumed that the phases initially do not contain any excess charge (ψ=0). When the sample and spectrometer are electrically connected, electrons will move from the spectrometer to the sample to align the Fermi levels E_F. As a result, an electrical field $\Delta\psi$ is created between the sample and spectrometer. This causes an acceleration of outgoing PEs and alters the measured KE_{PES}.

If E_F of the sample and spectrometer initially are different, electrons will move from the phase with higher E_F to the phase with lower E_F. As a result, one phase will have an excess of electrons and the other a deficiency, and a difference in outer electrostatic potential (or Volta potential) $\Delta\psi$ will exist between the sample and detector. This difference in ψ will alter the KE of the PE as it travels from the sample to the detector. It follows from the schematic diagram in Figure 4.4 that when E_F of the sample and the spectrometer are equal the *measured* KE_{PES} depends on the work function of the spectrometer Φ_{spec} (not the sample) according to [164, 167]:

$$KE_{PES} = h\nu - BE - \Phi_{spec} \qquad (4.4)$$

To obtain BE values that are comparable for different spectrometers, both Φ_{spec} and $h\nu$ need to be known with desired accuracy. In practice, this is often done by measuring a reference spectrum with the same photon energy used for measuring the sample. The reference spectrum can be of any PE peak with a well-known BE. A common choice is the Au 4f peak, that gives a strong photoionization signal. This type of calibration works well for conductive samples, where E_F of the sample and spectrometer are aligned [168]. For

samples containing insulating/semiconducting phases, this may not be the case. For these materials an internal BE calibration may be preferred, to account for any differences in E_F between the sample and the spectrometer. These can be inherent to the sample (e.g., due to different work functions) or a result of sample charging. To perform a valid calibration using an internal reference, the reference PE peak should stem from the same phase as the PE peak of interest. For a material containing several different phases (e.g., a composite electrode) it may be necessary to use a different calibration for different phases [42, 169]. For battery materials common methods for BE calibration includes using the metal oxide peak at ~530 eV or the graphitic carbon peak at ~284.5 eV (for the bulk material), or the hydrocarbon peak at ~285 eV (for the interphase layer) [169-171].

A common issue among PES (XPS) literature is that BE values sometimes rather arbitrarily are referenced to the adventitious carbon peak, without considering the origin, chemical nature or energy level alignment between this species and the sample substrate, which are effects known for many years. Practical consequences of this issue is extensively discussed in the recent reference [172]. An important result highlighted in this review is that the measured BE of the adventitious carbon peaks is highly dependent on the substrate and sample environment, and can vary as much as ~2.5 eV for different samples [173]. Thus, even though this calibration procedure is one of the most commonly used [174], the adventitious carbon peak cannot in general be used as a BE reference without further considerations [169, 172, 175, 176].

4.2.2.2 Theoretical description of binding energies

So far, it has only been mentioned that the BE of an electron depends on the orbital it stems from. This is partly correct, but not the whole picture. Since an electron is emitted in the photoionization process, the electronic structure of the sample is altered during the PES measurement, and the final state of the sample contains one electron less (an electron hole). The removal of an electron can affect the remaining electrons, and the energy of the emitted PE will therefore not directly represent the initial orbital energy.

A more rigorous definition of the BE can be made by considering the conservation of energy in the photoionization process. Thus, the energy of the initial state must be equal to the energy of the final state [163]. The initial state consists of a photon with energy $h\nu$ and a sample in its initial ground state with energy $E_{initial}(N)$. The final state consists of a PE with kinetic energy KE and a sample in a final state with energy $E_{final}(N-1)$. Setting the initial and final energy equal and rearranging, one obtains:

$$h\nu - KE = E_{final}(N-1) - E_{initial}(N) = BE. \qquad (4.5)$$

The energy difference between the final and initial state of the sample is defined as the BE versus the vacuum level. For a solid, Φ_{sample} has to be subtracted to obtain the BE with respect to E_F.

The definition of the BE as given in Eq. (4.5) is exact. However, calculating the total energies of the initial and final state can generally only be done using approximations. A simple approximation for the BE is given by Koopmans' theorem [177, 178], which states that the BE of an electron orbital is equal to the negative of the ground state orbital energy *if no rearrangement of the other electrons in the system occurs in the photoionization process*. This assumption is also called the "sudden" or "frozen orbital" approximation. In practice, the remaining electrons will redistribute in order to minimize the energy of the final state. This will alter the energy of the final state by a relaxation energy. A better approximation of the BE can then be given by trying to approximate this energy as well.

Another way to estimate the BE is by the "Z+1" or "equivalent-core" approximation, where the effect of the (core) electron hole is estimated by the hypothetical addition of a proton to the nucleus [163, 164]. The BE can then be estimated from the ionization energies of the Z and Z+1 atom in a Born-Haber(-Fajans) cycle [179-182]. This approximation works rather well when the interactions between the valence electrons and core electrons are small.

4.2.3 Shifts in binding energy

One of the main reasons for the usefulness of PES lies in its ability to measure shifts in electron energies arising from the local electronic structure of the material. This allows for identifying not only the type of elements, but also the presence of different chemical environments and oxidation states. In this section some of the factors that affect the measured BE are discussed. The shifts have been divided into chemical shifts, electrochemical shifts and shifts due to spin-orbit coupling.

4.2.3.1 Chemical shifts

As first discovered by Siegbahn *et al.* in the 1960s [183] the BE of an element can vary depending on its chemical environment. This variation in BE is called a chemical shift, and can be used to determine the local chemical environment and the oxidation state of an element. Due to this property, PES has also been called Electron Spectroscopy for Chemical Analysis (ESCA), an abbreviation used by Siegbahn and co-workers.

The difference of the measured BE of an element in a chemical compound, compared to the BE of the same element as a free atom in its ground state, can be explained by initial and final state effects. Initial state effects stem from how an atom or ion is bonded in a chemical compound. The chemical bonding will alter the energies of the valence electrons, which are directly involved in the bonding, but it will also affect the BE of the core electrons, due to changes

in the electron density around the atom. This is the main reason for the ability to differentiate between different chemical states with PES [164].

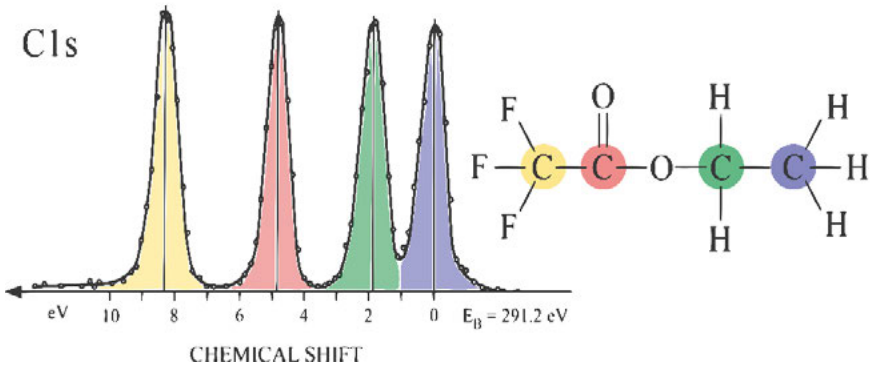

Figure 4.5: The chemical shift illustrated by the difference in binding energy of the four carbon atoms with different chemical environments in the "ESCA molecule".

As a rule of thumb, the BE increases when the electron density decreases [163, 164]. A decrease in electron density around an element can e.g., be a result of chemical bonds to strongly electronegative elements, such as F or O. This is illustrated for the classic "ESCA molecule" (ethyl trifluoroacetate) in Figure 4.5, where the BE of the carbon C 1s level increases when hydrogen bonds are substituted for the more electronegative elements O and F. A decrease in electron density can also be a result of the oxidation of an element, where a higher oxidation state corresponds to a lower electron density and generally a higher BE. These "classical" chemical shifts are due to intra-atomic initial state effects. If interatomic (also called extra-atomic) or final state effects instead are dominating, the change in BE can sometimes be negative, even if the electron density decreases. One example is barium, in which case interatomic initial state effects dominate, leading to a decrease in BE for BaO as compared to Ba metal [164, 167, 184].

Final state effects include the rearrangement of electrons as a result of the creation of a core hole. These effects are also referred to as relaxation effects. The relaxation of the final state results in a decreased BE compared to the expected orbital energy of the initial state [163]. Final state effects can also include excitations of valence electrons (to empty states or the continuum), resulting in a decrease of the KE of the outgoing PE. These peaks appear as so-called satellites at higher BEs in the PE spectra [163, 164, 185]. Satellites are commonly observed for transition metal oxides, where electron transfer can occur from filled ligand states to unoccupied conduction band states in the metal. This corresponds to a valence excited state. When the conduction band electron relaxes to the valence band, energy is released, which increases the KE of the outgoing PE. This relaxed final state corresponds to the main peak

(lowest BE) in the core level spectrum. Due to the electron rearrangement as a result of final state effects, the BE of transition metals with different oxidation states sometimes does not follow the trend expected from initial state effects. This is the case for e.g., Cu and Co, where an increased oxidation state can give rise to a small negative shift in BE [186-189].

4.2.3.2 Electrochemical shifts

The measured BE of a PE will also depend on the local electrostatic potential of the phase it stems from. In general, it is not possible to separate the contribution from the chemical and electrostatic potential of the electron in the measured BE. Thus, a measured BE shift of a core level can include contributions both from a change in ϕ and/or in μ. However, this can sometimes by circumvented, e.g., by aligning the E_F of the sample to E_F of the spectrometer. If the BE then is referenced towards this common E_F, the BE will be independent of ϕ (for conductive phases). This is because a change in ϕ shift all electron energy levels in the phase equally. Thus, the energy difference between e.g. a core level and the Fermi level remains constant. For samples containing electronically insulating phases, the situation is more complex. In this case differences in electron electrochemical potential $\bar{\mu}_e$ between different phases need to be accounted for when evaluating BEs.

The shifts in BE due to differences in $\bar{\mu}_e$ between different phases were investigated in the 1980s by in particular Kolb and Hansen. They showed that it was possible to remove an electrode from an electrolyte solution and maintain most of the EDL, while the bulk electrolyte was removed [190]. The thin EDL could then be probed by PES without obstruction from the bulk electrolyte. PES measurements performed in UHV showed that the EDL remained intact even after long exposure to radiation. The results gave new insights on ion concentration as a function of applied electrode voltage [190], as well as the presence of what they denoted electrochemical shifts. The latter are BE shifts induced by the difference in $\bar{\mu}_e$ over the EDL [191]. Species in electronic contact with the electrode showed no shifts in BE (specifically adsorbed) while non-specifically adsorbed species showed shifts between 0 and 1 eV/V, depending on their distance from the electrode surface [191-194].

More recently similar shifts have been observed between the bulk material and the interphase layer for cycled battery electrodes [169, 172, 195, 196]. The BE shifts of the interphase PE peaks relative to the bulk material are suggested to stem from a buried dipole layer at the interface, accommodating a difference in $\bar{\mu}_e$ between the phases [197]. By comparing the measured BE of the non-conductive phases to the expected BEs (from reference spectra), it is possible to estimate to what extent the shift stems from a difference in ϕ. A further help in this regard is that all core levels shift equally in the case of a change in ϕ. In this way it may be possible to separate contributions from ϕ and μ_e to the total shift in BE.

4.2.3.3 Spin-orbit coupling

Spin-orbit coupling arises as a result of the interaction of the magnetic moment of the electron, stemming from its spin, with the magnetic field resulting from the motion of the electron around the nucleus. These properties are described by the spin quantum number, m_s, and the orbital angular momentum quantum number, l. A detailed description of this phenomenon can be found in textbooks on quantum mechanics [153, 154].

The effect of spin-orbit coupling is visible in the PE spectra of orbitals with a non-zero orbital angular momentum, such as the p-, d- and f-orbitals. Depending on if the spin is parallel or antiparallel to the orbital angular momentum, the BE decreases or increases, respectively. The relative area of the two PE peaks can in addition be predicted from the degeneracy of the energy level (as determined from the total angular momentum, j) [164].

As an example, the 2p orbital ($l = 1, m_s = \pm ½$) will be split into two energy levels by the spin-orbit coupling; the $2p_{3/2}$ energy level and the $2p_{1/2}$ energy level (the subscript indicates the total angular momentum j). The $2p_{3/2}$ level have four available states and the $2p_{1/2}$ have two. Thus, in this case the peak area of the $2p_{3/2}$ level will be twice as large as the area of $2p_{1/2}$ level, and the $2p_{3/2}$ peak will be located at relatively lower BE. This is illustrated in Figure 4.6, where a Co 2p spectrum is shown. The spin-orbit splitting of p-, d- and f-orbitals and their known relative intensities can be helpful for identifying different elements or chemical compounds.

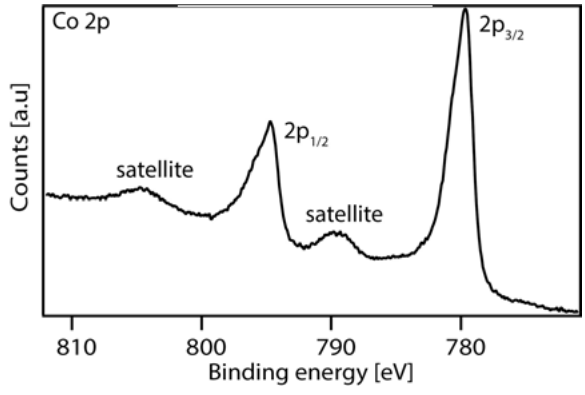

Figure 4.6: Photoelectron spectra of the Co 2p core level. The area under the Co $2p_{3/2}$ peak is approximately twice the area of the $2p_{1/2}$ peak.

4.2.4 Peak intensities

The intensity of each PE peak gives quantitative information regarding the sample composition [198], and depends on several factors. The most obvious one is perhaps the concentration of the different elements, where an increased concentration of an element results in a higher peak intensity. However, the

peak intensity does not directly reflect the sample composition, but also depends on the probability of photoionization, and the probability for the generated PE to escape from the sample [199]. The (absolute) measured intensity will also depend on the instrumental setup, including the photon flux, the beam size on the sample, the efficiency of the electron detector etc.

Often when PES is used to gain quantitative information regarding a sample or a sample series, the measurements are performed using the same instrument and all samples are measured consecutively. In this way, most of the factors affecting the intensity stemming from the experimental setup can be disregarded, since these are equal. In this way relative intensities of different elements or chemical compounds can be calculated and compared to other samples in the same series. An estimation of the relative amount n_i of an element i in a homogeneous sample can be achieved by dividing the peak area A_i with the photoionization cross section σ_i, and the IMFP λ_i [167, 200]:

$$n_i = A_i/(\sigma_i \lambda_i). \tag{4.6}$$

An even better estimation can be achieved if the quantification is made for the same element in different chemical states (e.g., a metal in different oxidation states or an element in different chemical environments). In this case uncertainties in the cross section and IMFP can be disregarded and the areas can be directly compared.

The photoionization cross section describes the probability that an electron from a certain core level will be emitted when irradiated by photons of a specific energy. The cross section is different for different subshells of an element, and depends on the transition probability between the final and initial state, as well as the density of states [163, 164]. The IMFP is the average length a PE will travel in a material before it becomes scattered. The IMFP governs the likelihood of electrons at different depths to escape from the sample. The IMFP depends on the KE of the PE, and on the material in which the PE travels, where factors such as band gap and density are crucial [201, 202]. Both the σ and λ can be calculated, and values can be found in for example references [201, 203-205].

It should be noted that quantity calculations performed from PES are often done using several approximations. In addition, Eq. (4.6) is only valid for homogeneous samples. In for example layered samples, the species in the outermost layer will have relatively higher intensities as these electrons are most likely to escape from the sample. The signal from buried layers will in this case be attenuated due to the limited probing depth. In this regard, absolute values of the sample composition can often contain large measurement errors and should be used with care. A sounder approach is to use PES quantification to discover trends and changes over one measurement series [167].

4.2.5 Surface sensitivity and depth profiling

PES is a very surface sensitive technique due to the short IMFP of the electrons. This makes PES an ideal technique to investigate surface properties without attenuation from a dominating bulk signal. The IMFP increases with an increased kinetic energy of the outgoing PE, and is also larger in less dense materials (e.g., gases and liquids compared to solids).

In Figure 4.7 the IMFP in liquid propylene carbonate (PC) is shown as a function of the KE of the outgoing electrons [201]. PC has been used as the electrolyte solvent in the APPES measurements performed in this thesis. The IMFP of PC thus determines the maximum thickness of the liquid layer in these measurements, which allows for probing the solid/liquid interface. From Figure 4.7 it can be seen that by going from very soft X-rays to hard X-rays, the probing depth can be increased more than 10 times. This is highly useful for reaching and optimizing the signal from buried interfaces [206], and also to perform a depth profiling of the interphase [23, 42, 207].

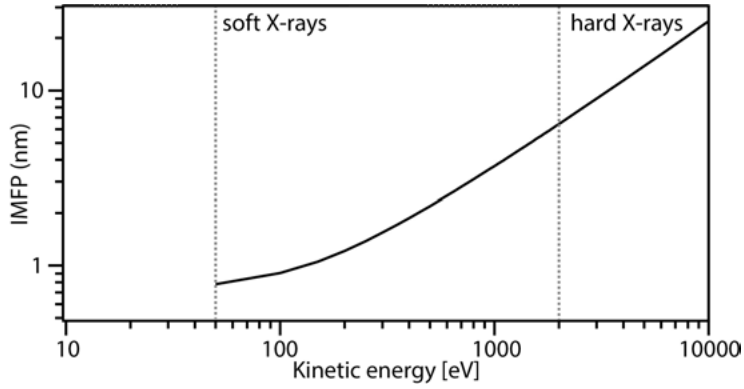

Figure 4.7: Inelastic mean free path of electrons traveling through PC as a function of kinetic energy of the photoelectrons.

The intensity (I) of PEs stemming from a specific depth (*d*) of the sample will be attenuated, compared to the intensity of the PEs stemming from the top layer. The attenuation can be described by the equation:

$$I = I_0 e^{-d/\lambda sin\theta}, \qquad (4.7)$$

where I_0 is the intensity from the top layer, λ the IMFP and θ the angle between the sample surface and the detector. The probing depth is usually defined as 3λ, corresponding to 95 % of the total detected intensity for θ=90°.

By changing the angle or the photon energy (and thus the IMFP) the probing depth can be altered. This allows for a non-destructive depth profiling of the sample. By the use of grazing angles or low photon energies, only the outermost surface layers are probed. These measurements can be compared to spectra measured with larger angles/higher photon energies, which contain

relatively more information from the (outer) bulk. By comparing peak intensities for different probing depths it is possible to estimate the thickness of a surface layer or detect chemical gradients in a sample. This is highly useful for understanding the degradation reactions occurring at battery interphases, since both the surface evolution and the redox reactions can be followed [208, 209].

4.3 Experimental setups

In this section the experimental setups used for the spectroscopic measurements performed in this thesis are described. Most of the experiments have been performed at synchrotron facilities. The main principles behind the generation of synchrotron light is briefly presented, and thereafter the hemispherical analyzer used for electron detection in PES is described. Finally, the experimental end-stations that have been used are discussed, with focus on their capabilities for studies of LIB interfaces.

4.3.1 Synchrotron radiation

Synchrotron radiation (SR) is generated by acceleration of electrons travelling at nearly the speed of light. The electrons are contained in a large electron storage ring (~100 m in diameter), where they are directed in a loop by the use of bending magnets. These apply a magnetic field in the vertical direction, causing a horizontally moving electron to accelerate inwards in a circular motion. The acceleration of the electron also causes emission of synchrotron radiation in a broad range of energies, ranging from infrared to hard X-rays. Due to the relativistic speed of the electrons the emission is concentrated in the forward direction [210, 211]. This results in a high brilliance and narrow bandwidth radiation that allows for fast, high resolution measurements using e.g., diffraction and spectroscopy [210, 212, 213].

In between the bending magnets there are also straight sections in the storage ring. In these sections insertion devices such as wigglers and undulators can be inserted. These devices consist of arrays of magnets with alternating polarity, causing the electron to move in an oscillating motion (“wiggle”). The wiggler contains an array of very strong magnets that gives a large amplitude to the electron oscillations. This gives a small interaction between the electron beam and the synchrotron radiation, resulting in a similar spectrum as for the bending magnet, but with an increased flux. In an undulator the magnetic field is weaker, resulting in a small oscillation of the electrons. In this case the radiation generated at each dipole magnet interferes with the radiation from the other magnets in the array. This gives rise to a more intense and focused beam concentrated at certain energies corresponding to constructive interference. The electron storage ring also contains a radio

frequency (RF) cavity with an oscillating electric field that is used to replenish the energy that the electrons lose by emitting radiation. A simplistic top view of the electron storage ring is shown in Figure 4.8.

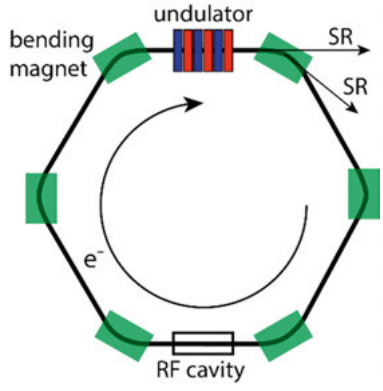

Figure 4.8: Illustration of the different components used to generate synchrotron radiation (SR).

Except for the high brilliance, one of the main advantages with synchrotron radiation is the tunable photon energy. A specific photon energy for a spectroscopic measurement can be selected by the use of a monochromator. This is one of several components included in a beamline. The beamline connects the storage ring to the end-stations, where the measurements are performed. Except for monochromatizing the light, the beamline is also used to focus the beam on the sample by the use of slits and mirrors.

The end-stations vary in design depending on the type of measurements it is designed for. Typically, a PES end-station can contain preparation chambers for sample modification (cleaning, deposition, gas exposure), a suitable sample holder, manipulators for moving the sample, and an electron detector. For this thesis synchrotron radiation was used to perform soft and hard X-ray PES. The synchrotron radiation sources used were Diamond Light Source (UK), BESSY II (Germany) and MAX IV (Sweden).

4.3.2 The hemispherical analyzer

To record a PE spectrum, the number of electrons are counted as a function of KE (or BE). There are various detectors that can be used for this purpose, but in this thesis a hemispherical electron analyzer was always used [214, 215].

The hemispherical analyzer consists of two concentric hemispherical electrodes, with different applied voltages. A simplified cross section of the analyzer is shown in Figure 4.9. The electrons enter the analyzer through an electron lens system, before reaching the entrance slit. The lens system is used to focus the electrons on the entrance slit to improve the collection efficiency, and it can also be used to accelerate/retard the electrons.

The trajectory of the electrons through the analyzer depends on their KE, and the voltage difference between the hemispherical electrodes. The voltage difference between the electrodes is configured by a pass energy, E_p. Electrons with a KE equal to E_p will move through the analyzer in a circular trajectory with radius $R_0=(R_1+R_2)/2$. Electrons that have a too high or too low KE relative to E_p, will collide into the outer or inner hemisphere, respectively. Thus, only electrons with an energy close to the E_p will reach the detector. The range of energies reaching the detector determines the energy resolution of the analyzer [214, 216, 217].

To avoid a different energy resolution for spectra of different elements (corresponding to different electron energies), a fixed E_p can be used. In this case, the electrons are accelerated/retarded (in addition to focused) by the lens system before arriving at the entrance slit. For every value of KE the number of electrons that reach the detector are counted, giving the resulting spectrum. The detector used is typically a microchannel plate detector.

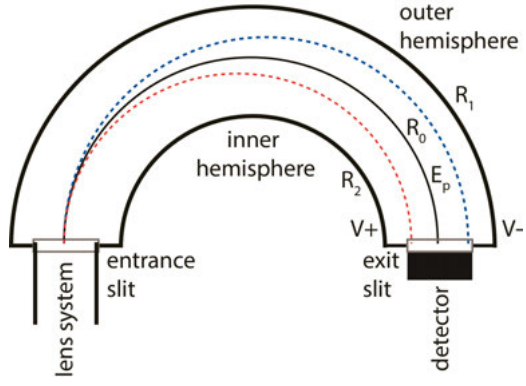

Figure 4.9: Cross section of the hemispherical electron analyzer showing the upper and lower boundary of electrons that can pass through the analyzer.

For ambient pressure instruments the electron lens system is also combined with a differential pumping system [218]. In this way the pressure can be decreased in steps from near ambient at the sample (~10 mbar) to UHV at the electron analyzer. Each pumping step can lower the pressure by ~2–3 orders of magnitude. By decreasing the pressure, the IMFP of the electrons is increased, and a larger number of electrons can be detected. This significantly improves the signal intensity of APPES instruments [217-220].

4.3.3 Experimental end-stations

In this thesis *ex situ* PES measurements are performed at the HIKE (BESSY II) and I09 (Diamond) end-stations. The range of available photon energies at the synchrotron facilities allows for a non-destructive depth profiling, and the hard X-rays can be used to probe buried interface layers.

Operando APPES measurements are performed at the HIPPIE beamline (MAX IV) using the electrochemical cell end-station. Here (near) ambient pressures are used to introduce a liquid phase in the measurements, and the electrochemical cell setup allows for spectroscopic measurements during battery cycling. A thorough description of the respective beamline and end-stations can be found in the beamline papers [221-223].

4.3.3.1 HIKE end-station at the KMC-1 beamline

At the HIKE end-station [221, 224, 225] synchrotron radiation is generated by a bending magnet. The beamline is equipped with a double crystal monochromator, where one of three pairs of crystals can be chosen; Si(111), Si(311), or Si(422) [225]. The choice of crystal pair can be switched during measurements to allow for a wide selection of photon energies. Altogether, the double crystal monochromator setup allows for photon energies with high flux and high energy resolution between 2–12 keV. The monochromatic beam is focused by hard X-ray mirrors. The minimum beam size on the sample is approximately 100 x 100 μm. In the normal setup the light irradiates the sample at grazing incidence. The spectrometer is placed at a 90° angle to the beamline, i.e., when grazing incidence is used this gives normal emission of the PEs (90° versus sample surface). This sample orientation maximizes the probing depth. However, the sample can also be rotated for other incident/emission angles. The electron analyzer at HIKE is a Scienta R4000 spectrometer, configured for high kinetic energies.

The samples can be transferred to the analysis chamber through the load lock by be use of a transfer rod [118, 171]. The transfer rod can be attached both to a glovebox for sample preparation of air sensitive samples, and to the load lock of the spectrometer. Transfer from the load lock chamber to the analyzer chamber is made in vacuum. The sample is mounted to a sample holder connected to motorized manipulators allowing for movement of the samples in the xyz-directions as well as sample rotation. The operative pressure of the analysis chamber during measurements of battery samples is typically in the ~10^{-7} mbar pressure range.

4.3.3.2 Surface science end-station at the I09 beamline

The I09 beamline at Diamond light source is unique as it can deliver both soft and hard X-rays focused to the same spot on the sample [222]. The X-rays are generated by the use of two undulators with different magnetic periods in order to generate both soft and hard X-rays. The desired photon energy for hard X-rays is selected by a Si(111) double-crystal monochromator and the beam is focused by hard X-ray mirrors. The soft X-ray beamline contains a plane grating monochromator and soft X-ray mirrors in order to collimate and focus the light. The beamlines also include diagnostics in order to focus both beams on the same focal spot of the electron analyzer. The combined range of photon energies accessible at the I09 beamline ranges from approximately 150

eV to up to ~18 000 eV. The large energy range gives excellent opportunities for non-destructive depth profiling of the samples. A Scienta EW4000 high-voltage electron analyzer is used for PES measurements.

The experimental end-station contains preparation chambers that allow for heating, sputtering and physical vapor deposition for sample preparation. A transfer "suitcase" is available for sample insertion under an inert environment (argon) or vacuum. The sample holder is connected to a manipulator that allows for sample positioning and rotation in two directions.

4.3.3.3 APPES end-station at the HIPPIE beamline

At the HIPPIE beamline [223] high flux synchrotron light in the soft X-rays regime is generated by an undulator. The beamline design is typical for soft X-rays, i.e., collimated light is irradiated on a plane grating monochromator and a series of soft X-ray mirrors are used for focusing the light. The photon energy range for HIPPIE is 250–2200 eV and the focused beam size is approximately 25 x 60 μm. The crucial feature of this beamline for the research performed in this thesis, is the ability to perform *operando* APPES measurements on electrochemical systems. This is enabled by the electrochemical cell design together with an APPES spectrometer [223].

The general idea for the design of APPES instruments, is to limit the distance the electrons have to travel in elevated pressures [219], as the IMFP is inversely proportional to the gas pressure. At a pressure of 1 mbar the IMFP is in the order of ~1 mm. Thus, the (maximum) distance the electrons need to travel in this pressure should be limited to the same range.

The end-station at HIPPIE is equipped with a Scienta HIPP-3 electron analyzer with a differential pumping system integrated into the electrostatic lens system [226]. Each differential pumping stage is separated from the previous by a small aperture. This setup allows for near ambient pressures in the analysis chamber, while UHV can be maintained in the hemispherical electron analyzer. The electron lenses minimize the loss of signal intensity from sample to detector. The closest distance the sample can be placed to analyzer cone is determined by the cone aperture. To keep the pressure at the sample close to the base pressure of the analysis chamber, the distance should be at least one aperture diameter [218, 227]. Thus, the aperture size is crucial for the maximum pressure that can be practically used in a measurement. However, a smaller aperture also decreases the PE detection efficiency, and limits the sample area that can be studied. The aperture size is therefore often chosen to approximately match the beam size. At HIPPIE the analyzer cone aperture used for the experiments in this thesis is 0.3 mm, allowing for pressures up to ~30 mbar.

There are currently two available cells that can be used at the APPES end-station at HIPPIE; a catalysis cell and an electrochemical cell. In this thesis the electrochemical cell has been used. A photograph of the analysis chamber is shown in Figure 4.10. A rather large vacuum vessel makes up the analysis

chamber. The vessel has a background pressure of ~10^{-5} mbar and can be backfilled with various gases. The load lock door can be connected to a custom-made glovebox for insertion of air sensitive samples. The chamber is equipped with a top and bottom manipulator that both can be moved in the xyz-direction, and the top one can in addition rotate. A sample holder with space for three electrodes is connected to the top manipulator. Each electrode position on the sample holder is equipped with electrical feedthroughs that can be connected to an external potentiostat in a three-electrode cell setup. The bottom manipulator is designed for placement of an electrolyte beaker, and also contain two electrical feedthroughs for alternative cell designs. This setup is ideal for creating a solid/liquid interface with the dip-and-pull method (see further in Section 6.2.2).

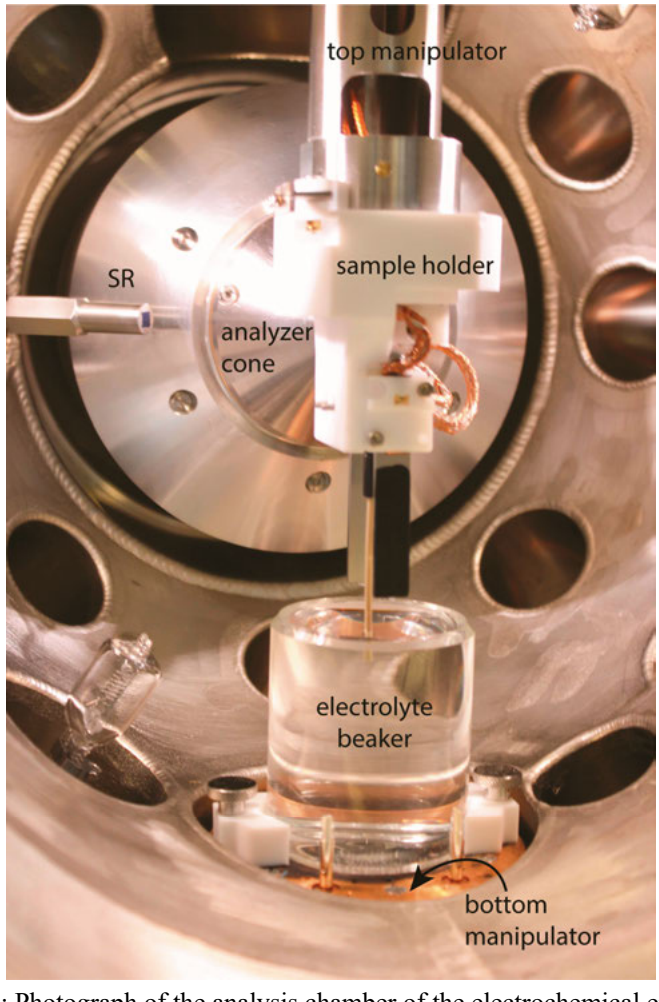

Figure 4.10: Photograph of the analysis chamber of the electrochemical end-station at HIPPIE. In the photograph a three-electrode cell is mounted and a water-based electrolyte is used in the electrolyte beaker.

5 Relating electrochemical potentials and spectroscopic energy levels

When electrochemical systems are studied by PES, it is essential to establish a common language to ensure that the results will be correctly interpreted by both electrochemists and spectroscopists. In this chapter, a connection between electrochemistry and PES is made, and some of the most common misconceptions in the fields are addressed.

5.1 Connecting "potentials" and energy levels

In physics, it is common to talk about the (electron) energy levels of a material, including core levels, the Fermi level, and the vacuum level. These concepts were introduced in Chapter 4. In electrochemistry, one rather talks about the "potential" of a species (or a reaction), and potentials such as the electrochemical, chemical and electrostatic potential were defined in Chapter 3. In both cases, denoting a potential energy to something (in this case most often an electron) only make sense if it is measured versus a defined reference. In this thesis, the "absolute" energy or potential of a species in a phase is defined versus the free species at rest in vacuum at infinity.

In practice, electron energies within the phase of interest are typically measured versus the Fermi level E_F (for condensed matter) in PES and versus the electron electrochemical potential $\bar{\mu}_e$ of a RE in electrochemistry. The possibly most important realization in order to combine PES with electrochemistry, is then that according to their definitions [119, 123, 228]:

$$E_F^\alpha \equiv \bar{\mu}_e^\alpha, \tag{5.1}$$

since both E_F^α and $\bar{\mu}_e^\alpha$ are defined as the energy required to bring an electron from an arbitrary reference (often vacuum at infinity for the definition) and add it to the phase α.

From the equality of E_F and $\bar{\mu}_e$, most of the other potentials and energies can also be related to each other. The different terms associated with electron energies that are mentioned in this thesis are summarized in Figure 5.1 and Table 5.1. In Figure 5.1 the relations between electron energies (blue vertical arrows), electric potentials (red vertical arrows) and energy levels (black

horizontal lines) are illustrated. This is highly useful for interpreting the *operando* APPES results. In Table 5.1 the corresponding terms and symbols are explained. The terms included are either measurements of electric potentials (in V), or electron energies (in eV). For the energy scale the potential energy of an electron at an electric potential V (i.e., –V in eV) is used.

A few things can be noted in Figure 5.1. First, it is drawn for the case of a condensed phase with an excess positive charge and a positive surface dipole, i.e., the electrostatic potentials lower the electron energy. This means that the vacuum level of the sample V_s is lower than the vacuum energy at infinity V_∞. In case of a negatively charged sample the opposite would be true. As all samples measured in this thesis are condensed phases, the BEs are referenced versus E_F, and the work function Φ of the sample is included in the figure. The direction of the arrows indicates in what direction the electron is moved according to the definition of the term. As can be seen the energies related to PES measurements (BE, Φ) are defined as energies to remove an electron, and the energies related to electrochemistry ($\bar{\mu}_e, \mu_e$) are defined for adding an electron. It is also illustrated that the total electrostatic potential ϕ (the Galvani potential) equals the sum of the surface potential χ and the Volta potential ψ.

Parameters that can be determined using electrochemical and/or spectroscopic tools include BEs, Φ, ψ, and $\bar{\mu}_e$. These parameters can for example be used to determine the work that can be performed by a chemical reaction, relative work functions of metals, or the chemical state of an element in a solid sample. However, the contribution from the chemical potential and the surface potential to the work function cannot be separated experimentally, and thus the Galvani potential cannot be directly measured [229, 230]. In addition, all electron energies are always measured relative to something, and in practice this is rarely the vacuum level at infinity. Thus, when electrochemistry is combined with spectroscopy, it is important to consider what practical reference is used for each measurement. This is in particular important to consider if several different phases, which are not in electronic equilibrium, are measured. This could for example be a solid/liquid interface. How these considerations affect measurements on LIB interfaces will be further discussed in Chapter 6.

Table 5.1: Different notations for electron energies used in electrochemistry and spectroscopy, and their description.

Term	Symbol	Unit	Description
Electrochemical potential	$\bar{\mu}_i^\alpha$	eV (or J/mol[6])	Total free energy of a species i in phase α relative to the same free species at vacuum at infinity.
Chemical potential	μ_i^α	eV (or J/mol[6])	Free energy of a species i in phase α, neglecting purely electrostatic contributions.
Galvani potential	ϕ	V	Electric work needed to move a unit positive test charge from infinity to the inside of a phase.
Surface potential	χ	V	Electrical work required to move a unit positive test charge from immediately outside the surface of a phase, to immediately inside the surface of a phase.
Volta potential	ψ	V	Electrical work required to move a unit positive test charge from vacuum to immediately outside the surface of a phase.
Fermi level	E_F	eV	Energy required to bring an electron from vacuum at infinity and add it to a phase α. Equal to $\bar{\mu}_e^\alpha$.
Binding energy	BE	eV	Energy required to remove an electron from a core level and bring it to the Fermi level of the phase.
Work function	Φ	eV	Minimum energy required to remove an electron from a phase and bring it to vacuum immediately outside the surface.

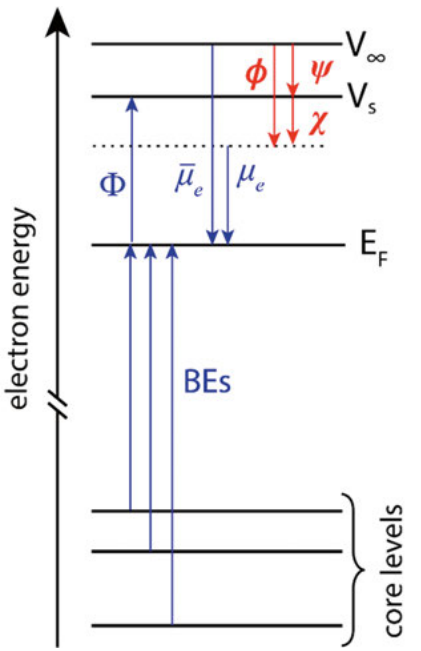

Figure 5.1: Illustration of electron energies and their relation to each other.

[6] J/mol is the more common unit in chemistry, however in this thesis the unit eV is used.

5.1.1 The Fermi level and the redox potential

In Section 4.1.2 the Fermi level of a solid was briefly discussed according to the physical definition; E_F is defined as an energy level where the probability of electron occupation is exactly ½. Since E_F is equal to $\bar{\mu}_e$, E_F can also be defined according to the electrochemical definition.

In section 3.1 it was described how the standard reduction potential of a reaction (EMF) could be defined from the Gibbs free energy of the reaction ΔG_{red} (Eq. (3.10)). According to the definition, the EMF of the reduction half-reaction is equal to E^0, or the negative of $\bar{\mu}_e$ (Eq.(3.5)). Thus, E_F or $\bar{\mu}_e$ of a phase can be defined according to [231]:

$$E_F = \bar{\mu}_e = -E_{rxn} = \bar{\mu}_R - \bar{\mu}_O \tag{5.2}$$

where $\bar{\mu}_R$ and $\bar{\mu}_O$ are the electrochemical potentials of the reduced and oxidized species, respectively. Consequently, E_F of any phase containing a redox couple can be defined from E_{rxn} (or alternatively from ΔG_{red}).

Over the years, there has been some controversy regarding the relation between E_F and the redox (reduction) potential of a reaction [232]. This controversy largely seems to stem from the different references used in physics and electrochemistry, and an inconsistent use of the term "absolute" electrode potential [128-130]. However, from the definitions of the terms it is nevertheless clear that E_F, corresponding to the work required to bring an electron from vacuum at infinity and add it to the phase α, must be equal to the reduction potential of the (virtual) redox reaction where a free electron in vacuum at infinity (denoted V) is added to a phase α according to [228, 231]:

$$O^+(\alpha) + e^-(V) \rightarrow R(\alpha). \tag{5.3}$$

The complications arise since there is no reliable way to determine the absolute reduction potential of this reaction (see Section 3.1.4). Instead, reduction potentials are typically measured versus a RE. In this case, the value equals the difference in Fermi level ($\Delta E_F = \Delta\bar{\mu}_e$) between the WE and the RE, and it will differ from the Fermi level versus absolute vacuum by a constant equal to the absolute voltage of the RE.

In PES the Fermi level is often referenced versus the vacuum just outside the sample. This is a measurable parameter, corresponding to the work function of the sample [128]. The work function differs from the Fermi level vs. vacuum at infinity by a constant equal to the Volta potential.

Thus, the Fermi level can always be correlated to the reduction potential, but the addition of a constant is necessary if different references are used for determining the two values.

5.1.2 The Fermi level of a solution

In line with Eq. (5.2), E_F can be defined for any solution containing a redox couple. If the energy corresponding to this work should be called a Fermi level, has however been argued [228]. The main arguments against using the notation E_F include that there are no free electrons in the solution, and that the solution might not exhibit Fermi-Dirac statistics. However, in solids E_F have been defined despite these conditions not being fulfilled (e.g., in semiconductors with bound electrons). Consequently, there is no particular reason for not calling it E_F in a liquid as well. Regardless of the preferred term for this quantity, any liquid with a redox couple will have a well-defined equilibrium (redox) potential, corresponding to the negative of the electron electrochemical potential of the liquid.

Even though the liquid phase does not contain any free electrons, electrons can still be accepted/donated from/to another phase by redox reactions. Thus, if a liquid solution with a redox couple is put in contact with a conductive phase, electrons will be transferred from the phase with higher $\bar{\mu}_e$ to the one with lower $\bar{\mu}_e$, until the electron electrochemical potentials are equal (corresponding to the alignment of "Fermi levels") [123, 130]. Electronic equilibrium will in this case be achieved, and there will be no voltage drop over the electrode/electrolyte interface. Instead, there will be a contact potential (electrostatic potential) difference $\Delta\phi$ between the phases, corresponding to the difference in chemical potential of the electron ($\Delta\mu_e$) in the solid and liquid phase. This potential difference cannot be directly measured, as first stated by J. W. Gibbs in the late 1800s [119, 120, 229, 233].

5.2 Avoiding some misconceptions

In both PES and electrochemistry one can study relative energies of electrons in different phases, and consequently also the energy required to transfer an electron from one phase to another. Extensive work was performed in the 1980s in order to connect these fields and establish a common ground in the interdisciplinary study of for example semiconductor/electrolyte interfaces. Despite these works [128-130, 228, 232], the connection between physical and electrochemical terms sometimes still causes confusion and misinterpretations [123]. In this section I therefore try to highlight some of the most common sources of misunderstandings in the fields of physics and electrochemistry, and specifically in the interdisciplinary research combining the two.

A first complication in this regard, is that the word "potential" is often poorly defined, and can refer to a voltage (electrode potential, cell potential etc.) as well as a relative electron energy (electrochemical potential, chemical potential etc.). This is highlighted in a recent perspective by Boettcher *et al.* [123]. The authors emphasize that to avoid these common confusions, it is

important to always define what type of potential is referred to, and in addition for what species and in what phase.

Possibly as a result of the poorly defined potentials, the electrochemical potential as defined in electrochemistry is sometimes referred to as the chemical potential, or the total chemical potential in physics. The chemical potential used in electrochemistry, would then be denoted by "inner chemical potential" [161, 234, 235]. This can of course be confusing, as the same term is used in different ways. Still, as long as the usage of a potential is explicitly defined, it should remain clear to the reader what quantity that is referred to.

In this thesis the term electrochemical potential is preferred, as it allows for the conceptual separation of the (electron) energy into contributions stemming from the chemical environment (μ), the surface properties (χ) and the external electrostatic fields (ψ) (where the sum of the latter two gives the total electrostatic potential, ϕ). This is in particular helpful for electrochemical systems, where applied external fields can induce electrostatic potential differences that are independent of the chemistry of the materials. Thus, throughout this thesis the chemical potential will only denote the contribution from the local chemical environment, and electrochemical potential will be used for the total potential energy of a species in a phase.

There are some special cases in which the electrochemical and chemical potential are the same, including (naturally) all neutral species. The movement of a neutral particle is independent of ϕ, and the driving force for movements only stems from differences in μ (e.g., due to concentration gradients). Another special case is for a single electronically conductive phase, where ϕ is constant everywhere. Also in this case the movement of a species within the phase will only be driven by a difference in μ, which in the case of a constant ϕ equals the difference in $\bar{\mu}_i^\alpha$ (i.e., $\Delta\bar{\mu}_i^\alpha = \Delta\mu_i^\alpha$). However, these special cases can in general not be applied to electrochemical systems.

Another source of confusion in electrochemistry is that the measured voltage of an electrochemical cell sometimes is referred to as an electric potential difference, $\Delta\phi$. This usage can be found in electrochemical textbooks [119, 120], and is inherently confusing since it is easy to misinterpret as $\Delta\phi$ between the electrodes, while it should mean $\Delta\phi$ between the contacts in the voltmeter. Here, it is important to recognize that **$\Delta\phi$ can only be measured between phases with the exact same chemical composition,** i.e., phases with equal chemical potential [119, 236]. Thus, while it is often true that the measured voltage equals $\Delta\phi$ between the two electric contacts in the voltmeter, this only holds since these contacts are made of the same material (commonly Cu). As the contacts are electrical conductors, they will be in electronic equilibrium with the electrodes and the measured voltage difference will therefore be equal to the negative of the electron electrochemical potential difference between the electrodes [123, 124]. The RE and WE are almost always made of different materials, and the voltage between them is thus *not* equal to $\Delta\phi$ between them.

The fact that a voltmeter measures $\Delta\bar{\mu}_e$, and not $\Delta\phi$, can be realized by considering the case where two different metals are put into contact [123]. In this case electrons will initially move from one metal to the other to compensate for the difference in μ_e. This generates a charged interface between the two metals. However, if the voltage between the two metals is measured with a voltmeter, it will show 0 V. This is because the voltmeter measures the overall driving force for the electrons to move from one phase to another (i.e., $\Delta\bar{\mu}_e$), which is zero when electronic equilibrium is achieved.

Another misconception in electrochemistry is that the stable voltage window of an electrolyte sometimes is denoted by the HOMO and LUMO of the solvent. This notation can be found in several highly influential papers [8, 48, 237]. Although the concepts sometimes can be related, the actual case is more complex and the stable voltage window of an electrolyte will depend on the chemistry of the entire electrolyte (salt, solvent and impurities) [238]. The stable voltage window should be defined as the voltage region in between the reduction and oxidation potential of the electrolyte. That the reduction potential does not coincide with the LUMO (and similarly the oxidation potential is not set by the HOMO of the solvent) can be understood by considering the case of liquid water. The energy difference between the HOMO and LUMO for liquid H_2O can be calculated to ~8.9 V [239]. However, it is well-known that the voltage stability window of water is ~1.2 V, making it an unsuitable choice for e.g., high voltage batteries. The stable voltage window of water is limited by the oxygen evolution reaction at high voltages (0.81 V vs. SHE) and the hydrogen evolution reaction at low voltages (-0.42 V vs. SHE) [127]. Similarly, the HOMO of the common LIB solvents EC and DMC have been calculated to ~9.1 V and ~8.3 V vs. Li/Li^+, respectively. The corresponding oxidation potentials are calculated to ~6.5 V vs. Li/Li^+ for EC and 5.7 V vs. Li/Li^+ for DMC [240]. Thus, using the HOMO/LUMO instead of the oxidation/reduction potential often leads to an overestimated electrolyte stability window.

6 Developing a methodology for *operando* APPES on LIB interfaces

Whenever PES measurements are performed on electrochemical systems, it is important to understand how the electrochemical processes affect the spectroscopic data [172, 173]. This is important both for *ex situ* and *operando* measurements. In Paper I, an *ex situ* study is performed that addresses a number of challenges associated with interpreting PES measurements of electrochemical systems. These results are summarized in Section 6.1.

Accounting for the BE shifts as a result of electrochemical processes will be even more crucial in *operando* APPES measurements, where also a liquid phase is present, and the electrode voltage is continuously changed. Moreover, *operando* APPES can be used as a tool to further understand these shifts, by probing the electrochemical reactions *operando*. In this way the shifts in BE/KE can be followed in detail for a controlled voltage.

A large part of the work in this thesis has been devoted to evaluating the practical and theoretical considerations in order to perform *operando* APPES measurements on LIB interfaces. This work is presented in Paper II-V and summarized in Section 6.2-6.4 of this chapter.

6.1 Effects of electrochemical processes on BE shifts

In Paper I, a general strategy towards reliable BE calibration of electrochemical systems on postmortem samples is outlined. The strategy is based on investigating the BE shifts that are measured as a result of SEI formation, changing the electrode voltage, and changing the state-of-charge of the electrode.

The effect of SEI formation on BE shifts has been observed in several studies [169, 172, 195, 196]. However, in many cases SEI formation occurs together with other electrochemical reactions, and it can be difficult to single out the effects stemming from this process. In Paper I, the SEI formation is therefore studied on a gold electrode, which is (essentially) inert in the voltage window (1.0–0.4 V vs. Li/Li^+) used for the electrochemical cycling. The PES results show a shift in BE for the carbon compounds associated with interphase formation as the SEI thickness increases. For a SEI thinner than the probing depth, both surface carbons directly adsorbed at the Au interface and

in the SEI are probed, and it can be expected that the carbon compounds can be located at different electrochemical potentials. This is indicated by broad C 1s peaks. After the formation of a thick SEI (50 and 150 cycles) the C 1s peaks are more distinct and the BE shifts of +2 eV relative to the pristine sample matches very well with the difference in electrode voltage (~3 V at OCV and 1 V for cycled samples, both vs. Li/Li^+).

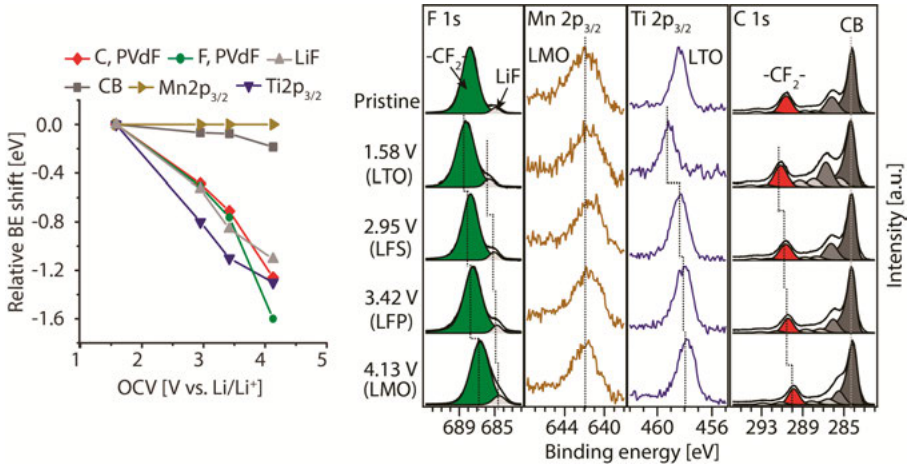

Figure 6.1: BE shifts for different electrode OCV of a mixed material composite electrode. Conductive phases show very small shifts in BE, while insulating/semi-conductive phases shift in BE when the voltage is changed. Adapted from Paper I.

The effect of altering the electrode voltage is further studied by preparing a mixed material electrode, consisting of four different AMs with different reduction potentials vs. Li/Li^+; $Li_4Ti_5O_{12}$ (LTO, 1.6 V), Li_2FeSiO_4 (LFS, 3.0 V), $LiFePO_4$ (LFP, 3.4 V), and $LiMn_2O_4$ (LMO, 4.1 V). Also, an electrode binder and a conductive additive (carbon black, CB) are added to improve the electrode performance. The mixed material composite electrode is cycled between 1.5–4.5 V vs. Li/Li^+ and four different samples stopped at each of the four lithiation plateaus are investigated with PES. The BE shifts as a function of electrode OCV after cycling are evaluated. The results displayed in Figure 6.1 show that the BE of the phases with mobile charges (LMO and CB) are essentially unaffected by the change in electrode OCV. This can be expected for phases that are well-aligned to E_F of the spectrometer, i.e., for conductive phases. The phases with poor conductivity on the other hand shifts to lower BE with an increased electrode OCV. As this shift occur even for electrochemically inactive phases such as the binder, this effect is attributed to a change in electrostatic potential rather than a change in chemical environment of the species.

The BE shifts during lithiation of a LMO electrode and a nano-Si electrode are also studied in Paper I. The BE shifts are found to be dependent on the type of redox reaction. For a phase transformation reaction new peaks

corresponding to the chemical environment in the new phase can be expected to grow as the phase transformation proceeds. This is largely the case for LMO. For a solid solution or alloying reaction, the lithium content is changed more gradually. In this case a more continuous BE shift of the PE peaks can be expected. This is observed for the nano-Si electrode.

Altogether, these results serve as a basis for interpreting the BE shifts of electrochemical systems. To further understand these shifts, it is desirable to perform *operando* APPES measurement where these effects can be observed directly during cycling. The requirements for these measurements and the obtained results are discussed in the following sections of this chapter.

6.2 Practical considerations

To be able to implement *operando* APPES measurements on real LIB interfaces there are several prerequisites. To begin with, it is necessary to characterize different liquid electrolytes, which cannot be studied with traditional PES due to the vacuum constraint. Further, to be able to probe the solid/liquid interface directly, an interface where either the solid or the liquid phase is thinner than the probing depth of the electrons needs to be prepared. Finally, to perform electrochemical cycling in *operando* measurements, a suitable cell that functions well from both an electrochemical and a PES perspective needs to be designed. In this section these aspects are discussed.

6.2.1 Liquid stability

In Paper II, APPES measurements are performed on a LIB electrolyte. The electrolyte consists of a solution of 1 M LiTFSI in PC. A static drop of both the electrolyte and only the pure PC solvent are probed. In order to stabilize the liquid during APPES measurements, the vapor pressure of PC needs to be close to saturation pressure in the chamber. This can be done by adding PC gas from a leak valve, or by keeping a large liquid container in the chamber from which “sacrificial” evaporation can occur. Stabilizing the droplet by a background pressure of another gas was not successful for the timescale needed for practical measurements.

When the droplet is irradiated by X-rays, it is observed that the salt components degrade due to beam damage. When high intensity synchrotron radiation is used, severe radiation damage is seen after 40 minutes of irradiation. The solvent on the other hand is essentially unaffected after the same time of X-ray exposure. When an in-house setup with Al Kα radiation is used, the salt is stable towards light exposure for at least 1 hour. The experiments also show that the convection of degradation products in the droplet seems limited, and by moving the measurement spot slightly sideways a fresh spot unaffected from beam damage can be obtained.

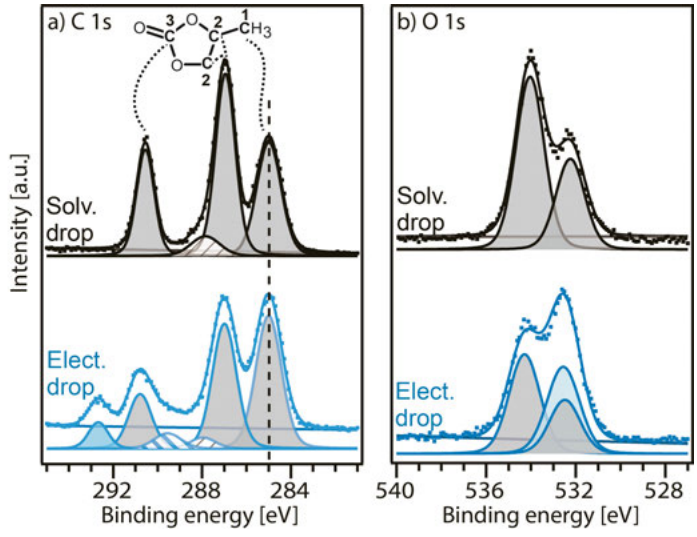

Figure 6.2: APPES spectra of the C 1s (a) and O 1s (b) core level for the pure PC solvent (solv. drop) and the electrolyte droplet (elect. drop). Adapted from Paper II.

The results presented in Paper II show that the spectra of the PC solvent are closely representative of the stoichiometry of the PC molecule. This is illustrated in Figure 6.2 where the C 1s peaks show a 1:2:1 ratio, and the O 1s peaks a 2:1 ratio for the solvent drop. For the electrolyte drop more adventitious carbon can be seen, which is believed to be related to an increased surface tension by the addition of salt. The relative quantities of salt and solvent are investigated by comparing the area of the CF_3 salt peak (blue peak at ~293 eV) and the CO_3 solvent peak (grey peak at ~291 eV). The calculations give a salt concentration that is approximately two times higher at the surface compared to the bulk (probing depth of ~6 nm and ~12 nm, respectively). The bulk concentration agrees well with the expected salt concentration for a 1 M solution. The results in Paper II show the importance of carefully characterizing the liquid prior to advancing to interface measurements, and in addition highlights the importance of the measurement conditions for the liquid stability.

6.2.2 Creating a solid/liquid interface

To be able to probe the solid/liquid interface either the solid or the liquid needs to be thinner than the probing depth of the outgoing PEs. In order to achieve this, either thin solid membranes or a thin liquid film can be used. A thin liquid film on a solid surface can be created by a variety of methods, including condensation, immersion of solid particles in a liquid jet, or by a dip-and-pull technique [206, 241, 242]. In this thesis the dip-and-pull method is used to create a solid/liquid interface, since this technique is relatively easy to combine with an electrochemical cell setup.

In the dip-and-pull technique a solid substrate is immersed into a liquid contained in a beaker [206, 243-245]. The solid is thereafter slowly retracted from the beaker, and as the solid is pulled up a thin liquid meniscus is created on the solid surface. This is illustrated in Figure 6.3 (not to scale). With this method it is easy to control e.g., the concentration or pH-value of the bulk solution, and the meniscus will (at least initially) to a large extent be representative of these properties. Any variations of salt concentration in the thin meniscus can also be measured directly by APPES by examining spectra of both solvent and salt, e.g., as in the measurements performed in Paper II.

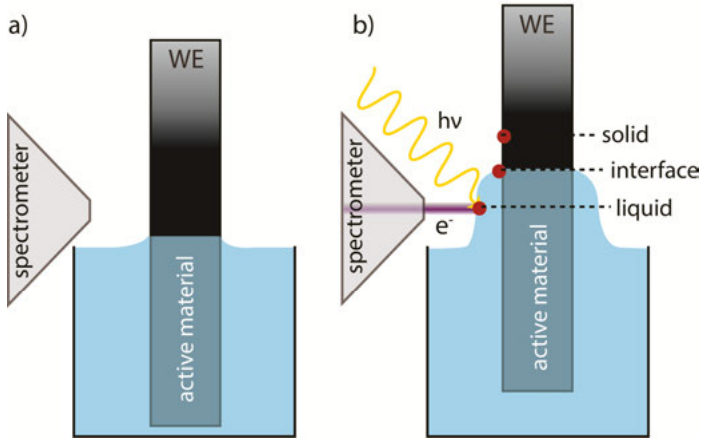

Figure 6.3: Illustration of the immersed electrode (a) for electrochemical cycling, and the retracted electrode (b) with a liquid meniscus for APPES measurements. The measurement positions where the solid, interface, and liquid can be probed are indicated. For simplicity only one electrode is shown. Adapted from Paper IV.

The thickness of the liquid meniscus created by the dip-and-pull method depends on the wetting properties, the withdrawal speed, the viscosity of the liquid, and the surface tension. This was described already in 1942 by Landau and Levich for a dip coating procedure [246, 247]. In several APPES measurements on water-based systems, the thickness of the liquid meniscus has been determined to be in the range of ~10-30 nm [244, 245, 248, 249]. The thickness is also seen to depend on the vapor pressure and the applied electrode voltage [244, 245, 248]. With a thickness in this range, the liquid film can be probed through with hard (tender) X-rays, but remains challenging to see through with soft X-rays.

The liquid meniscus created by the dip-and-pull method has been found to be reasonably stable for hours when a saturation pressure of the liquid solvent is kept in the chamber [250]. It is also confirmed that the liquid film is continuous and connected to the bulk electrolyte solution for films with a minimum thickness of ~10-20 nm [245, 248]. After extended measurement times (hours) the thickness of the liquid layer at the top of the meniscus becomes thinner. One reason for this discussed in the literature is the influence

of gravitational forces [243]. However, this can also be a result of the electrochemical cycling [251] or small changes in vapor pressure.

In the measurements performed in Papers III-V porous composite electrodes (typical for real batteries) as well as thin film electrodes are studied using the dip-and-pull method. Unfortunately, porous electrodes soak up the liquid electrolyte very efficiently and the entire electrode becomes covered by a liquid film, even though only the lower part of the electrode is immersed into the electrolyte. In this case it was not possible to see through the liquid layer with APPES.

In order to probe the solid/liquid interface directly, thin film electrodes were used instead. In this case, sputter deposition was used to apply a thin film coating consisting of only AM (no binder or conductive additives) to a polished substrate. This resulted in flat, dense sample surfaces. However, also in this case the region where both the solid and liquid could be probed simultaneously was very narrow. Thus, with soft X-rays (~2 keV) the solid/liquid interface could only be probed at the very edge of the meniscus.

During measurements on the solid/liquid interface, it is also found that the signal from the solid quickly decays during measurements. This is illustrated in Figure 6.4 for three consecutive O 1s spectra. The MO signal stemming from the bulk quickly decays during measurements, and surface species similar to the PC solvent is adsorbed on the sample surface. This is especially seen during high voltages/currents. The buildup is localized to the measurement spot, and by moving sideways on the sample an unaffected area can be found. Similar effects have also been noted in other publications [244, 249].

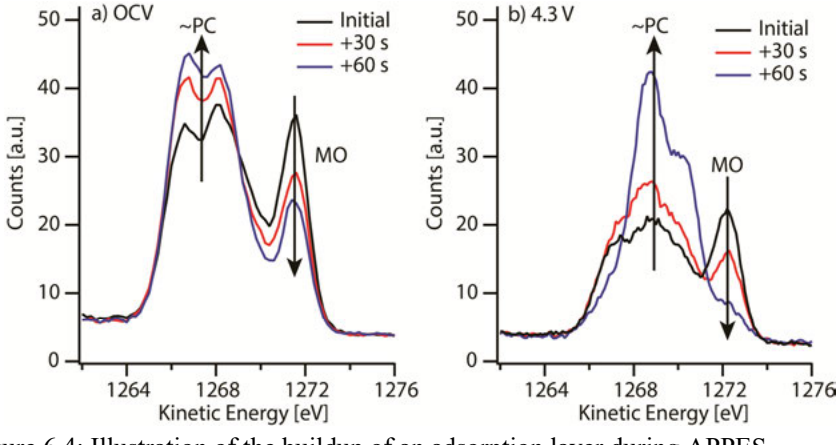

Figure 6.4: Illustration of the buildup of an adsorption layer during APPES measurements on the solid/liquid interface. Three consecutive O 1s spectra are measured at the same spot. Adapted from Paper V.

6.2.3 Functionality of the electrochemical cell

In the *operando* APPES measurements performed in this thesis (Paper III-V) the three-electrode setup available at the electrochemical end-station at HIPPIE is used (see Section 4.3.3.3). In order to precisely control the voltage of the WE electrode, it is desired that the RE behaves as an ideal non-polarizable electrode and that the resistance of the bulk electrolyte can be kept to a minimum. Further, if the aim is to study the kinetics of the redox reactions at the WE, it has to be ensured that the CE does not limit or interfere with these reactions. To achieve these conditions, the original setup at HIPPIE has been slightly modified for LIB measurements. The used three electrode setup is pictured in Figure 6.5.

The RE used in our APPES setup is a Li/Li^+ reference consisting of a small Li metal piece (approximately 2x5 mm) on a Cu wire. The Li/Li^+ RE is the most common for a LIB system, as it behaves close to an ideal non-polarizable electrode. Since essentially no current is drawn through the RE, it is sufficient with a small Li piece. By also using an electrolyte with high Li-ion concentration, the ideal non-polarizable behavior of the RE can be ensured.

Any effects from an iR_s-drop over the bulk electrolyte should also be limited in the voltage measurement. In order to do this, the ionic conductivity of the electrolyte should be high, and the RE should be placed close to the WE. For most liquid electrolytes the iR_s-drop is not a problem, as the Li-ion mobility generally is high (and especially much higher compared to the Li diffusion in the bulk electrodes) [252]. In the APPES setup the RE is also placed close to the WE by bending the Cu wire. To prevent a short circuit while keeping a small distance between WE and RE, the RE is covered in a thin polyethylene tube (see Figure 6.5).

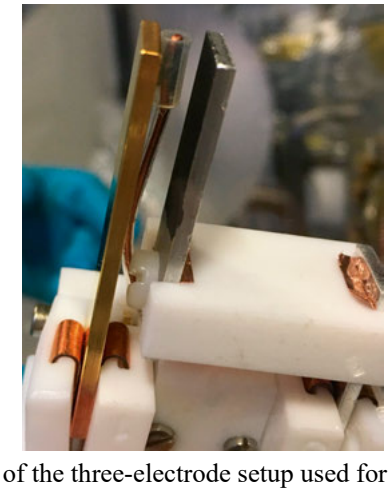

Figure 6.5: Photograph of the three-electrode setup used for operando APPES measurements. A white PTFE adapter is used to move the CE (here NMC) closer to the WE (here Au). A Li metal piece covered by a PE tube is attached to a Cu wire and placed close to the WE.

In the thin liquid meniscus on the other hand, the resistance will be significantly higher due to the limited number of ions in this small volume. In particular, the ion transport in the direction parallel to the WE surface is slow, especially for very thin films [206, 248, 251]. Thus, if *operando* APPES measurements are performed on the liquid meniscus, the ion transport in the meniscus can be rate determining for the redox reactions at the interface. This is especially an issue if the meniscus is probed "far" above (>4 mm) the bulk electrolyte. In this case, the measurements will not be representative of the kinetics for a regular battery cell. Further, if measurements are performed on the thin meniscus for a long time, it eventually starts to dry out and/or lose contact with the bulk electrolyte. Both these problems can be avoided by re-dipping the electrodes in between APPES measurements. The electrodes are then immersed in the electrolyte during electrochemical cycling and only withdrawn during the course of the APPES measurement. In this way a "snapshot" of the solid/liquid interface during more realistic cycling conditions can be gained.

The CE in a LIB provides both the electrons and Li-ions for the redox reactions at the WE. To avoid limiting the half-cell reaction at the WE, the chosen CE should always have a higher capacity than the WE, and the charge and mass transfer should be sufficiently fast. The mass transfer of Li^+ in a LIB is typically ensured by having a large excess of Li^+ in the electrolyte, so that the reaction rate is not limited by Li^+ diffusion from the bulk CE to the WE. The mass transfer can also be facilitated by decreasing the distance between the WE and CE. In our setup this is done by using an "adapter", as shown in Figure 6.5. The distance between WE and CE using this setup is around 1 cm. The electron conductivity is already fast for conductive electrode materials, and can otherwise be increased by adding conductive additives to the AM. In this thesis such additives are employed in the composite electrodes, while the model systems have sufficiently high conductivity.

6.3 Theoretical aspects

To connect the electrochemical and PES measurements in *operando* APPES, a common energy reference is necessary (as discussed in Chapter 5). This connection is usually made by electrically contacting one of the electrodes to the spectrometer. The most common choice is to connect the WE to the spectrometer to align their Fermi levels [244, 245, 248, 249, 253].

If the WE is electrically connected to the spectrometer, E_F^{WE} will be the energy reference that all PE peaks are measured against. This means that when the voltage of the WE (vs. the RE) is changed, the reference for the PES energies (KE or BE) is also changed. In this case a core level that is *unaffected* by the change in voltage (e.g., the electrolyte for an ideal polarizable interface)

will show a change in BE. This is illustrated in Figure 6.6 in the simplified case where no charge transfer occurs over the WE/electrolyte interface.

One could also imagine that it sometimes would be preferable to connect the RE to the spectrometer [254]. In this case, E_F^{RE} is the energy reference for both the electrochemical and the APPES measurements. Consequently, any core level unaffected by a change in WE voltage will have a constant BE, while the core levels that have an altered energy versus E_F^{RE} show a corresponding BE shift. However, since the voltage between WE and RE is known from the electrochemical measurements, an electron energy measured versus the WE can be converted to an energy versus the RE, and vice versa. In the APPES measurements performed in this thesis, the WE is always connected to the spectrometer. Thus, this case will be considered in the following model, presented in Paper III.

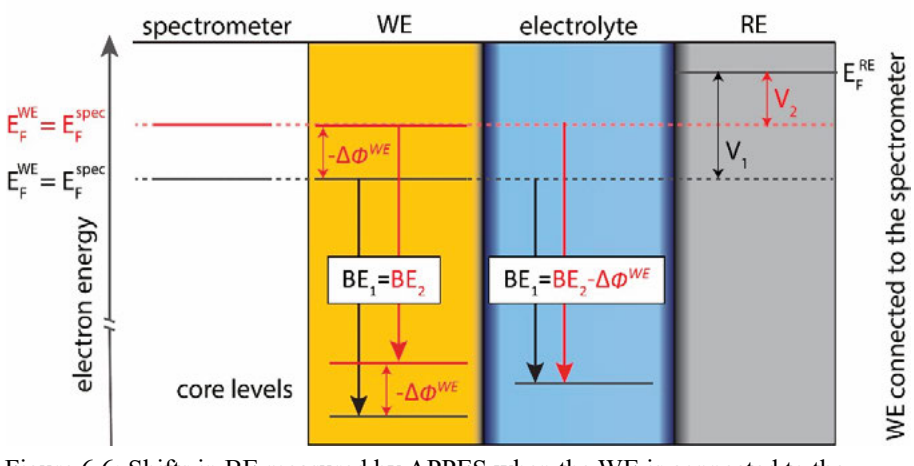

Figure 6.6: Shifts in BE measured by APPES when the WE is connected to the spectrometer. The BEs are shown for the case of no charge transfer when the voltage is changed from $V_1 > V_2$. Adapted from Paper III.

6.3.1 A model for interpreting *operando* APPES results of electrochemical interfaces

Operando APPES can be used to measure electrochemical potential differences between different phases. To measure the "true" difference in $\bar{\mu}_e$ between two phases, their Fermi levels should be measured. While this is possible for metals, with available energy states at the Fermi level, the case for semiconductors, insulators and liquids is different. For these materials E_F (if it is defined at all) is located in the gap between available states. Thus, measuring E_F of non-metals is not straightforward. Instead, it is interesting to consider what information that can be gained by measuring a core level by *operando* APPES.

The electron electrochemical potential $\bar{\mu}_e$ (or voltage) of an electrode can be changed either by changing the electron chemical potential μ_e, the electrostatic potential ϕ, or both. If $\bar{\mu}_e$ is changed solely by a change in ϕ, the energy of all electron levels within the phase are affected equally. This means that when the WE is electrically connected to the spectrometer, shifts in ϕ^{WE} will not affect the measured KE[7] of the electrons stemming from the WE (see Figure 6.6).

If the change in voltage instead stems from a change in μ_e, the KE shifts of different electron energy levels will in general not be equal. The KE shift will depend on the interaction between the electrons in a specific energy level and the added/removed electron(s). In this case the relative shift in energy of different core levels (vs. E_F^{WE}) can be measured by APPES, while the shift in energy of E_F (as always) can be measured by the voltage.

Thus, in an *operando* APPES setup where a conductive WE is electrically connected to the spectrometer, a shift in KE of PEs stemming from the WE is only expected for chemical shifts (see Section 4.2.3.1). KE shifts of the electrolyte PE peaks will on the other hand reflect the change in $\bar{\mu}_e$ of the electrolyte relative to the WE (i.e., the PES energy reference), and can be due to both a change in μ_e, and/or ϕ.

From the above discussion, it follows that the change in $\bar{\mu}_e$ cannot generally be obtained directly by measuring the KE shift of a core level. However, this can be done in the special case of a phase α with constant chemical potential μ_e^α. In this case $\Delta\bar{\mu}_e^\alpha = -\Delta\phi^\alpha$, and the change in $\Delta\bar{\mu}_e^\alpha$ can be evaluated from the KE shift of any core level of the phase. If this condition is met for the liquid electrolyte, it highly facilitates the APPES measurements. This is an important foundation for the data interpretation models presented in this thesis.

In Paper III, the three assumptions that; (i) the RE behaves as an ideal non-polarizable electrode, (ii) the iR_s-drop in the bulk electrolyte can be neglected, and (iii) the chemical potential of the liquid (electrolyte) is constant, are used to develop a general model for interpreting *operando* APPES results of solid/liquid interfaces.

According to assumptions (i) and (ii), the voltage of the RE is fixed ($\Delta\bar{\mu}_e^{RE} = 0$) and $iR_s \approx 0$. Thus, any change in voltage (ΔV) between the WE and RE solely stems from a change in $\Delta\bar{\mu}_e^{WE}$:

$$-\Delta V = \Delta\bar{\mu}_e^{WE}. \qquad (6.1)$$

Here, the WE voltage and also $\bar{\mu}_e^{WE}$ are considered versus an arbitrary (equal) fixed reference, such as the RE or the vacuum level at infinity.

In APPES, the KE of all PE peaks are measured relative to E_F of the electrode that is connected to the spectrometer. In our case this is the WE (i.e.,

[7] The shift in KE can also be directly converted to a shift in BE according to ΔKE=-ΔBE. In this model it is chosen to discuss the shifts in terms of KE.

not a fixed reference). If (iii) holds, $\Delta\bar{\mu}_e^{el} = -\Delta\phi^{el}$ and any electron level of the electrolyte can be measured to evaluate the shift in $\Delta\bar{\mu}_e^{el}$ versus E_F^{WE}. Under these conditions the measured change in kinetic energy (ΔKE) corresponds to the change in $\bar{\mu}_e$ between electrolyte and WE (both vs. an arbitrary fixed reference):

$$\Delta KE = \Delta\bar{\mu}_e^{el} - \Delta\bar{\mu}_e^{WE}. \tag{6.2}$$

Finally, $\Delta\bar{\mu}_e^{el}$ (vs. an arbitrary reference) is received by combining Eq. (6.1) and Eq. (6.2):

$$\Delta\bar{\mu}_e^{el} = -\Delta V + \Delta KE. \tag{6.3}$$

In accordance with this model, *operando* APPES can be used to directly evaluate a difference in $\bar{\mu}_e$ over the solid/liquid interface.

6.3.2 Two ideal cases

In Section 3.2.1 the ideal polarizable electrode and ideal non-polarizable electrode were introduced. These ideal cases can be useful to understand the behavior of an electrode or interface in specific voltage regions or during limited currents.

The ideal polarizable electrode represents an interface where no charge transfer occurs. In practice, this is the case in voltage regions where negligible redox (faradaic) reactions occur. If the electrode voltage is changed without inducing any faradaic reactions, this change of voltage will only stem from a change in ϕ, while μ remains constant. This will result in the buildup of an EDL between the solid and liquid, giving a voltage drop over the electrode/electrolyte interface. The (change in) voltage drop can be evaluated by measuring the KE shifts of the electrolyte PE peaks.

For an ideal non-polarizable RE and an ideal polarizable WE, the whole change in voltage can be expected to be located as a voltage drop at the WE/electrolyte interface. When *operando* APPES measurements are performed on such a system, a change in voltage is expected to be exactly replicated by a KE shift of the electrolyte PE peaks (versus E_F^{WE}). In this case plotting the KE shifts of the electrolyte as a function of WE voltage would result in a 1 eV/V slope. This has also been seen in a number of published studies [243, 245, 249, 250, 253, 255, 256].

If the WE instead is an ideal non-polarizable interface, the voltage would be constant, and thus measuring the KE as a function of voltage would not contain a lot of information. However, in the similar case of a (practically) reversible redox reaction, one can expect the electrochemical potential of the electrolyte $\bar{\mu}_e^{el}$ to be governed by the equilibrium potential of the redox reaction occurring at the WE. In the case of electronic equilibrium (for an

electrolyte containing a redox couple), $\bar{\mu}_e^{el}$ and $\bar{\mu}_e^{WE}$ (=E_F^{WE}) will be aligned. When measuring APPES on the solid/liquid interface of such a system, $\bar{\mu}_e^{el}$ will follow E_F^{WE} and the KE of the electrolyte PE peaks will be constant when measured versus E_F^{WE}. Thus, if the KE shifts of the electrolyte are plotted against the WE voltage, this would be expected to result in a slope of 0 eV/V.

In the next section it is discussed how these ideal cases can be used to interpret *operando* APPES results on LIB interfaces.

6.4 *Operando* APPES of LIB interfaces

Using the methodology as outlined in Section 6.2 and 6.3, *operando* APPES can be used to assess both differences in electron electrochemical potential and changes in chemical environment. In this thesis first studies on a liquid LIB electrolyte are performed with *operando* APPES (Paper III and IV). These results are used to develop a suggested model for interpreting *operando* APPES results on LIB systems. In Paper V, *operando* APPES measurements are performed directly on the solid/liquid interface for two real battery systems. This is, to my knowledge, the first time such measurements are performed on a solid/liquid LIB interface. The main results of Paper III-V are summarized and discussed in this section.

6.4.1 Probing the liquid phase

In our first *operando* APPES study, presented in Paper III, two LIB model interfaces are studied, consisting of a metallic WE (Au or Cu) and a 1 M $LiClO_4$ in PC electrolyte. A Li/Li^+ RE is used, and the CE is a NMC composite. The use of a metallic WE ensures that E_F of the WE remains constant, and the widely different lithiation potentials (~0.2 V for Au and ~2 V for CuO, both vs. Li/Li^+) allows to investigate the effect of charge transfer separated from effects stemming from the electrolyte behavior at certain voltages.

In Figure 6.7 the KE shift of the electrolyte PE peaks are shown as a function of WE voltage. During both EDL-charging and SEI formation a slope of ~1 eV/V is seen. During the charge transfer region (indicated in blue) both systems show a significantly lower slope.

The slope of 1 eV/V during EDL-charging can be expected, as the interface in this case will behave as an ideal polarizable interface. However, during SEI formation charge transfer of electrons occur from electrode to electrolyte, leading to a reduction of the electrolyte components. A new phase is in this case created (the SEI) that can have a different electrochemical potential than the electrolyte. Thus, if the SEI was probed, a different slope could be expected. However, in our case the SEI is confined to the surface region close to the electrode (~nm), while only the outer bulk electrolyte is probed with

APPES. The 1 eV/V slope then signifies that no charge transfer occurs over the SEI to the bulk electrolyte, which neither can be expected for an electronically insulating SEI.

The slope during lithiation is approximately 0.4 eV/V for the Au electrode (alloying reaction), and 0.7 eV/V for the Cu electrode (conversion reaction). Since the deviation from a 1 eV/V slope is directly correlated to the occurrence of a charge transfer reaction, and neither correlated to the absolute value of the WE voltage or the current, it is concluded that this effect seems to be related to the charge transfer reactions occurring at the WE/electrolyte interface.

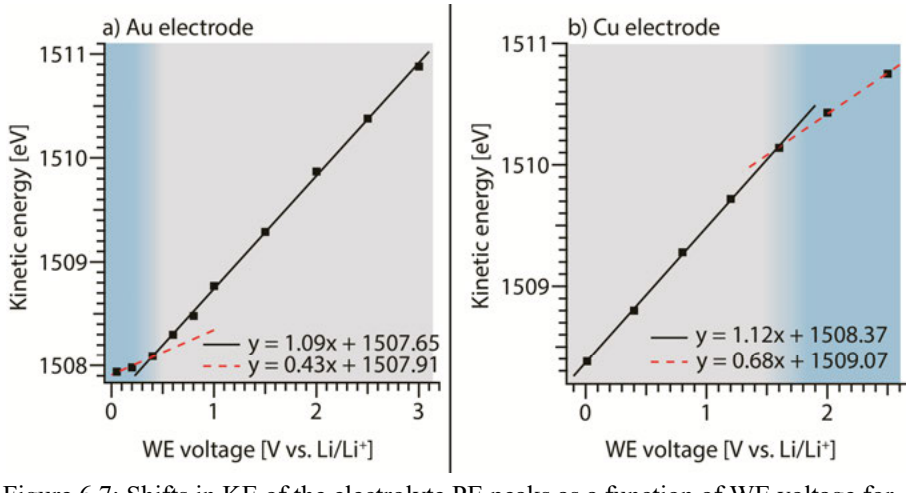

Figure 6.7: Shifts in KE of the electrolyte PE peaks as a function of WE voltage for a Au (a) and a Cu (b) electrode. The slope is close to 1 eV/V when no faradaic reactions occur, and significantly lower during lithiation. Adapted from Paper III.

The KE shifts of the electrolyte APPES peaks are further examined in Paper IV, where KE shifts are studied during different cycling conditions. In this case a LTO composite is used as WE, with the same electrolyte (1 M $LiClO_4$ in PC) as in Paper III. LTO is chosen as an ideal electrode material due to its very flat lithiation plateau, indicative of a first order phase transformation reaction. In addition, LTO has a quite high power capability, and a reduction potential above the onset of SEI formation. In this way the effect of current and/or applied voltage during lithiation can be studied with minimal influence from other effects.

The different voltage regions and the following changes in KE of the electrolyte PE peaks are summarized in Figure 6.8. The results show that the KE shift during initial charging (before onset of lithiation/reduction) follows the 1 eV/V behavior, just as in the case of Au and Cu. However, during charge transfer two different slopes are identified for LTO; a slope of ~0 eV/V during the phase transition reaction, and a slope of ~0.5 eV/V during a single phase lithiation. The KE of the electrolyte peaks at the lithiation plateau is further

investigated by the use of different overpotentials and/or currents, but this is not seen to have an effect on the KE in this (phase transformation) region. The interpretation of the different KE shifts is further discussed in Section 6.4.3.

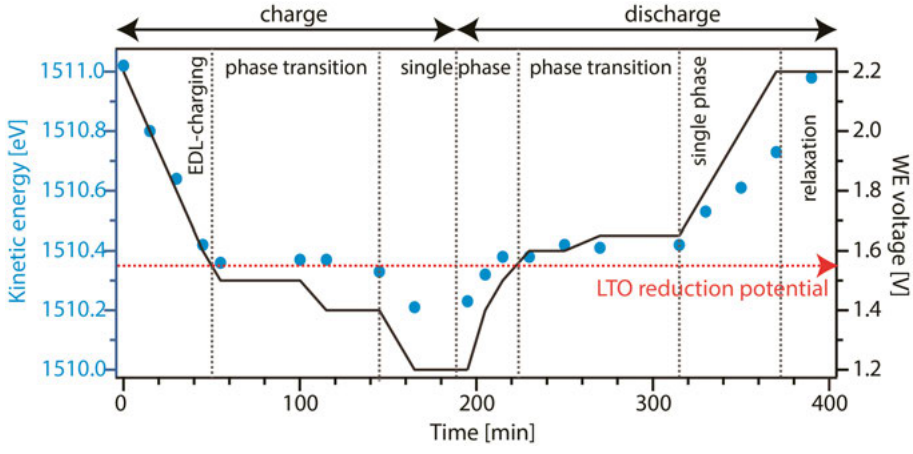

Figure 6.8: KE of the electrolyte PE peaks (blue dots), and WE voltage (black line) as a function of cycling time. The KE shift depends on the type of reaction occurring at the WE/electrolyte interface. Adapted from Paper IV.

6.4.2 An *operando* APPES model applicable to LIB interfaces

Based on the KE shifts seen during electrochemical cycling of Au, Cu and LTO, the model developed in Paper III (Section 6.3.1) is extended in Paper IV to be specifically applied for LIB systems.

The shift in KE of 1 eV/V for an ideal polarizable interface is already well understood, and attributed to the buildup of an EDL between the electrode and electrolyte when the WE voltage is changed. The deviation from this behavior during charge transfer has on the other hand been very scarcely studied. To understand the KE shifts seen for the electrolyte peaks in Paper III and IV, they need to be related to the electrochemical reactions.

The electrolyte in a LIB is an ionic conductor, but electronic insulator. The electrolyte does not contain free electrons or a reversible redox couple, and consequently electronic equilibrium cannot be achieved at the electrode/electrolyte interface. The transferable (charged) species is instead the Li-ion, and Li-ion equilibrium can be established at the interface during charge transfer (i.e., during (de)lithiation). Thus, to understand the KE shifts during LIB cycling, the electron electrochemical potentials measured by *operando* APPES need to be related to the Li-ion electrochemical potential. How this can be done is explained in the following.

The movement of Li-ions over the WE/electrolyte interface stems from a difference in electrochemical potential of the Li-ion in the different phases. To equilibrate this difference, either μ_{Li^+} or ϕ of at least one of the phases

must be changed. Assuming that the electrolyte composition is constant (high Li-ion concentration and mobility, and no degradation in the bulk electrolyte), μ^{el} will be constant (for all species). This means that a change in $\bar{\mu}$ of a species in the electrolyte will stem solely from a change in ϕ^{el}. As Li-ions are the only transferable species over the interface, a change in ϕ^{el} can be attributed to the movement of Li-ions. In the case of an electrolyte with constant chemical composition ($\Delta\mu^{el} = 0$) the electrochemical potential of the electron and Li-ion are related through:

$$\Delta\bar{\mu}_{Li^+}^{el} = \Delta\phi^{el} = -\Delta\bar{\mu}_{e}^{el}, \tag{6.4}$$

according to the definition of the electrochemical potential (Eq. (3.2)) used in this thesis. Further, if the reaction is occurring at limiting current conditions, set by the diffusion of Li in the bulk WE, the movement of Li^+ to the WE surface will be sufficiently fast to assume that Li-ion equilibrium is established at the WE/electrolyte interface. By definition, we have equilibrium of a species when the electrochemical potential of the species is equal in both phases [119, 120]:

$$\bar{\mu}_{Li^+}^{WE} = \bar{\mu}_{Li^+}^{el}. \tag{6.5}$$

Thus, during Li-ion equilibrium at the WE/electrolyte interface we can relate $\bar{\mu}_{Li^+}^{WE}$ to the measured shift in KE of the electrolyte peaks by combining Eq. (6.4) and Eq. (6.5), and substituting $\Delta\bar{\mu}_{e}^{el}$ according to (6.3). This gives:

$$\Delta\bar{\mu}_{Li^+}^{WE} = \Delta\bar{\mu}_{Li^+}^{el} = -\Delta\bar{\mu}_{e}^{el} = \Delta V - \Delta KE. \tag{6.6}$$

From thermodynamics we can write the Li chemical potential as the sum of the electrochemical potential of the Li-ion and electron, i.e., $\Delta\mu_{Li} = \Delta\bar{\mu}_{Li} = \Delta\bar{\mu}_{Li^+} + \Delta\bar{\mu}_{e}$ [119]. Using this relation together with Eq. (6.1) and Eq. (6.6) we arrive at:

$$\Delta\mu_{Li}^{WE} = \Delta\bar{\mu}_{Li^+}^{WE} + \Delta\bar{\mu}_{e}^{WE} = \Delta V - \Delta KE - \Delta V \rightarrow$$

$$\Delta\mu_{Li}^{WE} = -\Delta KE. \tag{6.7}$$

According to this model presented in Paper IV, *operando* APPES can be used to determine the change in Li chemical potential of the WE under Li-ion equilibrium conditions, in addition to the change in electron electrochemical potential of the electrolyte according to Eq. (6.3).

6.4.3 Interpreting the *operando* APPES results on a LIB electrolyte

Based on the two models presented in this thesis (from Paper III and IV), the KE shifts seen for the LIB electrolyte during charge transfer can be better understood. However, for the models to be applicable, the chemical composition of the probed electrolyte needs to be constant. In the studies performed in this thesis, this is ensured by using an electrolyte with high Li-ion concentration and high Li-ion mobility. Both these parameters are several orders of magnitude larger than the corresponding parameters for the WE. Under these conditions it can be assumed that any gradients in $\bar{\mu}_{Li^+}$ during (de)lithiation will exist within the bulk WE, while Li-ion equilibrium quickly is established at the WE/electrolyte interface.

The probed liquid meniscus also needs to be representative of the bulk electrolyte. To achieve this, the APPES measurements in Paper III and IV are performed on a thick part of the electrolyte meniscus, as close to the bulk electrolyte surface as possible. The electrodes are in addition re-dipped and moved sideways between every APPES measurement, to ensure that the meniscus is properly contacted and unaffected by beam damage. By using this methodology, it can be assumed that the chemical composition of the probed electrolyte is constant. In this case, the change in $\bar{\mu}_e^{el}$ stems solely from a change in ϕ^{el}, and the assumption that $\Delta\mu_e^{el} = 0$ made in our model holds.

The extent of the change in ϕ^{el} is then a measure of how much net charge that is transported over the electrode/electrolyte interface. A deviation from the 1 eV/V slope expected for an ideal polarizable electrode, implies that $\bar{\mu}_e^{el}$ has changed (relative to the RE). Assuming that $\bar{\mu}_e^{RE}$ is fixed, this means that $\bar{\mu}_e^{el}$ has changed. The change in ϕ^{el} (and consequently $\bar{\mu}_e^{el}$) can be attributed to the movement of Li-ions over the WE/electrolyte interface, in order to establish Li-ion equilibrium ($\bar{\mu}_{Li^+}^{el} = \bar{\mu}_{Li^+}^{WE}$).

During a phase transformation, the chemical potential μ_{Li}^{WE} is constant [56, 150], and a change in WE voltage only stems from a change in ϕ^{WE}. To maintain Li-ion equilibrium an equal shift in ϕ^{el} is needed. In this case the KE of the electrolyte is expected to be constant according to Eq. (6.7). This is seen for LTO on the (de)lithiation plateau. The other "extreme" case would be if the whole change in WE voltage stems from a change in μ_{Li}^{WE}. In this case $\bar{\mu}_{Li^+}^{WE}$ will remain constant and the Li-ion equilibrium is unaffected. In this case ϕ^{el} also remains constant. These two cases are illustrated in Figure 6.9. If the change in WE voltage change stems both from a change in μ_{Li}^{WE} and ϕ^{WE}, a slope in between 0 and 1 eV/V can be expected.

For LTO, a single-phase (de)lithiation reactions occurs after the phase transition, in which case μ_{Li}^{WE} is expected to change. During lithiation of LTO, the single-phase region for the spinel phase is not seen in the APPES measurements (Figure 6.8). This can be explained by the lithiation mechanism of the WE surface. Due to the large excess of Li-ions present at the

WE/electrolyte interface, the first lithiation of LTO can occur almost instantly, directly leading to a phase transition of the outermost surface, and after this μ_{Li}^{WE} will remain constant during the phase transition. During delithiation on the other hand, all lithium needs to diffuse out from the bulk of the WE, passing the surface on the way out. In this case the lithium content of the WE surface can be expected to change gradually during the single-phase delithiation, and the change in Li content (i.e., Li chemical potential) can be observed during APPES. The slope of Au and Cu during lithiation also indicate that μ_{Li}^{WE} is changed during cycling, in addition to an overpotential in order to account for the whole change in WE voltage.

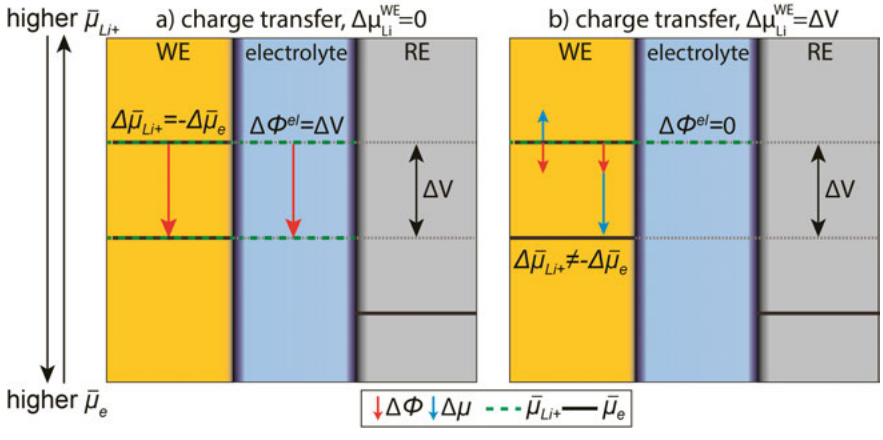

Figure 6.9: Shifts in chemical and electrostatic potential during charge transfer. When μ_{Li}^{WE} is constant (a) the electrolyte shifts together with the WE. When $\mu_{Li}^{WE} = \Delta V$ (b), the energy levels in the electrolyte are constant. Adapted from Paper IV.

From the results in Paper III and IV it follows that *operando* APPES can be used to study both the charge transfer (by the changes in $\bar{\mu}_e^{el}$) and the lithiation behavior (by the changes in μ_{Li}^{WE}) during cycling. This can be done even without direct access to the solid/liquid interface, showing the powerful capabilities of the *operando* APPES technique. These results are very interesting and show especially how the surface specific properties can be investigated with APPES. This information can be a valuable complement to e.g., electrochemical measurements and thermodynamic calculations that give information about the bulk material.

6.4.4 Probing the solid/liquid interface directly

In Paper V, the solid/liquid interface is studied directly for the state-of-the-art electrode materials LCO and NMC. The electrolyte used is 1 M $LiClO_4$ in PC. In order to access the electrode/electrolyte interface, flat thin film electrodes are used.

By moving the sample in the vertical direction, a region where the solid electrode and the liquid electrolyte can be probed simultaneously is found. This region is limited to the very edge of the liquid meniscus, over a distance of approximately ~60 µm. This distance can be compared to the vertical spot size of the beam, which is ~25 µm. Thus, we can be confident that there is a limited region on the sample where the electrode can be probed through the electrolyte. Measurements both further up and down on the sample are also performed, to be used as references for the pure solid and liquid phase, respectively.

In Figure 6.10 some of the spectra measured during charge of LCO (a) and NMC (b and c) are shown. A reference spectrum for the solid electrode at OCV (~3.1 V) is shown at the top of each graph, while the spectra below are recorded at the interface position using different WE voltages. From the O 1s spectra it can be confirmed that the solid and interface are probed simultaneously, as both the electrolyte solvent and salt, as well as the metal oxide is visible (light blue, green and grey peaks, respectively).

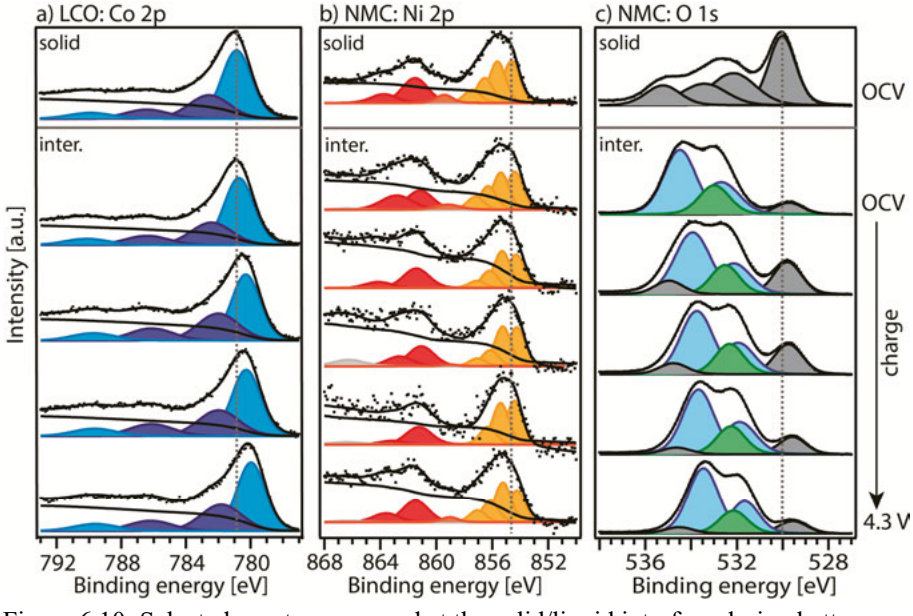

Figure 6.10: Selected spectra measured at the solid/liquid interface during battery charge. In (a) the Co 2p spectra for the LCO electrode is shown, and (b) and (c) show the Ni 2p and O 1s spectra for the NMC electrode, respectively.

When considering the peaks stemming from the AM, it is observed that these peaks shift slightly towards lower BEs as the voltage is increased. Since the WE is electrically connected to the spectrometer, this is not expected to result from a change in electrostatic potential. This is also supported by that the shifts in the Co, Ni and MO peak are different and non-reversible when the voltage is returned to OCV (as expected for electrostatic shifts). In

addition, no peak shifts are seen for the solid electrode measured far above the electrolyte when the WE voltage is changed. This shows that the electrical connection between the WE and spectrometer is functional.

In particular, the Ni 2p spectra show interesting changes in the shape of the satellite feature during cycling, indicating a redox activity of Ni during charge of the NMC electrode. However, the spectral analysis is complicated by the buildup of an adsorption layer during the *operando* measurements, and the signal-to-noise ratio is rather weak. Thus, although clear BE shifts of the AM are detected during cycling, it would be necessary to perform additional measurements with improved statistics for a more detailed analysis. This is especially important for the transition metals, as most information regarding their oxidation state can be gained from the satellite peaks. A higher signal-to-noise ratio from the interface could be achieved by the use of harder X-rays or by prolonged measurement where many spectra are taken for each potential. In the latter case, it is however important that the measurement spot is changed between each spectrum, to avoid beam damage and a decreasing signal from the electrode due to the buildup of an adsorption layer.

7 Stabilization of LIB interfaces[8]

To understand the chemistry of the charge transfer reactions occurring in a LIB, it is necessary to probe the interface directly. Due to the complexity and practical challenges of achieving this with *operando* APPES, *ex situ* PES can be a preferable technique for studying redox processes in the bulk material. *Ex situ* PES is also suitable to investigate the chemical composition of the (solid) interphase layer after cycling in detail.

Ideally, an interphase layer in a battery prevents side reactions while desired redox reactions proceeds unhindered. However, since the side reactions occurring are highly dependent on the specific chemistry of the battery, there is no "optimal" interphase that works for all systems. Thus, the interfacial reactions need to be understood for each specific material system, before one can try to optimize the interphase. This is important for the possible implementation of new battery materials. Often it is possible to significantly improve the battery performance by fine-tuning the interfacial chemistry. To do this, the main degradation mechanism(s) first needs to be identified. Different strategies can then be applied in order to stabilize the interface and improve cycling stability. Such strategies include (i) doping/substitution of the AM, (ii) using electrolyte additives, and (iii) AM coatings.

In this chapter the results gained from *ex situ* PES measurements of Li_2VO_2F are presented. The degradation mechanism of Li_2VO_2F is first studied in Paper VI. Building upon this knowledge, the different strategies (i)-(iii) are employed in Paper VI-IX to improve the cycling performance.

7.1 The degradation mechanism of Li_2VO_2F

In Paper VI, the degradation mechanism of Li_2VO_2F is investigated. The almost doubled theoretical capacity of Li_2VO_2F compared to NMC or LCO stems from its ability to store two Li-ions in the DRS structure. Experimentally, a maximum capacity of around 400 m Ah g^{-1} has been observed for low C-rates [99]. Unfortunately, these high initial capacities are followed by a rapid and continuous capacity fade, with only around 25 % of the initial capacity remaining after 50 cycles.

[8] Section 7.1 and 7.2.1 are loosely based on the same results reported in my Licentiate thesis: Källquist, I. (2019). Interfaces in Li-ion batteries seen through photoelectron spectroscopy.

In order to explain the poor cycling performance a series of Li_2VO_2F electrodes are investigated by PES. The samples are charged and discharged for a different number of cycles and stopped either in the fully lithiated state or fully delithiated state (labelled as "LX" and "DX", respectively, where X is the number of cycles). A pristine electrode (labelled "P") is used as a reference. Various photon energies ranging from very soft to hard X-rays are used to achieve a depth profile of the electrodes.

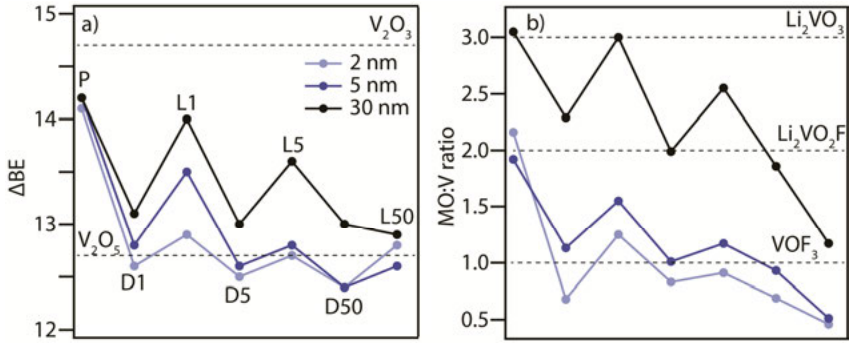

Figure 7.1: BE difference (a) and relative ratio (b) of the MO peak and V $2p_{3/2}$ peak. The ratio is calculated according to Eq.(4.6). Dashed lines indicated expected values for different compounds. The colors indicate different probing depths.

From the BE shifts of the V 2p peak during cycling, an oxidation of V towards V^{5+} can be identified. This is expected for the delithiated samples, where an oxidation of V compensates for the removal of Li. However, upon re-lithiation V should return to the V^{3+} if the cycling is reversible. This is not the case, as shown in Figure 7.1a. For all samples a gradual oxidation towards the V^{5+} state is seen, starting at the surface and proceeding towards the bulk with increased cycling. Additionally, the PES results show signs of oxygen redox reactions, indicated by a change in the ratio between V and MO during cycling. A significantly lower amount of MO is detected for the delithiated samples, and the MO:V ratio gradually decreases with number of cycles, as shown in Figure 7.1b. These results already give a general idea of the degradation of the material, by oxidation of V and conversion of the lattice oxygen. A more precise chemical degradation reaction can be suggested by investigating the spectra of different elements in detail.

In Figure 7.2 the O 1s and V 2p, C 1s, and P 2p spectra are shown for sample D5 and L5. The spectra are curve-fitted to identify different chemical compounds as indicated by labels. In the combined spectra of O 1s and V 2p, the oxidation of V can be evaluated, and the MO:V ratio can be determined from the relative peak areas, as summarized in Figure 7.1. Looking at the C 1s spectra in Figure 7.2b, it is seen that the capacity fade also can be coupled to the buildup of a surface layer upon lithiation. The surface compounds are partially removed from the electrode surface during delithiation, observed as

a relative increase in the intensity of the CB peak (stemming from the bulk), compared to the surface carbon peaks (dashed grey peaks). Due to the instability of the interphase layer towards dissolution, it fails to protect the electrode surface from further degradation. In the P 2p spectra (Figure 7.2c), it is also evident that salt degradation occurs. This is concluded from the identification of two different chemical environments, while the electrolyte salt ($LiPF_6$) is the only original source of P. The BE of the additional P 2p peak correspond well to the expected BE of PO_xF_y species.

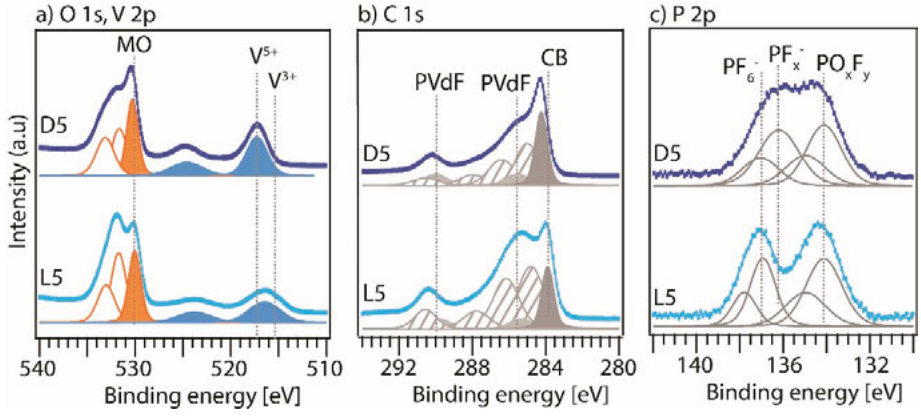

Figure 7.2: O 1s and V 2p (a), C 1s (b), and P 2p (c) spectra of the D5 and L5 sample. In (b) the striped peaks indicate surface compounds.

By considering all PES results, a suggested degradation reaction is proposed (see (7.1)). The origin of the AM degradation is proposed to be coupled to an oxidation O of, at sites in the disordered structure where V only is surrounded by O (rather than the stoichiometric ratio of two O and one F). This is also supported by other studies, suggesting a preferential location of F around the Li sites [257, 258]. At the VO_3 sites, V is in the 4+ oxidation state. Thus, to compensate for the removal of more than one Li, a partial oxidation of O must occur. Due to the highly reactive properties of oxidized O, O^- is prone to react with electrolyte ions. Coupling this to the formation of PO_xF_y, the following degradation reaction is proposed for the delithiated material:

$$VO_3 + PF_6^- + Li^+ + e^- \rightarrow VOF_3 + PO_2F_2^- + LiF. \qquad (7.1)$$

To summarize, the PES results shows that the oxidation of V and loss of lattice O starts at the electrode surface. According to the proposed degradation reaction, this leads to the formation of the redox inactive compound VOF_3 during delithiation, which is identified at the electrode surface together with other inorganic compounds resulting from salt degradation. Upon re-lithiation also an organic interphase layer is built up on the surface. These reactions are schematically illustrated in Figure 7.3. Due to the dissolution/detachment of

the interphase layer during delithiation, new parts of the AM are continuously exposed to the electrolyte. In this way the electrode degradation continues inwards to the bulk of the particles during extended cycling.

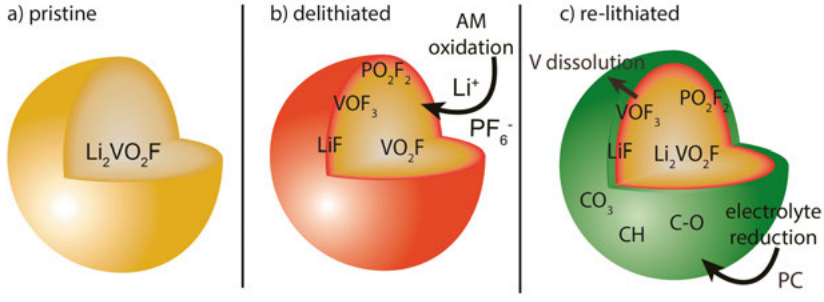

Figure 7.3: Schematic summary of the degradation reactions occurring in Li_2VO_2F, illustrating the breakdown of the AM as well as the buildup of a surface layer during cycling. Graphics adapted from Paper IX.

The knowledge about the mechanism behind the capacity fading for Li_2VO_2F is important not only for this particular material, but also to understand Li-rich materials in general. In particular, anion redox reactions have been found to be of high importance for the performance of these materials [79, 80, 259]. Involving anions in the redox processes can be beneficial as it allows for additional Li removal, giving an increased theoretical capacity. However, to achieve a reversible cycling involving anionic redox, the chemical stability of the DRS structure is crucial. In the case of Li_2VO_2F, our results indicate that the DRS structure is not sufficiently stable to prevent lattice oxygen loss and AM degradation during cycling.

7.2 Improved cycling stability of Li_2VO_2F

In order for Li-rich materials such as Li_2VO_2F to be viable choices for commercial batteries, their cycling performance needs to be considerably improved. In Paper VI-IX, three different approaches to achieve this are investigated. Since the degradation of the AM starts at the interface (Paper VI), there is a need to improve the interfacial stability. One way of doing this is to find a more thermodynamically stable DRS structure. This can be achieved by substituting part of the V atoms with other TMs. This route is investigated in Paper VII. In Paper VIII and IX, the aim is instead to improve the stability of the interphase layer, in order to prevent the AM from being continuously exposed to the electrolyte. In Paper VIII, the interphase is tuned by the use of electrolyte additives, and in Paper IX a surface modification of the AM particles is investigated. In the following sections these three strategies to improve cycling stability are discussed.

7.2.1 Active material substitution

Alternating the AM composition by doping or substitution is a possible route to increase the structural stability, the capacity, and/or the electrode voltage. For example, TM substitution was successfully used for NMC, where Co was substituted with Mn and Ni to improve both cycling stability and capacity in comparison to LCO [51, 85, 260]. Partial anion substitution can also be a way to improve both energy density and cycling performance [261-263]. In Li_2VO_2F the partial substitution of O for F increased both the voltage and the theoretical capacity compared to Li_2VO_3 [263].

In Paper VII, the approach with TM substitution is employed to Li_2VO_2F. Previous studies have shown that both Fe and Ti form more stable DRS structures compared to V, and therefore can be used to improve the structural stability [264]. Two materials where 50 % of the V atoms are substituted with either Fe or Ti are evaluated. The substituted materials $Li_2V_{0.5}Ti_{0.5}O_2F$ and $Li_2V_{0.5}Fe_{0.5}O_2F$ are successfully synthesized in the DRS phase, which is confirmed by X-ray diffraction. Density functional theory calculations also show that the disordered phase is more stable for the substituted materials, compared to the original composition (Li_2VO_2F). As expected, this leads to a significantly improved capacity retention, from 50 % for Li_2VO_2F, to around 80 % for $Li_2V_{0.5}Ti_{0.5}O_2F$ and $Li_2V_{0.5}Fe_{0.5}O_2F$ after 30 cycles.

A drawback of the substitution of V with Fe/Ti is the decrease of the theoretical capacity, since the maximum oxidation state of Fe and Ti is 3+ and 4+, respectively. Because of this, only 50 % ($Li_2V_{0.5}Fe_{0.5}O_2F$) or 75 % ($Li_2V_{0.5}Ti_{0.5}O_2F$) of the available Li can be extracted, unless O participates in the redox reaction. In this regard, it is necessary to make a tradeoff between improved structural stability, and decreased theoretical capacity.

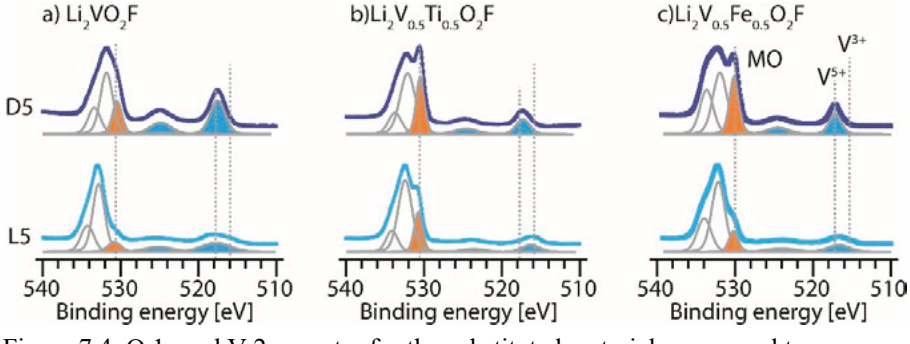

Figure 7.4: O 1s and V 2p spectra for the substituted materials compared to Li_2VO_2F. Adapted from Paper VII.

To further investigate the reason behind the improved cycling performance, PES measurements are carried out. The results for the Ti and Fe substituted samples are compared to the results for Li_2VO_2F. The most striking difference is that the substituted materials show a more stable MO:V ratio, indicating that

less lattice oxygen is converted to surface species. This is seen from the O 1s and V 2p spectra, shown for the D5 and L5 sample in Figure 7.4. Additionally, the surface layer dissolution seen for the Li_2VO_2F material is less prominent, further strengthening the hypothesis that the surface stability can be improved by increasing the stability of the DRS structure. Despite these improvements, an oxidation of V is still seen in the PES measurements. Just as for Li_2VO_2F, the oxidation starts at the surface and seems to continue into the bulk with cycling, although a relatively lower rate for the substituted materials.

The results of Paper VII show that the increased stability of the DRS phase is not by itself sufficient to prevent the irreversible reactions responsible for the AM degradation. To reach an acceptable cycling performance, it is therefore also necessary to consider the electrolyte composition and interphase layer formation.

7.2.2 Electrolyte additives

Using small amounts of electrolyte additives is a relatively cheap and straightforward way to improve the interfacial properties [40, 107, 108]. Common electrolyte additives used in LIBs include organic carbons such as vinylene carbonate, fluoroethylene carbonate and glycolide. The beneficial effects of these co-solvents stem from their passivating and film forming properties. These additives are in particular used to form beneficial interphase layers on negative electrodes [265-267]. To mitigate AM degradation at the positive electrode side, it is common to add co-salts to the electrolyte. Boron or phosphate containing salts have shown positive effects on the cycling performance in previous studies [268-272]. These salts are preferentially oxidized and form passivating interphase layers on the positive electrode.

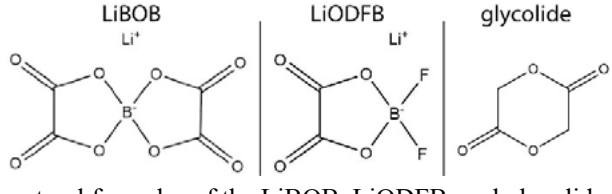

Figure 7.5: Structural formulas of the LiBOB, LiODFB, and glycolide additives.

To improve the interfacial stability of Li_2VO_2F both the performance at high and low voltages should be improved. In Paper VIII, three different electrolyte additives, as illustrated in Figure 7.5, are evaluated. The additives are lithium bis(oxalato)borate (LiBOB), lithium difluoro(oxalato)borate (LiODFB), and glycolide. All these additives are recognized for their film-forming properties [8, 28, 107]. Glycolide is particularly used to improve the stability of the SEI on negative electrodes [266], while the boron-containing additives LiBOB and LiODFB can mitigate detrimental oxidation reactions and TM dissolution occurring at the positive electrode [268, 273, 274].

In the measurements presented in Paper VIII 0.1 wt% of the different additives are added to the standard electrolyte (1 M $LiPF_6$ in EC/DMC, 1:1 v/v). The electrochemical cycling shows that all additives improve the capacity retention of Li_2VO_2F. Compared to the reference electrolyte without additives, the improvement is 5 %, 10 % and 12.5 % for glycolide, LiBOB and LiODFB, respectively. Both LiBOB and LiODFB improves the coulombic efficiency, but in the case of LiBOB this improvement is also coupled to a higher interfacial resistance, increasing the voltage polarization. This is not the case for LiODFB, that slightly decreases both the cell impedance and the voltage polarization. From the electrochemical testing, the LiODFB additive is thus seen to be the best performing additive.

To characterize the interphase for each additive, PES measurements are performed. By investigating the C 1s and O 1s spectra, which contain signal from PEs stemming from both the bulk material and the surface layer, the thickness of the surface layer can be estimated. In all cases it is seen that the surface layers formed with the electrolyte additives are generally thicker and contain a larger amount of O. This can be expected as the additives function through their film-forming properties where O containing compounds such as oxalates, borates, fluoroborates, and phosphates are created upon oxidation.

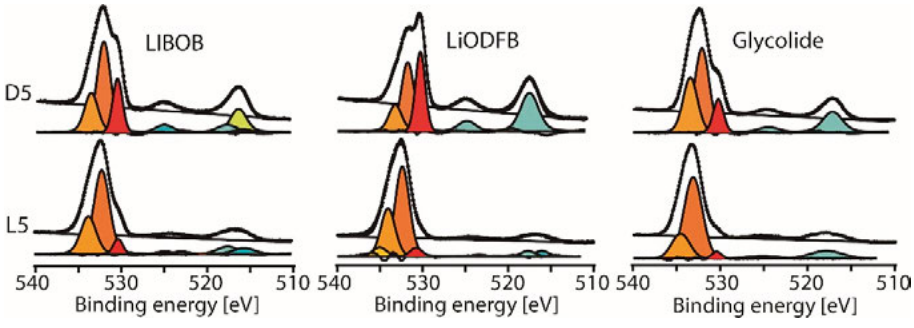

Figure 7.6: O 1s and V 2p spectra for electrode samples used with different electrolyte additives. Adapted from Paper VIII.

Evaluating the O 1s and V 2p spectra, shown for the D5 and L5 samples in Figure 7.6, it is found that the loss of lattice oxygen at high voltages is reduced. On the other hand, an increased amount of V is found in the interphase layer after lithiation, indicating that V dissolution at low voltages cannot be prevented by the electrolyte additives investigated here. The reversibility of the V^{3+}/V^{5+} redox couple is slightly improved by adding LiBOB or LiODFB.

Overall, the summarized results suggest that the boron salts can form an interphase layer that protects the electrode from extensive oxidation, i.e., one of the main degradation mechanisms seen for Li_2VO_2F. However, V dissolution and electrolyte reduction is still seen for all tested additives. This is also in agreement with the electrochemical cycling, which shows that although the capacity retention is improved, it is still not satisfactory.

7.2.3 Surface modification

Instead of tuning the electrode/electrolyte interphase by electrolyte additives, the interfacial properties can also be altered by adding a surface coating to the AM during synthesis. Coating the AM with a thin surface layer of an inorganic metal oxide, fluoride or phosphate has successfully improved the surface stability of other high capacity positive electrodes [275-278]. Common examples of coatings include e.g., AlF_3, Al_2O_3, TiO_2, and $AlPO_4$. By sacrificial degradation reactions between the surface layer and the salt anion (often PF_6^-), a beneficial inorganic surface layer can be formed. The formed interphase layer works as a physical barrier that prevents electrolyte compounds from reaching the AM. In this way detrimental reactions such as TM dissolution, HF formation and AM oxidation can be avoided. This can be done without altering the capacity of the bulk material, as compared to e.g., TM substitution. Thus, surface modifications can be an attractive option to improve the cycling performance of inherently reactive electrode materials.

In Paper IX, the Li_2VO_2F particles are coated with a thin layer of AlF_3, based on the successful results achieved for other Li-rich materials [279, 280]. The improved cycling performance with an AlF_3 coating is generally attributed to its insulating properties that can help prevent electron transfer between the electrode and the electrolyte [277]. A coating thickness corresponding to 2 or 3 mol% AlF_3 is seen to significantly improve both capacity retention and energy efficiency for Li_2VO_2F. The initial cycling capacity is however somewhat lower for the coated materials. This can be a result from a partial delitihation of the AM during synthesis with AlF_3, and/or from a mitigation of the side reactions between electrode and electrolyte.

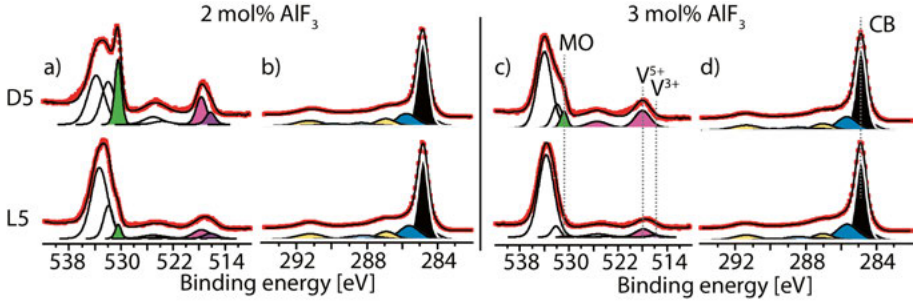

Figure 7.7: O 1s, V 2p (a and c) and C 1s (b and d) spectra of the coated electrodes. Adapted from Paper IX.

The effect of the AlF_3 surface modification on the interphase composition is studied by PES. The C 1s spectra (Figure 7.7b and d) show a significantly reduced amount of surface carbons, indicating that the coating can effectively prevent electrolyte reduction at low potentials. However, AM oxidation at high voltages is still seen, evident by a large amount of V^{5+} also for lithiated samples, and a decrease of the MO:V ratio indicating conversion of lattice O.

Also salt degradation is observed from the P 2p and F 1s spectra. Thus, as opposed to the interphase modification by electrolyte additives, the AlF_3 coating appears to successfully mitigate the reduction of the electrolyte, while oxidation reactions are not as efficiently prevented. This is attributed to a hindrance of electron transport between electrode and electrolyte solvent, while the $LiPF_6$ salt seem to be able to diffuse through the interphase layer and reach the active material.

In Figure 7.8 the effects of the three strategies for improving the interfacial stability are summarized and compared to the original Li_2VO_2F material.

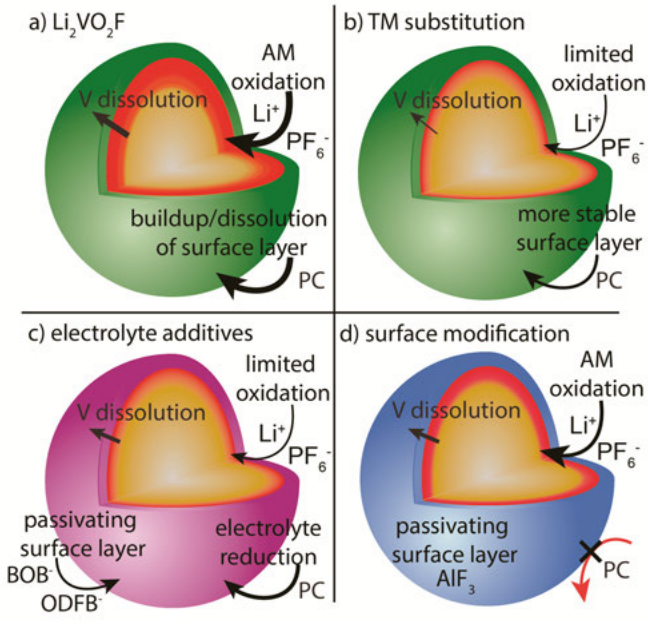

Figure 7.8: Illustration of the three main degradation mechanisms for Li_2VO_2F (a). By TM substitution (b), electrolyte additives (c), or surface modification (d) some of these mechanisms can be mitigated. The thickness of the arrows schematically represents the extent of the degradation.

8 Conclusion and outlook

After 50 years of researching the interphases in LIBs, the full understanding of their functionality, kinetics and mechanism of operation remain somewhat a mystery. Finding answers to these questions is essential for the rational design of batteries with better cycling performance.

In this thesis, focus is placed on the necessity to understand the general principles governing both the method of investigation and the physical or chemical processes one tries to study. This might seem obvious, as this is the general approach of any experimental work – the understanding we gain is a result of the models we have to interpret the data. However, this is important to remember whenever a new methodology is developed, as existing models may need to be adapted in order to describe the interplay between a specific method and a specific process. The main experimental contribution of this thesis to the research of LIB interfaces lies in the combination of the existing theories and models applied in PES and electrochemistry – in order to provide a methodology for studying LIB systems with *operando* APPES.

The results presented in this thesis can be divided into two main topics; the study of the potential differences over the LIB interfaces, and the detailed study of the chemical composition of the interphase layers in LIBs. For the first topic, primarily *operando* APPES is used, while *ex situ* PES has been used for the second topic.

8.1 Present and future use of ex situ and *operando* PES

Ex situ PES has for a long time been employed to successfully characterize the chemical composition, thickness and evolution of the surface layers in LIBs after extended battery cycling. The technique is also highly suitable for studying the changes in oxidation state of different elements upon (de)lithiation of the AM.

In this thesis *ex situ* PES is used to evaluate the redox mechanism in Li_2VO_2F, as well as the surface evolution of the same material. From these studies it is found that the poor capacity retention of Li_2VO_2F can be attributed to a combination of active material degradation through detrimental reactions with the salt, and continuous charge loss through a cyclic buildup and dissolution of interphase layers. These processes can to some extent be mitigated by TM substitution, by the use of electrolyte additives, and/or by a

surface coating of the AM particles. By improving the properties of the electrode/electrolyte interface, the cycling performance of Li_2VO_2F is significantly improved. To further optimize the capacity retention of the Li-rich material, all of these strategies could of course be used together, as it was seen that the different methods improved the interfacial stability in different ways (Figure 7.8).

Although a lot of useful information can be gained from *ex situ* PES, the static conditions during these measurements cannot provide any information regarding the kinetics of the interfacial reactions. To gain this type of information, characterization techniques that can be performed *operando* are necessary. In this thesis a step in this direction is taken by developing a methodology for performing *operando* APPES measurements on LIB interfaces. Both practical and theoretical aspects are considered, and a model for interpreting *operando* APPES data under certain measurement conditions is presented. The first model presented in this thesis can be applied to any electrode/electrolyte interface, and suggests how *operando* APPES can be a useful tool to directly probe the electron electrochemical potential difference over a solid/liquid interface. This cannot be achieved by electrochemical measurements, which require two electrically conductive materials to measure a voltage difference.

The model is further developed for the specific case of LIB systems and used to interpret the *operando* APPES results. It is seen that the KE shifts of different phases in a LIB are dependent on the electrochemical reactions occurring at the interface. In particular, two "extreme" cases can be highlighted; the shift in KE of the electrolyte APPES peaks is ~1 eV/V when no faradaic reactions occur, and ~0 eV/V during a first order phase transition. In both these cases the chemical potential of the WE is constant. In the case of a changing chemical potential, e.g., in the case of a single phase lithiation reaction, the behavior is more complex.

The work performed in this thesis provides a basis for interpreting *operando* APPES measurements on LIB interfaces. However, this methodology is still very novel, and there is much more to learn – both regarding the technique and the kinetics of the charge transfer reactions. For example, the studies performed in this thesis have to a large extent involved "simplified" measurements, where for example only the bulk liquid has been studied, and/or only one electrochemical process is occurring at a time. In this way the interpretation of the results is facilitated, and an understanding of the individual phases and processes can be developed. This is a necessity before proceeding to the study of full LIB interfaces, where a multitude of different reactions can occur simultaneously.

The logical follow up to the studies performed in this thesis would probably seem to be a merge of the two main topics in this thesis, i.e., experiments where the potential differences and detailed chemical composition of the LIB interfaces are probed simultaneously with *operando* APPES. In this way the

potential differences could be directly correlated to charge transfer reactions, which in turn could be identified through the chemical composition. While this would be a highly desirable study to perform, it is also a very difficult study, both practically and in terms of interpreting the results. In this regard, I think it is important to remember that *operando* APPES is not necessarily a better choice than *ex situ* PES for all research questions.

First and foremost, the availability of the techniques can be considered. While instruments capable of probing LIB interfaces *ex situ* are widely available, the number of instruments with capabilities of probing the whole electrode/interphase/electrolyte region are very scarce. To gain a sufficient signal from the interphase a tender X-ray source is essentially necessary, in addition to an APPES instrument compatible with an electrochemical setup. Currently there are only a few such setups in the world [281-283], and most of them are not yet available for general users. Secondly, even as these setups can be expected to become more and more common, the inherently dampened signal from the WE and interphase by the liquid and gas phase in APPES measurements will pose a challenge towards resolving small chemical shifts (e.g., of transition metals) in *operando* measurements. As a third remark, *operando* APPES will probably also be most useful for studying one battery cycle, or the behavior at specific potentials. Studies of ageing after prolonged cycling times (months or even years) are instead more suitable for *ex situ* measurements (or will at least involve pre-cycling).

Thus, even though I expect *operando* APPES to be an essential tool to understand questions regarding the EDL, the kinetics of SEI formation, and the onset and behavior of the lithiation reactions, I believe *ex situ* PES studies will remain highly useful for the study of e.g., battery ageing. The two different approaches can complement each other, where *operando* measurement for example can be used to identify the onset of charge transfer reactions, and *ex situ* measurement of samples stopped at these voltages can be used to further investigate the redox mechanism. A comparison of the results can also be useful to evaluate the effects of the sample environment/treatment on the composition of the interphase layer.

To conclude this thesis, I would thus like to highlight that, in the same way that there will probably never be such a thing as a perfect battery or an optimal interphase, there is no unique technique that can be used to understand all aspects of the processes occurring in a LIB. PES can be used to gain some pieces to the puzzle, while electrochemical measurements can be used to gain others. Doing both measurements simultaneously, can help puzzling these pieces together. However, to finish the puzzle, also other techniques will be helpful. A variety of *operando* methods may be used to gather currently missing pieces, which are needed for the completion of the intricate LIB interface puzzle.

Acknowledgements

The work performed in this thesis had never been possible without the help and support from co-workers, friends, and family. I am grateful for each and every one of you, and the list of people in this acknowledgement could be made very long. However, there are some people that have been particularly important for the finalization of this work, whom I would like to specifically mention.

First and foremost, to **Maria**, my outstanding main supervisor that has invaluable both for the scientific results and the enjoyment of my PhD journey. I was also lucky enough to be backed up by no less than three additional co-supervisors – **Håkan**, **Laurent** and **Kristina** – thank you for your advice, support and inspiration. This also extends to **Fredrik L** and **Julia**, who I consider my unofficial supervisors. Thank you for mentoring me in the art of curve-fitting and battery building, for the beamtime struggles and successes, and for the tremendous work with finalizing our APPES papers.

In my projects I have worked with many excellent researchers that I would like to acknowledge: to **Tove** and **Heyin**, for the more recent beamtimes and your contributions to the endless discussions of potentials. I hope this work will facilitate any upcoming *operando* APPES measurements! To **Leif**, for teaching me about electrochemistry and how Li-ion batteries really work.

To everyone involved in the LiRichFCC project, where I'm especially happy to have connected with the former PhD students (now Dr.) **Christian** and **Jin Hyun**. At UU also **Andy**, **Jolla** and **Daniel** were essential to make sure this project provided both successful research and good times. To all the synchrotron staff – making sure our experiments could run even at the most inconvenient times. A special thanks goes to **Andrey** at HIPPIE for his contributions to our APPES studies.

To everyone at the division, current and former co-workers, thank you for providing a friendly atmosphere, a fun place to work and countless good memories. The thesis writing without our fika, discussions and AWs have been a much less pleasant period of time (but possibly more productive). To the "senior" PhDs **Olof**, **Christofer**, **Clara** and **Fredrik J** – thank you for sharing your wisdom on how to master (PhD) life. To all the PhD students sharing this journey with me – thank you for trusting me with the power of the bedazzled gavel (aka as your PhD representative). I wish you all great successes with your upcoming research and life adventures. I can't wait to meet you all soon again to thank you in person.

Finally, to my covid-family **Ludde**, **Sebastian** and **Lídia**, to my yoga-and-handstand-family, and last but not least, to my "real" **family**. Thank you for giving me some kind of social community during this odd year, and keeping me (mostly) happy and healthy during this writing processes.

Mest av allt till Ludde – tack för all hjälp och stöd när det blivit lite för mycket kaaaaooooosss. Like you lotely.

References

[1] Blomgren, G.E., *The Development and Future of Lithium Ion Batteries.* Journal of the Electrochemical Society, 2017. **164**(1): p. A5019-A5025.

[2] Yamahira, T., Kato, H., and Anzai, M., *Nonaqueous Electrolyte Secondary Battery*. 1991, Google Patents.

[3] Julien, C., et al., *Lithium Batteries*, in *Lithium Batteries: Science and Technology*. 2016, Springer International Publishing: Cham. p. 29-68.

[4] Yang, Y., et al., *On the Sustainability of Lithium Ion Battery Industry – a Review and Perspective.* Energy Storage Materials, 2021. **36**: p. 186-212.

[5] Di Lecce, D., Verrelli, R., and Hassoun, J., *Lithium-Ion Batteries for Sustainable Energy Storage: Recent Advances Towards New Cell Configurations.* Green Chemistry, 2017. **19**(15): p. 3442-3467.

[6] NobelPrize.org. *Popular Information*. 2021 [cited 2021 2 Aug 2021]; Available from: https://www.nobelprize.org/prizes/chemistry/2019/popular-information/.

[7] Zubi, G., et al., *The Lithium-Ion Battery: State of the Art and Future Perspectives.* Renewable and Sustainable Energy Reviews, 2018. **89**: p. 292-308.

[8] Gauthier, M., et al., *Electrode–Electrolyte Interface in Li-Ion Batteries: Current Understanding and New Insights.* The Journal of Physical Chemistry Letters, 2015. **6**(22): p. 4653-4672.

[9] Peled, E. and Menkin, S., *Review—Sei: Past, Present and Future.* Journal of The Electrochemical Society, 2017. **164**(7): p. A1703-A1719.

[10] Winter, M., *The Solid Electrolyte Interphase – the Most Important and the Least Understood Solid Electrolyte in Rechargeable Li Batteries*, in *Zeitschrift für Physikalische Chemie*. 2009. p. 1395.

[11] Wurm, C., et al., *Anode Materials for Lithium-Ion Batteries*, in *Lithium-Ion Batteries: Basics and Applications*, R. Korthauer, Editor. 2018, Springer Berlin Heidelberg: Berlin, Heidelberg. p. 43-58.

[12] Nitta, N., et al., *Li-Ion Battery Materials: Present and Future.* Materials Today, 2015. **18**(5): p. 252-264.

[13] Ciez, R.E. and Whitacre, J.F., *Comparison between Cylindrical and Prismatic Lithium-Ion Cell Costs Using a Process Based Cost Model.* Journal of Power Sources, 2017. **340**: p. 273-281.

[14] Quinn, J.B., et al., *Energy Density of Cylindrical Li-Ion Cells: A Comparison of Commercial 18650 to the 21700 Cells.* Journal of The Electrochemical Society, 2018. **165**(14): p. A3284-A3291.

[15] Tarascon, J.M. and Armand, M., *Issues and Challenges Facing Rechargeable Lithium Batteries.* Nature, 2001. **414**(6861): p. 359-367.

[16] Armand, M. and Tarascon, J.M., *Building Better Batteries.* Nature, 2008. **451**: p. 652-657.

[17] Whittingham, M.S., *Lithium Batteries and Cathode Materials.* Chemical Reviews, 2004. **104**(10): p. 4271-4302.

[18] Qiu, B., et al., *Understanding and Controlling Anionic Electrochemical Activity in High-Capacity Oxides for Next Generation Li-Ion Batteries.* Chemistry of Materials, 2017. **29**(3): p. 908-915.
[19] Manthiram, A., *A Reflection on Lithium-Ion Battery Cathode Chemistry.* Nature Communications, 2020. **11**(1): p. 1550.
[20] Wu, X., et al., *Safety Issues in Lithium Ion Batteries: Materials and Cell Design.* Frontiers in Energy Research, 2019. **7**(65).
[21] Chen, Y., et al., *A Review of Lithium-Ion Battery Safety Concerns: The Issues, Strategies, and Testing Standards.* Journal of Energy Chemistry, 2021. **59**: p. 83-99.
[22] Doughty, D.H. and Roth, E.P., *A General Discussion of Li Ion Battery Safety.* The Electrochemical Society Interface, 2012. **21**(2): p. 37-44.
[23] Philippe, B., et al., *Nanosilicon Electrodes for Lithium-Ion Batteries: Interfacial Mechanisms Studied by Hard and Soft X-Ray Photoelectron Spectroscopy.* Chemistry of Materials, 2012. **24**(6): p. 1107-1115.
[24] Broussely, M., et al., *Main Aging Mechanisms in Li Ion Batteries.* Journal of Power Sources, 2005. **146**(1): p. 90-96.
[25] Harlow, J.E., et al., *A Wide Range of Testing Results on an Excellent Lithium-Ion Cell Chemistry to Be Used as Benchmarks for New Battery Technologies.* Journal of The Electrochemical Society, 2019. **166**(13): p. A3031-A3044.
[26] Lin, Z., et al., *Aligning Academia and Industry for Unified Battery Performance Metrics.* Nature Communications, 2018. **9**(1): p. 5262.
[27] Preger, Y., et al., *Degradation of Commercial Lithium-Ion Cells as a Function of Chemistry and Cycling Conditions.* Journal of The Electrochemical Society, 2020. **167**(12): p. 120532.
[28] Xu, K., *Electrolytes and Interphases in Li-Ion Batteries and Beyond.* Chemical Reviews, 2014. **114**(23): p. 11503-11618.
[29] Kabir, M.M. and Demirocak, D.E., *Degradation Mechanisms in Li-Ion Batteries: A State-of-the-Art Review.* International Journal of Energy Research, 2017. **41**(14): p. 1963-1986.
[30] Pender, J.P., et al., *Electrode Degradation in Lithium-Ion Batteries.* ACS Nano, 2020. **14**(2): p. 1243-1295.
[31] Woody, M., et al., *Strategies to Limit Degradation and Maximize Li-Ion Battery Service Lifetime - Critical Review and Guidance for Stakeholders.* Journal of Energy Storage, 2020. **28**: p. 101231.
[32] Edge, J.S., et al., *Lithium Ion Battery Degradation: What You Need to Know.* Physical Chemistry Chemical Physics, 2021. **23**(14): p. 8200-8221.
[33] Peled, E., *The Electrochemical Behavior of Alkali and Alkaline Earth Metals in Nonaqueous Battery Systems—the Solid Electrolyte Interphase Model.* Journal of The Electrochemical Society, 1979. **126**(12): p. 2047-2051.
[34] Aurbach, D., *Review of Selected Electrode–Solution Interactions Which Determine the Performance of Li and Li Ion Batteries.* Journal of Power Sources, 2000. **89**(2): p. 206-218.
[35] Verma, P., Maire, P., and Novak, P., *A Review of the Features and Analyses of the Solid Electrolyte Interphase in Li-Ion Batteries.* Electrochimica Acta, 2010. **55**(22): p. 6332-6341.
[36] Aurbach, D., et al., *Review on Electrode–Electrolyte Solution Interactions, Related to Cathode Materials for Li-Ion Batteries.* Journal of Power Sources, 2007. **165**(2): p. 491-499.
[37] Edström, K., Gustafsson, T., and Thomas, J.O., *The Cathode–Electrolyte Interface in the Li-Ion Battery.* Electrochimica Acta, 2004. **50**(2): p. 397-403.

[38] Zuo, X., et al., *High-Voltage Performance of Licoo2/Graphite Batteries with Methylene Methanedisulfonate as Electrolyte Additive.* Journal of Power Sources, 2012. **219**: p. 94-99.
[39] Gao, H., et al., *Mechanistic Study of Electrolyte Additives to Stabilize High-Voltage Cathode–Electrolyte Interface in Lithium-Ion Batteries.* ACS Applied Materials & Interfaces, 2017. **9**(51): p. 44542-44549.
[40] Tan, S., et al., *Recent Progress in Research on High-Voltage Electrolytes for Lithium-Ion Batteries.* ChemPhysChem, 2014. **15**(10): p. 1956-1969.
[41] Lee, T.J., et al., *Solid Permeable Interface (Spi) on a High-Voltage Positive Electrode of Lithium-Ion Batteries.* Journal of The Electrochemical Society, 2018. **165**(3): p. A575-A583.
[42] Malmgren, S., et al., *Comparing Anode and Cathode Electrode/Electrolyte Interface Composition and Morphology Using Soft and Hard X-Ray Photoelectron Spectroscopy.* Electrochimica Acta, 2013. **97**: p. 23-32.
[43] Qian, Y., et al., *Influence of Electrolyte Additives on the Cathode Electrolyte Interphase (Cei) Formation on Lini1/3mn1/3co1/3o2 in Half Cells with Li Metal Counter Electrode.* Journal of Power Sources, 2016. **329**: p. 31-40.
[44] Zhang, J.-N., et al., *Dynamic Evolution of Cathode Electrolyte Interphase (Cei) on High Voltage Licoo2 Cathode and Its Interaction with Li Anode.* Energy Storage Materials, 2018. **14**: p. 1-7.
[45] Hausbrand, R., Becker, D., and Jaegermann, W., *A Surface Science Approach to Cathode/Electrolyte Interfaces in Li-Ion Batteries: Contact Properties, Charge Transfer and Reactions.* Progress in Solid State Chemistry, 2014. **42**(4): p. 175-183.
[46] Li, Q., et al., *Investigations on the Fundamental Process of Cathode Electrolyte Interphase Formation and Evolution of High-Voltage Cathodes.* ACS Applied Materials & Interfaces, 2020. **12**(2): p. 2319-2326.
[47] Zaera, F., *Probing Liquid/Solid Interfaces at the Molecular Level.* Chemical Reviews, 2012. **112**(5): p. 2920-2986.
[48] Goodenough, J.B. and Park, K.-S., *The Li-Ion Rechargeable Battery: A Perspective.* Journal of the American Chemical Society, 2013. **135**(4): p. 1167-1176.
[49] Armand, M., et al., *Lithium-Ion Batteries – Current State of the Art and Anticipated Developments.* Journal of Power Sources, 2020. **479**: p. 228708.
[50] Mizushima, K., et al., *Lixcoo2 (0<X<-1): A New Cathode Material for Batteries of High Energy Density.* Materials Research Bulletin, 1980. **15**(6): p. 783-789.
[51] Lu, Z., MacNeil, D.D., and Dahn, J.R., *Layered Cathode Materials Li [Ni X Li (1 / 3 − 2x / 3) Mn (2 / 3 − X / 3)] O 2 for Lithium-Ion Batteries.* Electrochemical and Solid-State Letters, 2001. **4**(11): p. A191-A194.
[52] Ceder, G., et al., *Identification of Cathode Materials for Lithium Batteries Guided by First-Principles Calculations.* Nature, 1998. **392**(6677): p. 694-696.
[53] Ohzuku, T., Iwakoshi, Y., and Sawai, K., *Formation of Lithium-Graphite Intercalation Compounds in Nonaqueous Electrolytes and Their Application as a Negative Electrode for a Lithium Ion (Shuttlecock) Cell.* Journal of The Electrochemical Society, 1993. **140**(9): p. 2490-2498.
[54] Julien, C., et al., *Anodes for Li-Ion Batteries*, in *Lithium Batteries: Science and Technology*. 2016, Springer International Publishing: Cham. p. 323-429.
[55] Colbow, K.M., Dahn, J.R., and Haering, R.R., *Structure and Electrochemistry of the Spinel Oxides Liti2o4 and Li43ti53o4.* Journal of Power Sources, 1989. **26**(3): p. 397-402.

[56] Li, D. and Zhou, H., *Two-Phase Transition of Li-Intercalation Compounds in Li-Ion Batteries.* Materials Today, 2014. **17**(9): p. 451-463.
[57] Ohzuku, T., Ueda, A., and Yamamoto, N., *Zero-Strain Insertion Material of Li [Li1 / 3ti5 / 3] O 4 for Rechargeable Lithium Cells.* Journal of The Electrochemical Society, 1995. **142**(5): p. 1431-1435.
[58] Cicconi, P., et al., *A Life Cycle Costing of Compacted Lithium Titanium Oxide Batteries for Industrial Applications.* Journal of Power Sources, 2019. **436**: p. 226837.
[59] Christensen, J., Srinivasan, V., and Newman, J., *Optimization of Lithium Titanate Electrodes for High-Power Cells.* Journal of The Electrochemical Society, 2006. **153**(3): p. A560.
[60] Zhu, Y.-R., et al., *Electrochemical Performance and Lithium-Ion Intercalation Kinetics of Submicron-Sized Li4ti5o12 Anode Material.* Journal of Alloys and Compounds, 2013. **547**: p. 107-112.
[61] Liu, H., et al., *Elucidating the Limit of Li Insertion into the Spinel Li4ti5o12.* ACS Materials Letters, 2019. **1**(1): p. 96-102.
[62] Xu, K., *Nonaqueous Liquid Electrolytes for Lithium-Based Rechargeable Batteries.* Chemical Reviews, 2004. **104**(10): p. 4303-4418.
[63] Julien, C., et al., *Electrolytes and Separators for Lithium Batteries*, in *Lithium Batteries: Science and Technology*. 2016, Springer International Publishing: Cham. p. 431-460.
[64] Li, Q., et al., *Progress in Electrolytes for Rechargeable Li-Based Batteries and Beyond.* Green Energy & Environment, 2016. **1**(1): p. 18-42.
[65] Ge, M., et al., *Review of Porous Silicon Preparation and Its Application for Lithium-Ion Battery Anodes.* Nanotechnology, 2013. **24**(42): p. 422001.
[66] Zamfir, M.R., et al., *Silicon Nanowires for Li-Based Battery Anodes: A Review.* Journal of Materials Chemistry A, 2013. **1**(34): p. 9566-9586.
[67] Zuo, X., et al., *Silicon Based Lithium-Ion Battery Anodes: A Chronicle Perspective Review.* Nano Energy, 2017. **31**: p. 113-143.
[68] Poizot, P., et al., *Nano-Sized Transition-Metal Oxides as Negative-Electrode Materials for Lithium-Ion Batteries.* Nature, 2000. **407**(6803): p. 496-499.
[69] Cabana, J., et al., *Beyond Intercalation-Based Li-Ion Batteries: The State of the Art and Challenges of Electrode Materials Reacting through Conversion Reactions.* Advanced Materials, 2010. **22**(35): p. E170-E192.
[70] Reddy, M.V., Subba Rao, G.V., and Chowdari, B.V.R., *Metal Oxides and Oxysalts as Anode Materials for Li Ion Batteries.* Chemical Reviews, 2013. **113**(7): p. 5364-5457.
[71] Luo, F., et al., *Review—Nano-Silicon/Carbon Composite Anode Materials Towards Practical Application for Next Generation Li-Ion Batteries.* Journal of The Electrochemical Society, 2015. **162**(14): p. A2509-A2528.
[72] Bach, P., et al., *Lithiation and Delithiation Mechanisms of Gold Thin Film Model Anodes for Lithium Ion Batteries: Electrochemical Characterization.* Electrochimica Acta, 2015. **164**: p. 81-89.
[73] Grugeon, S., et al., *Particle Size Effects on the Electrochemical Performance of Copper Oxides toward Lithium.* Journal of The Electrochemical Society, 2001. **148**(4): p. A285.
[74] Rehnlund, D., et al., *Electrochemical Fabrication and Characterization of Cu/Cu2o Multi-Layered Micro and Nanorods in Li-Ion Batteries.* Nanoscale, 2015. **7**(32): p. 13591-13604.
[75] Sahay, R., et al., *High Aspect Ratio Electrospun Cuo Nanofibers as Anode Material for Lithium-Ion Batteries with Superior Cycleability.* The Journal of Physical Chemistry C, 2012. **116**(34): p. 18087-18092.

[76] Yang, Y., et al., *An Efficient Route to Cu2o Nanorod Array Film for High-Performance Li-Ion Batteries.* Thin Solid Films, 2016. **608**: p. 79-87.
[77] Amatucci, G.G., Tarascon, J.M., and Klein, L.C., *Coo2, the End Member of the Li X Coo2 Solid Solution.* Journal of The Electrochemical Society, 1996. **143**(3): p. 1114-1123.
[78] Li, J., et al., *Structural Origin of the High-Voltage Instability of Lithium Cobalt Oxide.* Nature Nanotechnology, 2021. **16**(5): p. 599-605.
[79] Seo, D.-H., et al., *The Structural and Chemical Origin of the Oxygen Redox Activity in Layered and Cation-Disordered Li-Excess Cathode Materials.* Nature Chemistry, 2016. **8**: p. 692-697.
[80] Yabuuchi, N., et al., *Origin of Stabilization and Destabilization in Solid-State Redox Reaction of Oxide Ions for Lithium-Ion Batteries.* Nature Communications, 2016. **7**: p. 13814.
[81] Van der Ven, A., Aydinol, M.K., and Ceder, G., *First-Principles Evidence for Stage Ordering in Li X Coo2.* Journal of The Electrochemical Society, 1998. **145**(6): p. 2149-2155.
[82] Ménétrier, M., et al., *The Insulator-Metal Transition Upon Lithium Deintercalation from Licoo2: Electronic Properties and 7li Nmr Study.* Journal of Materials Chemistry, 1999. **9**(5): p. 1135-1140.
[83] Ceder, G. and Van der Ven, A., *Phase Diagrams of Lithium Transition Metal Oxides: Investigations from First Principles.* Electrochimica Acta, 1999. **45**(1): p. 131-150.
[84] Liu, Q., et al., *Approaching the Capacity Limit of Lithium Cobalt Oxide in Lithium Ion Batteries Via Lanthanum and Aluminium Doping.* Nature Energy, 2018. **3**(11): p. 936-943.
[85] Yabuuchi, N. and Ohzuku, T., *Novel Lithium Insertion Material of Lico1/3ni1/3mn1/3o2 for Advanced Lithium-Ion Batteries.* Journal of Power Sources, 2003. **119-121**: p. 171-174.
[86] Kobayashi, H., et al., *Investigation on Lithium De-Intercalation Mechanism for Li1−Yni1/3mn1/3co1/3o2.* Journal of Power Sources, 2005. **146**(1): p. 640-644.
[87] Julien, C., et al., *Optimization of Layered Cathode Materials for Lithium-Ion Batteries.* Materials, 2016. **9**(7): p. 595.
[88] Kim, J.-M. and Chung, H.-T., *The First Cycle Characteristics of Li[Ni1/3co1/3mn1/3]O2 Charged up to 4.7 V.* Electrochimica Acta, 2004. **49**(6): p. 937-944.
[89] Yan, J., Liu, X., and Li, B., *Recent Progress in Li-Rich Layered Oxides as Cathode Materials for Li-Ion Batteries.* Rsc Advances, 2014. **4**(108): p. 63268-63284.
[90] Rozier, P. and Tarascon, J.M., *Review—Li-Rich Layered Oxide Cathodes for Next-Generation Li-Ion Batteries: Chances and Challenges.* Journal of The Electrochemical Society, 2015. **162**(14): p. A2490-A2499.
[91] Hu, S., et al., *Li-Rich Layered Oxides and Their Practical Challenges: Recent Progress and Perspectives.* Electrochemical Energy Reviews, 2019. **2**(2): p. 277-311.
[92] Liu, J., et al., *Recent Breakthroughs and Perspectives of High-Energy Layered Oxide Cathode Materials for Lithium Ion Batteries.* Materials Today, 2021. **43**: p. 132-165.
[93] Lee, J., et al., *Unlocking the Potential of Cation-Disordered Oxides for Rechargeable Lithium Batteries.* Science, 2014. **343**(6170): p. 519-522.

[94] Urban, A., Lee, J., and Ceder, G., *The Configurational Space of Rocksalt-Type Oxides for High-Capacity Lithium Battery Electrodes.* Advanced Energy Materials, 2014. **4**(13): p. 1400478.
[95] Yabuuchi, N., et al., *High-Capacity Electrode Materials for Rechargeable Lithium Batteries: Li3nbo4-Based System with Cation-Disordered Rocksalt Structure.* Proceedings of the National Academy of Sciences, 2015. **112**(25): p. 7650-7655.
[96] Wang, R., et al., *A Disordered Rock-Salt Li-Excess Cathode Material with High Capacity and Substantial Oxygen Redox Activity: Li1.25nb0.25mn0.5o2.* Electrochemistry Communications, 2015. **60**: p. 70-73.
[97] Assat, G., et al., *Fundamental Interplay between Anionic/Cationic Redox Governing the Kinetics and Thermodynamics of Lithium-Rich Cathodes.* Nature Communications, 2017. **8**(1): p. 2219.
[98] Sathiya, M., et al., *Reversible Anionic Redox Chemistry in High-Capacity Layered-Oxide Electrodes.* Nature Materials, 2013. **12**: p. 827-835.
[99] Chen, R., et al., *Disordered Lithium-Rich Oxyfluoride as a Stable Host for Enhanced Li+ Intercalation Storage.* Advanced Energy Materials, 2015. **5**(9): p. 1401814.
[100] Ren, S., et al., *Improved Voltage and Cycling for Li+ Intercalation in High-Capacity Disordered Oxyfluoride Cathodes.* Advanced Science, 2015. **2**(10): p. 1500128.
[101] Song, B., et al., *Structural Evolution and the Capacity Fade Mechanism Upon Long-Term Cycling in Li-Rich Cathode Material.* Physical Chemistry Chemical Physics, 2012. **14**(37): p. 12875-12883.
[102] Sathiya, M., et al., *Origin of Voltage Decay in High-Capacity Layered Oxide Electrodes.* Nature Materials, 2014. **14**: p. 230-238.
[103] Lee, J., et al., *Mitigating Oxygen Loss to Improve the Cycling Performance of High Capacity Cation-Disordered Cathode Materials.* Nature communications, 2017. **8**(1): p. 981.
[104] Hartnig, C. and Schmidt, M., *Electrolytes and Conducting Salts*, in *Lithium-Ion Batteries: Basics and Applications*, R. Korthauer, Editor. 2018, Springer Berlin Heidelberg: Berlin, Heidelberg. p. 59-74.
[105] Montanino, M., Passerini, S., and Appetecchi, G.B., *4 - Electrolytes for Rechargeable Lithium Batteries*, in *Rechargeable Lithium Batteries*, A.A. Franco, Editor. 2015, Woodhead Publishing. p. 73-116.
[106] Edström, K., Herstedt, M., and Abraham, D.P., *A New Look at the Solid Electrolyte Interphase on Graphite Anodes in Li-Ion Batteries.* Journal of Power Sources, 2006. **153**(2): p. 380-384.
[107] Haregewoin, A.M., Wotango, A.S., and Hwang, B.-J., *Electrolyte Additives for Lithium Ion Battery Electrodes: Progress and Perspectives.* Energy & Environmental Science, 2016. **9**(6): p. 1955-1988.
[108] Zhang, S.S., *A Review on Electrolyte Additives for Lithium-Ion Batteries.* Journal of Power Sources, 2006. **162**(2): p. 1379-1394.
[109] Manthiram, A., Yu, X., and Wang, S., *Lithium Battery Chemistries Enabled by Solid-State Electrolytes.* Nature Reviews Materials, 2017. **2**: p. 16103.
[110] Quartarone, E. and Mustarelli, P., *Electrolytes for Solid-State Lithium Rechargeable Batteries: Recent Advances and Perspectives.* Chemical Society Reviews, 2011. **40**(5): p. 2525-2540.
[111] Lewandowski, A. and Świderska-Mocek, A., *Ionic Liquids as Electrolytes for Li-Ion Batteries—an Overview of Electrochemical Studies.* Journal of Power Sources, 2009. **194**(2): p. 601-609.

[112] Armand, M., et al., *Ionic-Liquid Materials for the Electrochemical Challenges of the Future.* Nature Materials, 2009. **8**: p. 621.
[113] Ravdel, B., et al., *Thermal Stability of Lithium-Ion Battery Electrolytes.* Journal of Power Sources, 2003. **119-121**: p. 805-810.
[114] Solchenbach, S., et al., *Quantification of Pf5 and Pof3 from Side Reactions of Lipf6 in Li-Ion Batteries.* Journal of The Electrochemical Society, 2018. **165**(13): p. A3022-A3028.
[115] Somerville, L., et al., *The Effect of Pre-Analysis Washing on the Surface Film of Graphite Electrodes.* Electrochimica Acta, 2016. **206**: p. 70-76.
[116] Fink, K., et al., *Impacts of Solvent Washing on the Electrochemical Remediation of Commercial End-of-Life Cathodes.* ACS Applied Energy Materials, 2020. **3**(12): p. 12212-12229.
[117] Fang, C., et al., *Gradient Polarity Solvent Wash for Separation and Analysis of Electrolyte Decomposition Products on Electrode Surfaces.* Journal of The Electrochemical Society, 2020. **167**(2): p. 020506.
[118] Malmgren, S., et al., *Consequences of Air Exposure on the Lithiated Graphite Sei.* Electrochimica Acta, 2013. **105**: p. 83-91.
[119] Bard, A.J. and Faulkner, L.R., *Electrochemical Methods: Fundamentals and Applications*. 2. ed. 2001, New York: Wiley.
[120] Koryta, J., Dvořák, J., and Kavan, L., *Principles of Electrochemistry*. 1993: John Wiley & Sons Inc.
[121] Scholz, F. and Bond, A.M., *Electroanalytical Methods: Guide to Experiments and Applications*. 2nd, rev. and extend;2. Aufl.; ed, ed. F. Scholz, et al. 2010, Heidelberg;New York;: Springer.
[122] Seeber, R., Zanardi, C., and Inzelt, G., *Links between Electrochemical Thermodynamics and Kinetics.* ChemTexts, 2015. **1**(4): p. 18.
[123] Boettcher, S.W., et al., *Potentially Confusing: Potentials in Electrochemistry.* ACS Energy Letters, 2021. **6**(1): p. 261-266.
[124] Riess, I., *What Does a Voltmeter Measure?* Solid State Ionics, 1997. **95**(3): p. 327-328.
[125] Bard, A., *Standard Potentials in Aqueous Solution*. 2017: Routledge.
[126] Arning, M.D. and Minteer, S.D., *18 - Electrode Potentials*, in *Handbook of Electrochemistry*, C.G. Zoski, Editor. 2007, Elsevier: Amsterdam. p. 813-827.
[127] Haynes, W.M., *Crc Handbook of Chemistry and Physics*. 2014: CRC press.
[128] Trasatti, S., *The Absolute Electrode Potential: An Explanatory Note (Recommendations 1986).* Pure and Applied Chemistry, 1986. **58**(7): p. 955-966.
[129] Trasatti, S., *The Concept and Physical Meaning of Absolute Electrode Potential: A Reassessment.* Journal of Electroanalytical Chemistry and Interfacial Electrochemistry, 1982. **139**(1): p. 1-13.
[130] Gerischer, H. and Ekardt, W., *Fermi Levels in Electrolytes and the Absolute Scale of Redox Potentials.* Applied physics letters, 1983. **43**(4): p. 393-395.
[131] Donald, W.A., et al., *Absolute Standard Hydrogen Electrode Potential Measured by Reduction of Aqueous Nanodrops in the Gas Phase.* Journal of the American Chemical Society, 2008. **130**(11): p. 3371-3381.
[132] Isse, A.A. and Gennaro, A., *Absolute Potential of the Standard Hydrogen Electrode and the Problem of Interconversion of Potentials in Different Solvents.* The Journal of Physical Chemistry B, 2010. **114**(23): p. 7894-7899.
[133] Lauks, I., *Polarizable Electrodes.* Sensors and Actuators, 1981. **1**: p. 261-288.
[134] Méry, A., et al., *A Critical Review for an Accurate Electrochemical Stability Window Measurement of Solid Polymer and Composite Electrolytes.* Materials, 2021. **14**(14): p. 3840.

[135] Yokoyama, Y., et al., *Origin of the Electrochemical Stability of Aqueous Concentrated Electrolyte Solutions.* Journal of The Electrochemical Society, 2018. **165**(14): p. A3299-A3303.
[136] Helmholtz, H.v., *Ueber Einige Gesetze Der Vertheilung Elektrischer Ströme in Körperlichen Leitern, Mit Anwendung Auf Die Thierisch-Elektrischen Versuche (Schluss.).* Annalen der Physik, 1853. **165**(7): p. 353-377.
[137] Gouy, M., *Sur La Constitution De La Charge Électrique À La Surface D'un Électrolyte.* J. Phys. Theor. Appl., 1910. **9**(1): p. 457-468.
[138] Chapman, D.L., *Li. A Contribution to the Theory of Electrocapillarity.* The London, Edinburgh, and Dublin Philosophical Magazine and Journal of Science, 1913. **25**(148): p. 475-481.
[139] Stern, O., *The Theory of the Electrolytic Double-Layer.* Z. Elektrochem, 1924. **30**(508): p. 1014-1020.
[140] Frumkin, A., *Die Kapillarkurve Der Höheren Fettsäuren Und Die Zustandsgleichung Der Oberflächenschicht.* Zeitschrift für Physikalische Chemie, 1925. **116**(1): p. 466-484.
[141] Grahame, D.C., *The Electrical Double Layer and the Theory of Electrocapillarity.* Chemical Reviews, 1947. **41**(3): p. 441-501.
[142] Parsons, R., *The Electrical Double Layer in Non-Aqueous Solvents.* Electrochimica Acta, 1976. **21**(9): p. 681-686.
[143] Parsons, R., *The Electrical Double Layer: Recent Experimental and Theoretical Developments.* Chemical Reviews, 1990. **90**(5): p. 813-826.
[144] Ito, M., *Structures of Water at Electrified Interfaces: Microscopic Understanding of Electrode Potential in Electric Double Layers on Electrode Surfaces.* Surface Science Reports, 2008. **63**(8): p. 329-389.
[145] Dunwell, M., Yan, Y., and Xu, B., *Understanding the Influence of the Electrochemical Double-Layer on Heterogeneous Electrochemical Reactions.* Current Opinion in Chemical Engineering, 2018. **20**: p. 151-158.
[146] Burt, R., Birkett, G., and Zhao, X.S., *A Review of Molecular Modelling of Electric Double Layer Capacitors.* Physical Chemistry Chemical Physics, 2014. **16**(14): p. 6519-6538.
[147] Nattino, F., et al., *Continuum Models of the Electrochemical Diffuse Layer in Electronic-Structure Calculations.* The Journal of Chemical Physics, 2019. **150**(4): p. 041722.
[148] Dryden, M.D.M. and Wheeler, A.R., *Dstat: A Versatile, Open-Source Potentiostat for Electroanalysis and Integration.* PLOS ONE, 2015. **10**(10): p. e0140349.
[149] Martin, S.M., et al., *A Fully Differential Potentiostat.* IEEE Sensors Journal, 2009. **9**(2): p. 135-142.
[150] Van der Ven, A., Bhattacharya, J., and Belak, A.A., *Understanding Li Diffusion in Li-Intercalation Compounds.* Accounts of Chemical Research, 2013. **46**(5): p. 1216-1225.
[151] Karlsson, L., et al., *Atomic Physics*. Fourth edition ed. 2005, Uppsala: Fysiska instutionen, Uppsala Universitet.
[152] Blinder, S.M., *Introduction to Quantum Mechanics (Second Edition)*. 2021, S.l.: Academic Press.
[153] Griffiths, D.J. and Schroeter, D.F., *Introduction to Quantum Mechanics*. Third ed. 2018, Cambridge, United Kingdom: Cambridge University Press.
[154] Sakurai, J.J. and Napolitano, J., *Modern Quantum Mechanics*. Third ed. 2021, Cambridge: Cambridge University Press.

[155] Kirchhoff and Bunsen, *Xxiv.—on Chemical Analysis by Spectrum-Observations.* Quarterly Journal of the Chemical Society of London, 1861. **13**(3): p. 270-289.
[156] Bohr, N., *I. On the Constitution of Atoms and Molecules.* The London, Edinburgh, and Dublin Philosophical Magazine and Journal of Science, 1913. **26**(151): p. 1-25.
[157] Aspect, A. and Villain, J., *The Birth of Wave Mechanics (1923–1926).* Comptes Rendus Physique, 2017. **18**(9): p. 583-585.
[158] De Broglie, L., *Waves and Quanta.* Nature, 1923. **112**(2815): p. 540-540.
[159] Heisenberg, W., *Über Quantentheoretische Umdeutung Kinematischer Und Mechanischer Beziehungen.* Zeitschrift für Physik, 1925. **33**(1): p. 879-893.
[160] Schrödinger, E., *Quantisierung Als Eigenwertproblem.* Annalen der physik, 1926. **385**(13): p. 437-490.
[161] Kittel, C., *Introduction to Solid State Physics Eighth Edition.* 2021.
[162] Streetman, B.G. and Banerjee, S., *Solid State Electronic Devices*. Vol. 10. 2006: Pearson/Prentice Hall Upper Saddle River, NJ.
[163] Hüfner, S. and SpringerLink, *Photoelectron Spectroscopy: Principles and Applications*. Third Revis and Enlarg ed. 2003, Berlin, Heidelberg: Springer Berlin Heidelberg.
[164] van der Heide, P., *X-Ray Photoelectron Spectroscopy : An Introduction to Principles and Practices*. 2011, Hoboken, UNITED STATES: Wiley.
[165] Hertz, H., *Ueber Einen Einfluss Des Ultravioletten Lichtes Auf Die Electrische Entladung.* Annalen der Physik, 1887. **267**(8): p. 983-1000.
[166] Einstein, A., *Über Einen Die Erzeugung Und Verwandlung Des Lichtes Betreffenden Heuristischen Gesichtspunkt.* Annalen der Physik, 1905. **322**(6): p. 132-148.
[167] Moulder, J.F. and Chastain, J., *Handbook of X-Ray Photoelectron Spectroscopy: A Reference Book of Standard Spectra for Identification and Interpretation of Xps Data*. 1992: Physical Electronics Division, Perkin-Elmer Corporation.
[168] Greczynski, G., Primetzhofer, D., and Hultman, L., *Reference Binding Energies of Transition Metal Carbides by Core-Level X-Ray Photoelectron Spectroscopy Free from Ar+ Etching Artefacts.* Applied Surface Science, 2018. **436**: p. 102-110.
[169] Oswald, S., et al., *Binding Energy Referencing for Xps in Alkali Metal-Based Battery Materials Research (Ii): Application to Complex Composite Electrodes.* Batteries, 2018. **4**(3): p. 36.
[170] Lindgren, F., et al., *Breaking Down a Complex System: Interpreting Pes Peak Positions for Cycled Li-Ion Battery Electrodes.* The Journal of Physical Chemistry C, 2017. **121**(49): p. 27303-27312.
[171] Philippe, B., et al., *Photoelectron Spectroscopy for Lithium Battery Interface Studies.* Journal of the Electrochemical Society, 2016. **163**(2): p. A178-A191.
[172] Greczynski, G. and Hultman, L., *X-Ray Photoelectron Spectroscopy: Towards Reliable Binding Energy Referencing.* Progress in Materials Science, 2020. **107**: p. 100591.
[173] Greczynski, G. and Hultman, L., *C 1s Peak of Adventitious Carbon Aligns to the Vacuum Level: Dire Consequences for Material's Bonding Assignment by Photoelectron Spectroscopy.* ChemPhysChem, 2017. **18**(12): p. 1507-1512.
[174] Baer, D.R., *Summary of Iso/Tc 201 Standard: Xviii, Iso 19318:2004—Surface Chemical Analysis—X-Ray Photoelectron Spectroscopy—Reporting of Methods Used for Charge Control and Charge Correction.* Surface and Interface Analysis, 2005. **37**(5): p. 524-526.

[175] Bird, R.J. and Swift, P., *Energy Calibration in Electron Spectroscopy and the Re-Determination of Some Reference Electron Binding Energies.* Journal of Electron Spectroscopy and Related Phenomena, 1980. **21**(3): p. 227-240.
[176] Jacquemin, M., et al., *Calibration of the X-Ray Photoelectron Spectroscopy Binding Energy Scale for the Characterization of Heterogeneous Catalysts: Is Everything Really under Control?* ChemPhysChem, 2013. **14**(15): p. 3618-3626.
[177] Koopmans, T., *Über Die Zuordnung Von Wellenfunktionen Und Eigenwerten Zu Den Einzelnen Elektronen Eines Atoms.* Physica, 1934. **1**(1): p. 104-113.
[178] Tsuneda, T., et al., *On Koopmans' Theorem in Density Functional Theory.* The Journal of Chemical Physics, 2010. **133**(17): p. 174101.
[179] Born, M., *Eine Thermochemische Anwendung Der Gittertheorie.* Verhandlungen der Deutschen Physikalischen Gesellschaft, 1919. **21**: p. 13-24.
[180] Haber, F., *Betrachtungen Zur Theorie Der Wärmetönung.* Verhandlungen der Deutschen Physikalischen Gesellschaft, 1919. **21**: p. 750-768.
[181] Fajans, K., *Die Elektronenaffinität Der Halogenatome Und Die Ionisierungsenergie Der Halogenwasserstoffe.* Verhandl Deut Phys Ges, 1919. **21**: p. 714-722.
[182] Glasser, L. and von Szentpály, L., *Born−Haber−Fajans Cycle Generalized: Linear Energy Relation between Molecules, Crystals, and Metals.* Journal of the American Chemical Society, 2006. **128**(37): p. 12314-12321.
[183] Fahlman, A., Nordling, C., and Siegbahn, K., *Esca : Atomic, Molecular and Solid State Structure Studied by Means of Electron Spectroscopy*. 1967: Uppsala : Almqvist and Wiksell.
[184] Wertheim, O.K., *Anomalous Chemical Shifts: Barium Compounds.* Journal of Electron Spectroscopy and Related Phenomena, 1984. **34**(3): p. 309-312.
[185] Veal, B.W. and Paulikas, A.P., *Final-State Screening and Chemical Shifts in Photoelectron Spectroscopy.* Physical Review B, 1985. **31**(8): p. 5399-5416.
[186] Biesinger, M.C., et al., *Resolving Surface Chemical States in Xps Analysis of First Row Transition Metals, Oxides and Hydroxides: Cr, Mn, Fe, Co and Ni.* Applied Surface Science, 2011. **257**(7): p. 2717-2730.
[187] Biesinger, M.C., et al., *Resolving Surface Chemical States in Xps Analysis of First Row Transition Metals, Oxides and Hydroxides: Sc, Ti, V, Cu and Zn.* Applied Surface Science, 2010. **257**(3): p. 887-898.
[188] Biesinger, M.C., *Advanced Analysis of Copper X-Ray Photoelectron Spectra.* Surface and Interface Analysis, 2017. **49**(13): p. 1325-1334.
[189] Biesinger, M.C., et al., *The Role of the Auger Parameter in Xps Studies of Nickel Metal, Halides and Oxides.* Physical Chemistry Chemical Physics, 2012. **14**(7): p. 2434-2442.
[190] Hansen, W.N., *The Emersed Double Layer.* Journal of Electroanalytical Chemistry and Interfacial Electrochemistry, 1983. **150**(1): p. 133-140.
[191] D'Agostino, A.T. and Hansen, W.N., *Observation of Systematic Electrochemically Induced Binding Energy Shift in the Xps Spectra of Emersed Cs+ Double Layer Species.* Surface Science, 1986. **165**(1): p. 268-276.
[192] D'Agostino, A.T. and Hansen, W.N., *Shift in Core Level Binding Energy in Double-Layer Species on Potentiostatically Emersed Electrodes.* Journal of Electron Spectroscopy and Related Phenomena, 1988. **46**(1): p. 155-164.
[193] Hamm, U.W., Lazarescu, V., and Kolb, D.M., *Adsorption of Pyrazine on Au(111) and Ag(111) Electrodes an Ex Situ Xps Study.* Journal of the Chemical Society, Faraday Transactions, 1996. **92**(20): p. 3785-3790.

[194] Zhou, W. and Kolb, D.M., *Influence of an Electrostatic Potential at the Metal/Electrolyte Interface on the Electron Binding Energy of Adsorbates as Probed by X-Ray Photoelectron Spectroscopy.* Surface Science, 2004. **573**(2): p. 176-182.
[195] Wood, K.N. and Teeter, G., *Xps on Li-Battery-Related Compounds: Analysis of Inorganic Sei Phases and a Methodology for Charge Correction.* ACS Applied Energy Materials, 2018. **1**(9): p. 4493-4504.
[196] Oswald, S., Hoffmann, M., and Zier, M., *Peak Position Differences Observed During Xps Sputter Depth Profiling of the Sei on Lithiated and Delithiated Carbon-Based Anode Material for Li-Ion Batteries.* Applied Surface Science, 2017. **401**: p. 408-413.
[197] Maibach, J., et al., *Electric Potential Gradient at the Buried Interface between Lithium-Ion Battery Electrodes and the Sei Observed Using Photoelectron Spectroscopy.* The journal of physical chemistry letters, 2016. **7**(10): p. 1775-1780.
[198] Powell, C.J. and Jablonski, A., *Progress in Quantitative Surface Analysis by X-Ray Photoelectron Spectroscopy: Current Status and Perspectives.* Journal of Electron Spectroscopy and Related Phenomena, 2010. **178-179**: p. 331-346.
[199] Berglund, C.N. and Spicer, W.E., *Photoemission Studies of Copper and Silver: Theory.* Physical Review, 1964. **136**(4A): p. A1030-A1044.
[200] Wagner, C.D., et al., *Empirical Atomic Sensitivity Factors for Quantitative Analysis by Electron Spectroscopy for Chemical Analysis.* Surface and Interface Analysis, 1981. **3**(5): p. 211-225.
[201] Powell, C.J. and Jablonski, A., *Nist Electron Inelastic-Mean-Free-Path Database 71, Version 1.0*. 1999.
[202] Powell, C.J. and Jablonski, A., *Evaluation of Calculated and Measured Electron Inelastic Mean Free Paths near Solid Surfaces.* Journal of physical and chemical reference data, 1999. **28**(1): p. 19-62.
[203] Yeh, J.J. and Lindau, I., *Atomic Subshell Photoionization Cross Sections and Asymmetry Parameters: $1 \leqslant Z \leqslant 103$.* Atomic Data and Nuclear Data Tables, 1985. **32**(1): p. 1-155.
[204] Scofield, J.H., *Theoretical Photoionization Cross Sections from 1 to 1500 Kev*. 1973, California Univ.
[205] Seah, M.P. and Dench, W.A., *Quantitative Electron Spectroscopy of Surfaces: A Standard Data Base for Electron Inelastic Mean Free Paths in Solids.* Surface and Interface Analysis, 1979. **1**(1): p. 2-11.
[206] Favaro, M., et al., *Interface Science Using Ambient Pressure Hard X-Ray Photoelectron Spectroscopy.* Surfaces, 2019. **2**(1): p. 78-99.
[207] Starr, D.E., et al., *Combined Soft and Hard X-Ray Ambient Pressure Photoelectron Spectroscopy Studies of Semiconductor/Electrolyte Interfaces.* Journal of Electron Spectroscopy and Related Phenomena, 2017. **221**: p. 106-115.
[208] Malmgren, S., et al., *Nondestructive Depth Profiling of the Solid Electrolyte Interphase on Lifepo4 and Graphite Electrodes.* ECS Transactions, 2010. **25**(36): p. 201-210.
[209] Nordh, T., et al., *Depth Profiling the Solid Electrolyte Interphase on Lithium Titanate (Li4ti5o12) Using Synchrotron-Based Photoelectron Spectroscopy.* Journal of Power Sources, 2015. **294**: p. 173-179.
[210] Rubensson, J.-E., *Synchrotron Radiation*, in *An everyday application of special relativity*. 2016, Morgan & Claypool Publishers.
[211] Attwood, D., *Soft X-Rays and Extreme Ultraviolet Radiation: Principles and Applications*. 2000: Cambridge university press.

[212] Fan, C. and Zhao, Z., *Synchrotron Radiation in Materials Science : Light Sources, Techniques and Applications*. 2018, Newark, GERMANY: John Wiley & Sons, Incorporated.
[213] Lin, F., et al., *Synchrotron X-Ray Analytical Techniques for Studying Materials Electrochemistry in Rechargeable Batteries.* Chemical Reviews, 2017. **117**(21): p. 13123-13186.
[214] Mårtensson, N., et al., *A Very High Resolution Electron Spectrometer.* Journal of Electron Spectroscopy and Related Phenomena, 1994. **70**(2): p. 117-128.
[215] Gelius, U., et al., *A New Esca Instrument with Improved Surface Sensitivity, Fast Imaging Properties and Excellent Energy Resolution.* Journal of Electron Spectroscopy and Related Phenomena, 1990. **52**: p. 747-785.
[216] Wannberg, B., Gelius, U., and Siegbahn, K., *Design Principles in Electron Spectroscopy.* Journal of Physics E: Scientific Instruments, 1974. **7**(3): p. 149-159.
[217] Eriksson, S.K., et al., *A Versatile Photoelectron Spectrometer for Pressures up to 30 Mbar.* Review of Scientific Instruments, 2014. **85**(7): p. 075119.
[218] Ogletree, D.F., et al., *A Differentially Pumped Electrostatic Lens System for Photoemission Studies in the Millibar Range.* Review of Scientific Instruments, 2002. **73**(11): p. 3872-3877.
[219] Ogletree, D.F., et al., *Photoelectron Spectroscopy under Ambient Pressure and Temperature Conditions.* Nuclear Instruments & Methods in Physics Research Section a-Accelerators Spectrometers Detectors and Associated Equipment, 2009. **601**(1-2): p. 151-160.
[220] Shavorskiy, A., et al., *Synchrotron-Based Ambient Pressure X-Ray Photoelectron Spectroscopy.* Synchrotron Radiation News, 2014. **27**(2): p. 14-23.
[221] Gorgoi, M., et al., *Hard X-Ray High Kinetic Energy Photoelectron Spectroscopy at the Kmc-1 Beamline at Bessy.* The European Physical Journal Special Topics, 2009. **169**(1): p. 221-225.
[222] Lee, T.-L. and Duncan, D.A., *A Two-Color Beamline for Electron Spectroscopies at Diamond Light Source.* Synchrotron Radiation News, 2018. **31**(4): p. 16-22.
[223] Zhu, S., et al., *Hippie: A New Platform for Ambient-Pressure X-Ray Photoelectron Spectroscopy at the Max Iv Laboratory.* Journal of Synchrotron Radiation, 2021. **28**(2): p. 624-636.
[224] Gorgoi, M., et al., *The High Kinetic Energy Photoelectron Spectroscopy Facility at Bessy Progress and First Results.* Nuclear Instruments and Methods in Physics Research Section A: Accelerators, Spectrometers, Detectors and Associated Equipment, 2009. **601**(1): p. 48-53.
[225] Schaefers, F., Mertin, M., and Gorgoi, M., *Kmc-1: A High Resolution and High Flux Soft X-Ray Beamline at Bessy.* Review of Scientific Instruments, 2007. **78**(12): p. 123102.
[226] Cai, J., et al., *An Apxps Endstation for Gas–Solid and Liquid–Solid Interface Studies at Ssrf.* Nuclear Science and Techniques, 2019. **30**(5): p. 81.
[227] Kahk, J.M., et al., *A Study of the Pressure Profiles near the First Pumping Aperture in a High Pressure Photoelectron Spectrometer.* Journal of Electron Spectroscopy and Related Phenomena, 2015. **205**: p. 57-65.
[228] Reiss, H., *The Fermi Level and the Redox Potential.* The Journal of Physical Chemistry, 1985. **89**(18): p. 3783-3791.
[229] Lyklema, J., *Interfacial Potentials: Measuring the Immeasurable?* Substantia, 2017. **1**(2).

[230] Kahn, A., *Fermi Level, Work Function and Vacuum Level.* Materials Horizons, 2016. **3**(1): p. 7-10.
[231] Scanlon, M.D., et al., *Charging and Discharging at the Nanoscale: Fermi Level Equilibration of Metallic Nanoparticles.* Chemical Science, 2015. **6**(5): p. 2705-2720.
[232] Khan, S.U.M., Kainthla, R.C., and Bockris, J.O.M., *The Redox Potential and the Fermi Level in Solution.* The Journal of Physical Chemistry, 1987. **91**(23): p. 5974-5977.
[233] Pethica, B.A., *Are Electrostatic Potentials between Regions of Different Chemical Composition Measurable? The Gibbs–Guggenheim Principle Reconsidered, Extended and Its Consequences Revisited.* Physical Chemistry Chemical Physics, 2007. **9**(47): p. 6253-6262.
[234] Kittel, C. and Kroemer, H., *Thermal Physics*. Vol. 9690. 1970: Wiley New York.
[235] Ganguly, J., *Thermodynamics in Earth and Planetary Sciences*. 2008: Springer.
[236] Garrido, J., *Thermodynamics of Electrochemical Systems.* The Journal of Physical Chemistry B, 2004. **108**(47): p. 18336-18340.
[237] Melot, B.C. and Tarascon, J.M., *Design and Preparation of Materials for Advanced Electrochemical Storage.* Accounts of Chemical Research, 2013. **46**(5): p. 1226-1238.
[238] Peljo, P. and Girault, H.H., *Electrochemical Potential Window of Battery Electrolytes: The Homo–Lumo Misconception.* Energy & Environmental Science, 2018. **11**(9): p. 2306-2309.
[239] Chen, W., et al., *Ab Initio Electronic Structure of Liquid Water.* Physical Review Letters, 2016. **117**(18): p. 186401.
[240] Barnes, T.A., et al., *Ab Initio Characterization of the Electrochemical Stability and Solvation Properties of Condensed-Phase Ethylene Carbonate and Dimethyl Carbonate Mixtures.* The Journal of Physical Chemistry C, 2015. **119**(8): p. 3865-3880.
[241] Trotochaud, L., et al., *Ambient Pressure Photoelectron Spectroscopy: Practical Considerations and Experimental Frontiers.* J Phys Condens Matter, 2017. **29**(5): p. 053002.
[242] Crumlin, E.J., et al., *X-Ray Spectroscopy of Energy Materials under in Situ/Operando Conditions.* Journal of Electron Spectroscopy and Related Phenomena, 2015. **200**: p. 264-273.
[243] Favaro, M., et al., *Unravelling the Electrochemical Double Layer by Direct Probing of the Solid/Liquid Interface.* Nature communications, 2016. **7**: p. 12695.
[244] Karslıoğlu, O., et al., *Aqueous Solution/Metal Interfaces Investigated in Operando by Photoelectron Spectroscopy.* Faraday Discussions, 2015. **180**(0): p. 35-53.
[245] Axnanda, S., et al., *Using "Tender" X-Ray Ambient Pressure X-Ray Photoelectron Spectroscopy as a Direct Probe of Solid-Liquid Interface.* Scientific Reports, 2015. **5**: p. 9788.
[246] Landau, L. and Levich, B., *Dragging of a Liquid by a Moving Plate*, in *Dynamics of Curved Fronts*, P. Pelcé, Editor. 1988, Academic Press: San Diego. p. 141-153.
[247] Maleki, M., et al., *Landau–Levich Menisci.* Journal of Colloid and Interface Science, 2011. **354**(1): p. 359-363.

[248] Ali-Löytty, H., et al., *Ambient-Pressure Xps Study of a Ni–Fe Electrocatalyst for the Oxygen Evolution Reaction.* The Journal of Physical Chemistry C, 2016. **120**(4): p. 2247-2253.
[249] Lichterman, M.F., et al., *Direct Observation of the Energetics at a Semiconductor/Liquid Junction by Operando X-Ray Photoelectron Spectroscopy.* Energy & Environmental Science, 2015. **8**(8): p. 2409-2416.
[250] Favaro, M., et al., *Elucidating the Alkaline Oxygen Evolution Reaction Mechanism on Platinum.* Journal of Materials Chemistry A, 2017. **5**(23): p. 11634-11643.
[251] Stoerzinger, K.A., et al., *Stabilizing the Meniscus for Operando Characterization of Platinum During the Electrolyte-Consuming Alkaline Oxygen Evolution Reaction.* Topics in Catalysis, 2018. **61**(20): p. 2152-2160.
[252] Park, M., et al., *A Review of Conduction Phenomena in Li-Ion Batteries.* Journal of Power Sources, 2010. **195**(24): p. 7904-7929.
[253] Lichterman, M.F., et al., *An Electrochemical, Microtopographical and Ambient Pressure X-Ray Photoelectron Spectroscopic Investigation of Si/Tio2/Ni/Electrolyte Interfaces.* Journal of The Electrochemical Society, 2016. **163**(2): p. H139-H146.
[254] Wu, X., et al., *Monitoring the Chemical and Electronic Properties of Electrolyte–Electrode Interfaces in All-Solid-State Batteries Using Operando X-Ray Photoelectron Spectroscopy.* Physical Chemistry Chemical Physics, 2018. **20**(16): p. 11123-11129.
[255] Shavorskiy, A., et al., *Direct Mapping of Band Positions in Doped and Undoped Hematite During Photoelectrochemical Water Splitting.* The Journal of Physical Chemistry Letters, 2017. **8**(22): p. 5579-5586.
[256] Han, Y., et al., *Observing the Electrochemical Oxidation of Co Metal at the Solid/Liquid Interface Using Ambient Pressure X-Ray Photoelectron Spectroscopy.* The Journal of Physical Chemistry B, 2018. **122**(2): p. 666-671.
[257] Richards, W.D., et al., *Fluorination of Lithium-Excess Transition Metal Oxide Cathode Materials.* Advanced Energy Materials, 2018. **8**(5): p. 1701533.
[258] Ji, H., et al., *Hidden Structural and Chemical Order Controls Lithium Transport in Cation-Disordered Oxides for Rechargeable Batteries.* Nature Communications, 2019. **10**(1): p. 592.
[259] Saubanère, M., et al., *The Intriguing Question of Anionic Redox in High-Energy Density Cathodes for Li-Ion Batteries.* Energy & Environmental Science, 2016. **9**(3): p. 984-991.
[260] Lu, Z., MacNeil, D.D., and Dahn, J.R., *Layered Li[Ni[Sub X]Co[Sub 1−2x]Mn[Sub X]]O[Sub 2] Cathode Materials for Lithium-Ion Batteries.* Electrochemical and Solid-State Letters, 2001. **4**(12): p. A200.
[261] Choi, W. and Manthiram, A., *Superior Capacity Retention Spinel Oxyfluoride Cathodes for Lithium-Ion Batteries.* Electrochemical and Solid-State Letters, 2006. **9**(5): p. A245-A248.
[262] Gutierrez, A. and Manthiram, A., *Understanding the Effects of Cationic and Anionic Substitutions in Spinel Cathodes of Lithium-Ion Batteries.* Journal of The Electrochemical Society, 2013. **160**(6): p. A901-A905.
[263] Chen, R., et al., *Li+ Intercalation in Isostructural Li2vo3 and Li2vo2f with O2− and Mixed O2−/F− Anions.* Physical Chemistry Chemical Physics, 2015. **17**(26): p. 17288-17295.
[264] Urban, A., et al., *Electronic-Structure Origin of Cation Disorder in Transition-Metal Oxides.* Physical Review Letters, 2017. **119**(17): p. 176402.

[265] Aurbach, D., et al., *On the Use of Vinylene Carbonate (Vc) as an Additive to Electrolyte Solutions for Li-Ion Batteries.* Electrochimica Acta, 2002. **47**(9): p. 1423-1439.
[266] Jeon, J., et al., *Tuning Glycolide as an Sei-Forming Additive for Thermally Robust Li-Ion Batteries.* Journal of Materials Chemistry, 2012. **22**(39): p. 21003-21008.
[267] Liao, L., et al., *Fluoroethylene Carbonate as Electrolyte Additive to Improve Low Temperature Performance of Lifepo4 Electrode.* Electrochimica Acta, 2013. **87**: p. 466-472.
[268] Dalavi, S., et al., *Effect of Added Libob on High Voltage (Lini0.5mn1.5o4) Spinel Cathodes.* Electrochemical and Solid-State Letters, 2011. **15**(2): p. A28-A31.
[269] Ha, S.-Y., et al., *Using a Lithium Bis(Oxalato) Borate Additive to Improve Electrochemical Performance of High-Voltage Spinel Lini0.5mn1.5o4 Cathodes at 60°C.* Electrochimica Acta, 2013. **104**: p. 170-177.
[270] Lee, S.J., et al., *A Bi-Functional Lithium Difluoro(Oxalato)Borate Additive for Lithium Cobalt Oxide/Lithium Nickel Manganese Cobalt Oxide Cathodes and Silicon/Graphite Anodes in Lithium-Ion Batteries at Elevated Temperatures.* Electrochimica Acta, 2014. **137**: p. 1-8.
[271] Liu, J., et al., *Lithium Difluoro(Oxalato)Borate as a Functional Additive for Lithium-Ion Batteries.* Electrochemistry Communications, 2007. **9**(3): p. 475-479.
[272] Zhao, D., et al., *Tailoring Interfacial Architecture of High-Voltage Cathode with Lithium Difluoro(Bisoxalato) Phosphate for High Energy Density Battery.* Journal of Power Sources, 2020. **456**: p. 228006.
[273] Xu, M., et al., *Improving the Performance of Graphite/ Lini0.5mn1.5o4 Cells at High Voltage and Elevated Temperature with Added Lithium Bis(Oxalato) Borate (Libob).* Journal of The Electrochemical Society, 2013. **160**(11): p. A2005-A2013.
[274] Wu, Q., et al., *Effects of Lithium Difluoro(Oxalate)Borate on the Performance of Li-Rich Composite Cathode in Li-Ion Battery.* Electrochemistry Communications, 2012. **24**: p. 78-81.
[275] Verdier, S., et al., *Xps Study on Al[Sub 2]O[Sub 3]- and Alpo[Sub 4]-Coated Licoo[Sub 2] Cathode Material for High-Capacity Li Ion Batteries.* Journal of The Electrochemical Society, 2007. **154**(12): p. A1088.
[276] Wang, X., Wang, X., and Lu, Y., *Realizing High Voltage Lithium Cobalt Oxide in Lithium-Ion Batteries.* Industrial & Engineering Chemistry Research, 2019. **58**(24): p. 10119-10139.
[277] Zheng, J., et al., *Functioning Mechanism of Alf3 Coating on the Li- and Mn-Rich Cathode Materials.* Chemistry of Materials, 2014. **26**(22): p. 6320-6327.
[278] Erickson, E.M., et al., *Review—Recent Advances and Remaining Challenges for Lithium Ion Battery Cathodes.* Journal of The Electrochemical Society, 2017. **164**(1): p. A6341-A6348.
[279] Rosina, K.J., et al., *Structure of Aluminum Fluoride Coated Li[Li1/9ni1/3mn5/9]O2 Cathodes for Secondary Lithium-Ion Batteries.* Journal of Materials Chemistry, 2012. **22**(38): p. 20602-20610.
[280] Amalraj, F., et al., *Studies of Li and Mn-Rich Lix[Mnnico]O2electrodes: Electrochemical Performance, Structure, and the Effect of the Aluminum Fluoride Coating.* Journal of The Electrochemical Society, 2013. **160**(11): p. A2220-A2233.

[281] Grass, M.E., et al., *New Ambient Pressure Photoemission Endstation at Advanced Light Source Beamline 9.3.2.* Review of Scientific Instruments, 2010. **81**(5): p. 053106.
[282] Follath, R., et al., *The Energy Materials in-Situ Laboratory Berlin (Emil) at Bessy Ii.* Journal of Physics: Conference Series, 2013. **425**(21): p. 212003.
[283] Novotny, Z., et al., *Probing the Solid-Liquid Interface with Tender X Rays: A New Ambient-Pressure X-Ray Photoelectron Spectroscopy Endstation at the Swiss Light Source.* Rev Sci Instrum, 2020. **91**(2): p. 023103.

Acta Universitatis Upsaliensis

Digital Comprehensive Summaries of Uppsala Dissertations from the Faculty of Science and Technology 2069

Editor: The Dean of the Faculty of Science and Technology

A doctoral dissertation from the Faculty of Science and Technology, Uppsala University, is usually a summary of a number of papers. A few copies of the complete dissertation are kept at major Swedish research libraries, while the summary alone is distributed internationally through the series Digital Comprehensive Summaries of Uppsala Dissertations from the Faculty of Science and Technology. (Prior to January, 2005, the series was published under the title "Comprehensive Summaries of Uppsala Dissertations from the Faculty of Science and Technology".)

Distribution: publications.uu.se
urn:nbn:se:uu:diva-452281

ACTA
UNIVERSITATIS
UPSALIENSIS
UPPSALA
2021